ABSTRACT

Title of Dissertation: CHARACTERIZATION OF PROGRAMMED CELL DEATH PATHWAYS ACTIVATED IN MYCOBACTERIUM TUBERCULOSIS-INFECTED THP-1 CELLS AND HUMAN MONOCYTE-DERIVED MACROPHAGES

Guanchao Ding, Doctor of Philosophy, 2026

Dissertation directed by: Professor, Volker Briken, Ph.D., Cell Biology and Molecular Genetics

Mycobacterium tuberculosis (Mtb) primarily infects human lung macrophages, which serve as its major replication niche. Mtb can manipulate host macrophage cell death pathways to its advantage by inhibiting apoptosis and inducing necrotic cell death. However, the specific necrotic cell death pathway activated in human macrophages after Mtb infection remains unclear. Here, we used the THP-1 cell line and primary human monocyte-derived macrophages (hMDMs) to analyze multiple programmed cell death pathways during days 1-3 after Mtb infection. Regarding apoptosis, confocal microscopic analysis demonstrates that Mtb rarely induces apoptosis in THP-1 cells or hMDMs. Immunoblotting shows that Mtb induces significant CASP3 and GSDME activation in THP-1 cells, but not in hMDMs. We show that Mtb induces a significant

increase in GSDMD cleavage, a hallmark of pyroptosis, in THP-1 cells but not in hMDMs. MLKL phosphorylation was not observed in THP-1 cells or hMDMs during Mtb infections, indicating an absence of necroptosis. No changes in ferroptosis markers such as GPX4 expression or lipid peroxidation levels were detected. Time-lapse live-cell imaging revealed no lysosomal membrane permeabilization prior to plasma membrane rupture (PMR). However, we observed DNA release from Mtb-infected THP-1 cells and hMDMs after PMR. The DNA released from THP-1 cells exhibits low levels of myeloperoxidase and histone H3 citrullination. High-resolution confocal imaging shows that Mtb is associated with the released DNA. We demonstrate that pyroptosis induction is dispensable for the DNA release and cell death induction. In conclusion, our results reveal that Mtb-triggered cell death in hMDMs bypasses canonical cell death pathways, including apoptosis, pyroptosis, necroptosis, and ferroptosis. Instead, cell death in both THP-1 cells and hMDMs correlates with DNA release that shares partial features with METosis or NETosis.

CHARACTERIZATION OF PROGRAMMED CELL DEATH PATHWAYS ACTIVATED IN MYCOBACTERIUM TUBERCULOSIS-INFECTED THP-1 CELLS AND HUMAN MONOCYTE-DERIVED MACROPHAGES

by

Guanchao Ding

Dissertation submitted to the Faculty of the Graduate School of the
University of Maryland, College Park, in partial fulfillment
of the requirements for the degree of
Doctor of Philosophy
2026

Advisory Committee:
Professor Volker Briken, Ph.D., Chair
Professor David Mosser, Ph.D.
Professor Wenxia Song, Ph.D.
Professor Margaret Scull, Ph.D.
Professor Daniel Nelson, Ph.D., Dean's Representative

Acknowledgements

I have studied at the University of Maryland, College Park (UMD) for nearly seven years in pursuit of my Ph.D. degree in biology. I am deeply grateful to the university, my department, and my laboratory for providing a supportive, inclusive, and protective environment throughout my training as an international student. I was supported by NIAID grants R01AI147630 and R01AI139492, as well as by teaching assistantships provided by the department during my first two years of study.

I would like to express my sincere gratitude to my advisor, Dr. Volker Briken, for his mentorship in project development, experimental design, and data presentation, and for his consistent support as I pursued my scientific and personal aspirations. I am especially thankful to my former colleague, Dr. Jacques Augenstreich, who generously shared his ideas, techniques, and expertise, and whose guidance was instrumental in helping me bring this work to completion. I am also grateful to my current colleagues and collaborators, Akshaya Ganesh, Ravin Fisher, and Tasmim Hossain, for sharing this scientific journey with me. I thank my former lab members as well, whose discussions and insights contributed meaningfully to my development as a scientist.

I would like to acknowledge my dissertation committee members—Dr. Daniel Nelson, Dr. David Mosser, Dr. Wenxia Song, and Dr. Margaret Scull—for their thoughtful evaluation of my work and for their encouragement and guidance regarding my future career. As I began incorporating Python-based analysis into my research, I received generous assistance from Zizheng Zhang, Xiangyu Liu, and Junzheng Chu, who shared their expertise and greatly facilitated my learning process. Some schematics and graphical elements in this dissertation were created using BioRender.com.

Although we interacted primarily through scientific discussions rather than frequent in-person meetings, I am grateful to peer scientists—particularly Dr. Katrin Mayer-Barber and Dr. Eduardo Amaral at the NIAID—for their insightful feedback, which strengthened the rigor of our experiments and broadened the scope of this study. I also sincerely thank Dr. Liron David (Ben-Gurion University of the Negev) and Dr. Clare Bryant (University of Cambridge) for generously sharing valuable experimental materials.

I am profoundly grateful to my parents and grandparents for their unwavering support during the seven years I spent abroad. While distance often prevented me from being present, they carried both their responsibilities and challenges with remarkable strength, always choosing resilience so that I could focus on my work and so that we could look forward to a better reunion. Their patience, courage, and devotion sustained me more than they know, and words cannot fully express my gratitude for everything they have endured and given.

Finally, I would like to thank my friends, roommates, and the many individuals I encountered on campus, in my neighborhood, and throughout daily life at UMD. Together, they shaped some of the most meaningful and cherished memories of my graduate studies. Although many more names could be included, I will conclude here with sincere appreciation for all who made this journey possible.

Statement on the Use of Artificial Intelligence (AI) Tools

During the preparation of this dissertation, large language models (LLMs), including ChatGPT 5.2, Gemini 3, and their older versions, were used to improve clarity, grammar, and organization of the text, and to assist with formatting and revision of figure legends. All scientific ideas, experimental design, data analysis, interpretation, and conclusions were developed by me in collaboration with colleagues and do not originate from AI-assisted tools. I reviewed, verified, and edited all AI-assisted content to ensure accuracy and originality. AI tools were not used to generate experimental data, analyze raw data, or make scientific decisions.

Table of Contents

Acknowledgements ..... **ii**
Statement on the Use of Artificial Intelligence (AI) Tools ..... **iv**
Table of Contents ..... **v**
List of Figures ..... **viii**
List of Abbreviations ..... **ix**
Chapter 1: Introduction **1**
1.1 Tuberculosis (TB) pathology 1
1.1.1 General introduction of TB 1
1.1.2 Early infection 1
1.1.3 Host cells involved in subsequent Mtb infection 2
1.1.4 Granuloma formation 5
1.1.5 Symptoms and transmission of TB 7
1.2 Epidemiology of TB 9
1.3 Immunoprophylaxis and treatment of TB 10
1.3.1 Bacillus Calmette-Guérin (BCG) vaccine 10
1.3.2 Treatment of TB 12
1.4 Mtb biology 12
1.4.1 General biology of Mtb 12
1.4.2 Mtb membrane structure 13
1.4.3 Mtb virulence factors 15
1.5 General defense mechanisms of host macrophages against Mtb invasion 16
1.5.1 Intracellular defense mechanisms 16
1.5.2 Cytokine-mediated defense responses of macrophages 19
1.6 The roles of IFN-β in macrophage-Mtb interactions 20
1.7 General programmed cell death pathways related to Mtb infection 22
1.7.1 Apoptosis 22
1.7.2 Pyroptosis 25
1.7.3 Necroptosis 28
1.7.4 Ferropotosis 33
1.8 Manipulation of host cell death pathways in infected macrophages by Mtb 36
1.8.1 Mtb and apoptosis 36
1.8.2 Mtb and pyroptosis 40
1.8.3 Mtb and necroptosis 43
1.8.4 Induction of ferroptosis by Mtb 45
1.8.5 Induction of other programmed necrosis by Mtb 46
1.9 Importance of cell death pathways for Mtb virulence in vivo 48
1.10 Targeting cell death pathways for host-directed therapy (HDT) 49
1.11 Summary 50
Chapter 2: Assessment of the role Type I IFN plays in cell death induced by Mtb H37Rv in THP-1 cells **52**
2.1 Abstract 52
2.2 Materials and Methods 52

2.3 Results 55
2.3.1 Kinetics of cell death induced by Mtb H37Rv in THP-1 cells and hMDMs 55
2.4 Discussion 62
Chapter 3: Analysis of apoptosis induction after Mtb infection 63
3.1 Abstract 63
3.2 Materials and Methods 63
3.3 Data availability (applied throughout this dissertation) 65
3.4 Results 65
3.3.1 Analysis of apoptosis induction in THP-1 cells and hMDMs during the first three days of Mtb infection 65
3.5 Discussion 75
Chapter 4: Analysis of pyroptosis and necroptosis after Mtb infection 76
4.1 Abstract 76
4.2 Materials and Methods 77
4.3 Results 77
4.3.1 Analysis of pyroptosis induction in THP-1 cells and hMDMs during Mtb infection . 77
4.3.2 Analysis of necroptosis induction in THP-1 cells and hMDMs during Mtb infection 83
4.4 Discussion 86
Chapter 5: Analysis of GPX-4-regulated ferroptosis after Mtb infection 88
5.1 Abstract 88
5.2 Materials and Methods 88
5.3 Results 89
5.3.1 Analysis of the involvement of GPX-4 regulated ferroptosis in THP-1 cells and hMDMs during Mtb infection 89
5.4 Discussion 95
Chapter 6: Analysis of Lysosomal Membrane Permeabilization during Mtb Infection in THP-1 Cells 96
6.1 Abstract 96
6.2 Materials and Methods 97
6.3 Results 98
6.3.1 Analysis of LMP induction in THP-1 cells 2 hours prior to cell death 98
6.4 Discussion 103
Chapter 7: Analysis of DNA-Release-Associated Necrosis (DRAN) in THP-1 Cells and hMDMs During Mtb Infection 104
7.1 Abstract 104
7.2 Materials and Methods 106
7.3 Results 109
7.3.1 Frequency and kinetics of DNA release induced by Mtb H37Rv in THP-1 cells and hMDMs 109
7.3.2 Characterization of the molecular composition and biological relevance of eDNA released by Mtb-infected THP-1 cells 114
7.3.3 Assessment of whether pyroptosis induction is required for eDNA release 121
7.4 Discussion 129
Chapter 8: Comprehensive Discussion 130
8.1 Conclusions 130
8.2 Novelty 132

8.3 Limitations 133
8.4 Biological significance 136
8.5 Future directions 138
Appendices 141
Bibliography 146

This Table of Contents is automatically generated by MS Word, linked to the Heading formats used within the Chapter text.

List of Figures

Fig. 1: Extrinsic and intrinsic apoptosis pathways and their link to secondary necrosis. 23
Fig. 2: Canonical and non-canonical pyroptosis pathways. 26
Fig. 3: Receptor-dependent and -independent necroptosis pathways. 29
Fig. 4: The ferroptosis signaling pathway. 34
Fig. 5: Kinetics of Mtb-mediated cell death induction. 57
Fig. 6: Optimization of the Interferon-alpha/beta receptor (IFNAR) neutralizing assay. 60
Fig. 7: Evaluation of the involvement of IFN-β in Mtb-induced cell death. 61
Fig. 8: Validation of YO-PRO-1 and Draq7 staining in distinct cell death modalities. 67
Fig. 9: Assessing early apoptosis by YO-PRO-1 and Draq7 staining in Mtb-infected THP-1 cells. 69
Fig. 10: Mtb H37Rv induces marginal CASP3 activation in THP-1 cells but not in hMDMs. 72
Fig. 11: Mtb H37Rv does not induce CASP8 or 9 activation in THP-1 cells. 74
Fig. 12: H37Rv Mtb induces GSDMD cleavage in THP-1 cells but not in hMDMs. 80
Fig. 13: Mycobacterial species induce variable GSDMD cleavage, and different cell types have distinct sensitivity to necroptosis induction. 81
Fig. 14: H37Rv Mtb does not induce MLKL phosphorylation in THP-1 cells or hMDMs. 84
Fig. 15: Validation of anti-pMLKL antibody and quantifications supplement previous WB analysis. 85
Fig. 16: Mtb does not induce GPX4-regulated ferroptosis in THP-1 cells or hMDMs at the examined time points. 93
Fig. 17: Nested plot showing normalized Liperfluo fluorescence intensities in THP-1 cells. 94
Fig. 18: Mtb does not induce detectable LMP in THP-1 cells 2 hours prior to cell death. 100
Fig. 19: Single-cell analysis of lysosomal membrane integrity in THP-1 cells during Mtb infection. 102
Fig. 20: Mtb induces DNA release in THP-1 cells and hMDMs during the infection. 111
Fig. 21: Zoomed-in images illustrating the structures of released or expelled DNA. 112
Fig. 22: Markers of NETosis are detected on the extracellular DNA released by Mtb-infected THP-1 cells. 116
Fig. 23: Isotype control stainings for anti-MPO and anti-CitH3 antibodies. 118
Fig. 24: Assessment of the effect of eDNA on host THP-1 cells and Mtb bacilli 119
Fig. 25: GSDMD does not promote DNA release. 122
Fig. 26: CASP4 or 5 does not promote DNA release. 125
Fig. 27: NINJ1 promotes cell lysis of Mtb-infected THP-1 cells but is not required for DNA release. 128

List of Abbreviations

AI – artificial intelligence

AK – adenylate kinase

AM – alveolar macrophage

AMP – antimicrobial peptide

ASC – Apoptosis-associated speck-like protein containing a CARD

BCG – Bacillus Calmette-Guérin

BMDC – bone marrow-derived dendritic cell

BMDM – bone marrow-derived macrophage

BI – band intensity

Casp/CASP – caspase (murine/human)

Cat – cathepsin

Cat. No. – Catalog number

CDC – Centers for Disease Control and Prevention

$cFLIP_S$ – cellular FLICE-like inhibitory protein short form

CFU – colony-forming unit

cIAP – cellular Inhibitor of Apoptosis Protein

Conc. – concentration

CT – carboxyl-terminus

CYLD – cylindromatosis lysine 63 deubiquitinase

CYPD – cyclophilin D

cyt *c* – cytochrome *c*

DAPI – 4′,6-diamidino-2-phenylindole

DAT – di-and poly-acyltrehaloses

DC – dendritic cell

DD – death domain

DIABLO – direct IAP-binding protein with low pI

DIS – disulfiram

DISC – death-inducing signaling complex

DMSO – dimethyl sulfoxide

DNA – deoxyribonucleic acid

DPBS – Dulbecco's Phosphate-Buffered Saline

DR – drug-resistant

DRAN – DNA release-associated necrosis

eDNA – extracellular DNA

ETC – electron transport chain

EM – electron microscopy

ESX-1 – ESAT-6 secretion system-1

EsxA – Type VII secretion system extracellular protein A

FADD – Fas-associated death domain protein

Fer-1 – ferrostatin-1

FLICE – FADD-like IL-1β-converting enzyme

$FLIP_L$ – FADD-like IL-1β-converting enzyme-inhibitory protein long form

FoV – field of view

Fig. – Figure

Glu – glutamine

GoF – gain of function

GPX4 – glutathione peroxidase 4

GSDMD/E – gasdermin D/E

GSH – glutathione

GSR – glutathione-disulfide reductase

GSSG – glutathione disulfide

hAM – human alveolar macrophage

HBHA – heparin-binding hemagglutinin

HDT – host-directed therapy

hMDM – human monocyte-derived macrophage

HO• – hydroxyl radical

HOO• – hydroperoxyl radical

H_2O_2 – hydrogen peroxide

IM – interstitial macrophage

IAP – Inhibitor of Apoptosis protein

IFN – Interferon

IFNAR – Interferon-alpha and beta receptor

IL-1β – Interleukin-1 beta

IL-1R – Interleukin-1 receptor

KatG – catalase-peroxidase

KO – knock out

LAM – lipoarabinomannan

LDH – lactate dehydrogenase

LF – liperfluo

LLM – large language model

LM – lipomannan

LMP – lysosomal membrane permeabilization

LPS – lipopolysaccharide

LTB – latent TB

LV – Lysoview

LXA_4 – lipoxin A4

ManLAM – mannose-capped lipoarabinomannan

Mbo – *Mycobacterium bovis*

MCE – mammalian cell entry protein

MDM – monocyte-derived macrophages

MDR – multidrug-resistant

METosis – macrophage extracellular-trap formation/cell death

Mka – *Mycobacterium Kansasii*

MLKL – mixed lineage kinase domain-like pseudokinase

Mm – *Mycobacterium marinum*

MOI:x – multiplicity of infection of x

MOMP – mitochondrial outer membrane permeabilization

MPT – mitochondrial permeability transition

MPTP – mitochondrial permeability transition pore

mROS – mitochondrial reactive oxygen species

MS – mass spectrometry

Msm – *Mycobacterium smegmatis*

Mtb – *Mycobacterium tuberculosis*

MTBC – *Mycobacterium tuberculosis* complex

NAD^+ – nicotinamide adenine dinucleotide

NADPH – nicotinamide adenine dinucleotide phosphate

NIG – nigericin

NINJ1 – ninjurin-1

NK – natural killer

$NO^{\cdot}$ – nitric oxide radicals

NOX – NADPH Oxidase 2

NT – Amino-terminus

NETosis – neutrophil extracellular-trap formation/cell death

ONOO- – peroxynitrite

$O_2^{\cdot -}$ – superoxide

PAD4 – peptidyl arginine deiminase Type IV

PBMC – peripheral blood mononuclear cell

PBS – phosphate-buffered saline

PCD – programmed cell death

pDC – plasmacytoid dendritic cell

PDIM – phthiocerol pimycocerosate

PFA – paraformaldehyde

PGE_2 – prostaglandin E2

PHB2 – prohibitin 2

PIM – phosphatidylinositol mannoside

pknF – serine/threonine-protein kinase F

PMA – phorbol 12-myristate 13-acetate

PMR – plasma membrane rupture

PS – 1,2-diacyl-sn-glycero-3-phospho-L-serine/phosphatidylserine

PtpB – protein tyrosine phosphatase B

PUFA – poly-unsaturated fatty acid

RAP – raptinal

RawIntDen – raw integrated density

RIPK3 – receptor-interacting serine/threonine-protein kinase 3

RNS – reactive nitrogen species

RT – room temperature

ROI – region of interest

ROS – reactive oxygen species

RR – rifampicin-resistant

SARM1 – sterile alpha and TIR Motif containing 1.

SD – standard deviation

SL-1 – sulfolipid-1

SodA – superoxide dismutase

STS – Staurosporine

Syt G – Sytox Green

SV – supplementary video

TB – tuberculosis

tBid – truncated Bid

TCA – Tricarboxylic Acid Cycle

TDM – trehalose dimycolate

TLR – toll-like receptor

TNF-α – tumor necrosis factor-alpha

TNT – tuberculosis necrotizing toxin

T-PMT – transmitted-light photomultiplier tube microscopy

t(protein) – total(protein)

TRADD – Tumor Necrosis Factor receptor type 1-associated DEATH domain protein

TRAF – Tumor Necrosis Factor receptor-associated factor

Ub – ubiquitin

UI – uninfected

UT – untreated

WHO – World Health Organization

w.t./WT – wild type

WB – western blot

YO – YO-PRO-1

ZBP-1 – Z-DNA binding protein 1

Chapter 1: Introduction

1.1 Tuberculosis (TB) pathology

1.1.1 General introduction of TB

Tuberculosis (TB) remains a major global health threat and is one of the most fatal airborne infectious diseases worldwide. The disease is caused by *Mycobacterium tuberculosis* (Mtb), a member of the Mycobacteriaceae family. According to the World Health Organization (WHO), more than ten million people developed TB in 2023[1].

Mtb infection primarily involves the lungs, where it can give rise to active pulmonary TB. Classic symptoms include persistent cough, fever, and night sweats[2]. Although the lungs are the principal site of infection, TB is not restricted to the respiratory system. Mtb can disseminate to extrapulmonary sites such as the lymph nodes, bones, kidneys, and brain, resulting in a broad spectrum of clinical manifestations[2,3].

A key distinction in TB pathophysiology lies between active TB and latent TB. Individuals with active TB are symptomatic and capable of transmitting the bacterium to others. In contrast, individuals with latent TB harbor Mtb without clinical symptoms and are not infectious[2–4]. Despite the absence of symptoms, latent infection carries a lifelong risk of reactivation into active TB, especially in hosts with a compromised immune system[2–4].

1.1.2 Early infection

Mtb infection begins when aerosolized droplets containing Mtb are inhaled and enter the host respiratory tract[5,6]. Although bacilli may contact the nasal or bronchial mucosa, successful

infection typically requires the pathogen to reach the alveolar spaces of the lungs. Alveoli are specialized structures responsible for gas exchange and act as an immunological interface that detects, contains, and eliminates airborne pathogens.

Upon reaching the alveoli, Mtb encounters alveolar macrophages (AMs) and interstitial dendritic cells, which phagocytose the bacteria and serve as the initial cellular niche for infection[7]. A few Mtb bacilli are sufficient to establish a robust infection in the host, as demonstrated in multiple mammalian models[8–11]. Mtb can resist intracellular killing and begin to replicate. Once the bacterial load in a macrophage surpasses a threshold, estimated to be roughly >20 bacilli per cell[12], Mtb can induce necrotic cell death, releasing bacilli that infect neighboring cells and expand the initial infection foci.

During early infection, innate immune responses are initiated by alveolar macrophages and interstitial dendritic cells, leading to cytokine secretion and the recruitment of additional immune cells[7,13]. However, these early defenses are often insufficient to eliminate the pathogen. Mtb can also infect alveolar epithelial cells, potentially facilitating its traversal across the epithelial barrier and contributing to dissemination[14,15]. Infected macrophages are capable of migrating from the alveolar space into the lung interstitium and draining lymph nodes, where the bacteria can further disseminate and establish systemic infection[7,13,16,17].

1.1.3 Host cells involved in subsequent Mtb infection

After alveolar macrophages (AMs) migrate into the interstitium, Mtb disseminates from dead, infected AMs, and the resulting inflammatory response recruits additional immune cell populations to the infection site. At this stage, professional phagocytes, including macrophages, dendritic cells (DCs), and neutrophils, serve as the first responders to Mtb infection[18,19].

Interstitial macrophages (IMs) are tissue-resident macrophages that primarily originate from the bone marrow but can also be replenished by monocyte-derived macrophages (MDMs)[20]. These macrophages are highly heterogeneous and exhibit distinct immune responses depending on the specific stimuli and infection context[18,19]. In tuberculosis, IMs polarize into different functional subtypes in response to local signals. Classically activated M1 macrophages are pro-inflammatory and contribute to bacterial clearance or containment[19]. In contrast, M2 macrophages exert immunoregulatory functions; several M2 subsets are even immunosuppressive, facilitating the downregulation of host inflammatory responses and promoting intracellular Mtb survival[19].

Neutrophils constitute a large proportion of immune cells infiltrating the infection site. They can suppress Mtb infection through physical confinement of the bacilli and bactericidal mechanisms[21]. For instance, neutrophils generate reactive oxygen species (ROS) and antimicrobial peptides (AMPs) to kill Mtb. They also undergo neutrophil extracellular trap cell death (NETosis), releasing extracellular traps that entangle and restrict Mtb motility[21,22]. However, recent studies indicate that NETosis alone is insufficient to eliminate trapped Mtb and may even exacerbate tuberculosis progression[23]. Additionally, phagocytosis of neutrophil debris by other cells can promote intracellular Mtb growth. Neutrophils engage in extensive crosstalk with DCs, macrophages, B cells, and T cells, shaping the local inflammatory milieu. Overall, neutrophils are now regarded as a permissive niche that can facilitate Mtb replication and dissemination[21].

Dendritic cells phagocytose disseminated Mtb or Mtb-containing cell debris to initiate its maturation and migration[18,24,25]. A key function of DCs during Mtb infection is the presentation of Mtb antigens to $CD4^+$ T cells, thereby facilitating the development of effective adaptive immunity[18,24,25]. DCs interact dynamically with multiple immune cell types, substantially influencing the host response to Mtb[24]. Nevertheless, Mtb has evolved mechanisms to inhibit DC

maturation and migration to regional lymph nodes, impairing antigen presentation and dampening adaptive immune activation[25].

B cells and T cells are lymphocytes essential for adaptive immunity. In tuberculosis, B-cell-mediated humoral immunity plays an important role in host defense against Mtb. As reviewed by Stewart et al., studies using B-cell-deficient mouse models demonstrate an impaired immune response during Mtb infection[26]. Upon infection, B cells can differentiate into plasma cells and secrete antibodies targeting Mtb components[26]. Canonical mechanisms by which antibodies enhance host defense include opsonization, complement activation, and antibody-mediated phagocytosis of Mtb[27–29]. In addition, B cells interact with other immune cells to modulate their antimicrobial activity[27]. For example, B1 cells can polarize macrophages into an M2 phenotype during Mtb infection[27,30]. B cells also produce antibodies that influence the Th1 response. Finally, B cells regulate neutrophilia. Under experimental conditions, B-cell deficiency leads to increased neutrophil recruitment and mobility in Mtb-infected mice[27].

$CD4^+$ T cells comprise multiple subsets with distinct functions during anti-Mtb immunity. Th1 cells promote a pro-inflammatory response and activate and recruit macrophages to sites of infection[22]. In contrast, Th2 cells are immunoregulatory and may attenuate excessive inflammation[22]. Th17 cells contribute to neutrophilic tissue inflammation, which can lead to tissue damage. Interleukin (IL)-17, secreted by Th17 cells, also recruits interferon (IFN)-γ–producing $CD4^+$ T cells to infected tissues[22].

$CD8^+$ T cells contribute to anti-Mtb immunity by secreting perforin, granzymes, and granulysin to directly kill Mtb-infected host cells. They also produce pro-inflammatory cytokines, such as tumor necrosis factor (TNF)-α and IFN-γ, to modulate the local immune response[18,22].

However, due to discrepancies among published studies, the extent to which $CD8^+$ T cells are required to control TB progression remains controversial[18].

Other immune cell types also play important roles in host defense against Mtb infection. Their functions, however, are beyond the scope of this research. Because the host immune response elicited by TB is a broad and complex topic, it cannot be comprehensively reviewed in this dissertation. For further reading, two relevant review articles are recommended[18,22].

1.1.4 Granuloma formation

Granuloma formation is a key immunological hallmark of TB pathogenesis. A granuloma is a distinct histopathological structure composed of aggregated macrophages and various immune cell populations that organize in response to persistent Mtb infection[31–35]. Traditionally, granulomas were regarded as protective host structures that restrict Mtb replication and dissemination; however, accumulating evidence indicates that granulomas can also provide a permissive niche that supports mycobacterial survival and spread[31].

Granuloma formation begins when AMs become infected with Mtb and migrate into the lung interstitium. Infected macrophages eventually undergo cell death, releasing both viable bacilli and intracellular components that trigger the recruitment of additional macrophages and other immune cells, including neutrophils, dendritic cells, natural killer (NK) cells, B cells, and T cells etc[31,33]. Among these recruited lymphocytes, Th1 $CD4^+$ T cells play a critical role by secreting TNF-α, which amplifies immune cell recruitment and supports granuloma maintenance. TNF-α, together with IFN-γ, enhances the microbicidal activity of macrophages and sustains their antimicrobial functions[31,35]. Within the granuloma, macrophages exhibit remarkable phenotypic plasticity. They can fuse to form multinucleated giant cells or differentiate into lipid-laden foamy macrophages that often serve as reservoirs for Mtb. Some macrophages also transform into

epithelioid cells, characterized by elongated morphology and ruffled membranes that facilitate tight intercellular connections with neighboring cells[31,33]. Historically, granulomas were considered protective to the host because the spatial segregation of Mtb within these organized immune structures appeared to limit bacterial dissemination[31], while the coordinated bactericidal activities of diverse immune cells were believed to promote bacterial killing[35]. Clinical observations support this notion: immunocompromised individuals who are highly susceptible to TB often exhibit poorly formed or absent granulomas[34], highlighting the critical role of these structures in host defense against TB.

Granuloma formation represents the host's attempt to contain the infectious agent. However, granulomas paradoxically provide a replication niche for Mtb, contributing to chronic infection and dissemination[31,35]. To survive and replicate within the granuloma, Mtb exploits multiple strategies, including: (1) expressing virulence factors that induce epithelial cells to secrete MMP9, thereby recruiting uninfected macrophages to the infection foci[31]; (2) inhibiting phagosome maturation and phagolysosome fusion to evade intracellular killing[36,37]; (3) inhibiting host cell apoptosis while inducing necrosis[38]; and (4) expressing virulence factors that drive macrophage differentiation into foamy macrophages, which supply abundant fatty acids for Mtb survival and the synthesis of virulence-associated lipids[39]. Ultimately, this manipulation culminates in the development of caseous necrosis, in which the granuloma's center liquefies and ruptures, allowing Mtb to escape into the airways and infect a new host[40].

Granulomas also exhibit substantial heterogeneity during the progression of tuberculosis. The classification of granulomas has not been standardized. Here, we adopt the system proposed by Marakalala et al.[41]. Based on the number of histologically distinct regions, granulomas can be categorized as solid, caseous, or cavitary. Remarkably, heterogeneous granulomas often coexist

within the same infected individual, and their types are strongly correlated with disease outcomes[42,43]. Effective host control of Mtb typically leads to the formation of resolved granulomas, whereas extensive necrosis at the granuloma core results in a semi-liquid caseous mass devoid of nuclei or intact cellular structures. This caseous material is produced through proteolysis, and when the liquefied core erodes into the airway, it can be expelled, forming cavities enclosed by a fibrotic capsule—hallmarks of cavitary granulomas[43]. Multiple factors contribute to granuloma formation and determine its eventual fate, including bacterial heterogeneity, local immune responses, and vascularization. Notably, the degree of vascularization varies not only among granulomas but also within a single lesion. Peripheral cellular layers of a necrotic granuloma often exhibit higher vascular density than the core, leading to differences in blood flow, drug penetration, and therapeutic efficacy[43]. Both caseous and cavitary granulomas are associated with a high intracellular and extracellular burden of Mtb[43].

In summary, granuloma is an immunopathological hallmark of tuberculosis. It serves as a double-edged sword, embodying the complex and dynamic interface between host and pathogen. A deeper understanding of granuloma biology will provide crucial insights into the development of effective anti-TB therapies and preventive strategies.

1.1.5 Symptoms and transmission of TB

The major clinical manifestations of pulmonary TB include a persistent cough, fever, and night sweats, often accompanied by chest pain, fatigue, and hemoptysis. These symptoms arise as a result of the host immune response to Mtb infection and the progressive tissue damage within the lungs.

Fever is primarily triggered by a T-cell-mediated pro-inflammatory immune response that occurs during granuloma formation[44,45]. Activated Th1 cells secrete cytokines such as IFN-γ and

TNF-α, which enhance macrophage activation but also lead to systemic inflammatory responses[44,45]. As granulomas mature and undergo necrosis, damage to the bronchi and surrounding tissues facilitates the absorption of mycobacterial antigens and toxins into the bloodstream. These circulating factors stimulate the hypothalamic thermoregulatory center, resulting in an elevated set point and persistent high-grade fever in some TB patients[44,45].

The mechanisms underlying night sweats remain less well defined. One hypothesis posits that TB alters serum cortisol rhythms, a key modulator of both innate and adaptive immune responses and of body temperature regulation. Reduced cortisol levels during the night may lower the thermoregulatory threshold, leading to transient fever spikes and excessive perspiration as the body attempts to restore normothermia[44,45]. Additional factors such as cyclic cytokine release (e.g., IL-1β, IL-6) and autonomic dysregulation have also been implicated in this phenomenon[44,45].

Coughing is one of the most characteristic and consequential symptoms of pulmonary TB, playing a central role in Mtb transmission. It has been demonstrated that the Mtb-specific surface lipid sulfolipid-1 (SL-1) can induce cough in rodent models, linking bacterial components to the initiation of this symptom[46]. However, whether SL-1 exerts a similar effect in humans remains controversial[47]. Coughing facilitates the aerosolization of Mtb-containing droplets, which can remain airborne for prolonged periods and are readily inhaled by new hosts. Experimental studies using guinea pig infection models have shown that cough-generated aerosols are sufficient to initiate infection and sustain transmission cycles[48,49].

While coughing is the most efficient means of generating infectious droplet nuclei, it is not the only one. Other respiratory activities, such as sneezing, shouting, or singing, can also disperse viable Mtb bacilli into the air[48,49]. Once aerosolized, Mtb can survive for extended periods under desiccated conditions, maintaining its infectivity until inhaled by a susceptible individual. Upon

deposition in the alveoli of a new host, the bacilli are phagocytosed by alveolar macrophages, initiating a new cycle of infection and disease progression[40,49].

1.2 Epidemiology of TB

Mtb, the causative agent of TB, was responsible for an estimated 1.25 million deaths in 2023[1]. In the same year, approximately 10.8 million individuals, including 1.3 million children, developed TB[1]. These statistics highlight the resurgence of TB as a leading cause of death from infectious diseases following the COVID-19 pandemic.

Compared with previous years, the incidence of TB in 2023 increased slightly by about 0.2%, reflecting ongoing transmission despite intensified control efforts. However, the number of TB-related deaths declined, suggesting that expanded access to diagnostics, timely treatment, and recovery of health services after the pandemic contributed to improved survival rates[1]. The introduction of rapid molecular diagnostic tools, the increased deployment of shorter drug-sensitive and drug-resistant TB regimens, and strengthened case-finding strategies may also contribute to this positive trend.

Demographically, adult males accounted for the largest proportion of new TB cases, consistent with long-standing epidemiological patterns linked to higher exposure risks, occupational factors, and health-seeking behavior disparities[1]. Asia remained the epicenter of the disease, representing nearly 60% of all global cases, with India, Indonesia, China, the Philippines, and Pakistan collectively contributing the majority of the global TB burden[1].

Besides, more than 180,000 individuals developed drug-resistant TB (DR-TB) in 2023, marking an increase relative to 2022. The rise of multidrug-resistant (MDR) and rifampicin-resistant (RR) Mtb strains continues to pose a serious public health threat, particularly in regions

with limited access to second-line therapies and diagnostic infrastructure. Addressing DR-TB requires sustained investment in surveillance systems and novel therapeutic strategies[1].

Although ending the global TB epidemic remains a difficult and long-term goal, positive trends in TB mortality reduction, improved case detection, and broader access to effective treatments indicate that progress is being made. Continued political commitment, international collaboration, and research into host-directed therapies and novel vaccines will be essential to accelerate this trajectory toward TB elimination.

1.3 Immunoprophylaxis and treatment of TB

1.3.1 Bacillus Calmette-Guérin (BCG) vaccine

The BCG vaccine is the only broadly used vaccine for immunoprophylaxis of TB[50]. It contains an attenuated strain of *Mycobacterium bovis* (Mbo), a member of the *Mycobacterium tuberculosis* complex (MTBC) that is genetically closely related to Mtb. The vaccine was developed by Albert Calmette and Camille Guérin through continuous passaging of Mbo for 13 years[51]. Compared with its parental Mbo strain and the virulent Mtb strains, Mbo BCG lacks the RD1 genomic region, which encodes the ESAT-6 secretion system. The absence of ESAT-6, a critical virulence factor responsible for phagosomal rupture and necrosis induction in host cells, contributes to the attenuation of BCG[52].

The protective efficacy of the BCG vaccine is most evident in infants and young children, in whom it prevents severe and disseminated forms of TB, such as tuberculous meningitis[51]. This protection is primarily mediated through the activation of Mbo-specific $CD4^+$ T cells that provide cross-protective immunity against Mtb[50]. Additionally, infection with BCG has been shown to polarize macrophages toward a pro-inflammatory M1 phenotype, which may further limit the

intracellular replication of Mtb[50]. In contrast, in adults and elderly individuals, the vaccine provides variable and generally limited protection against pulmonary TB[53]. Importantly, BCG is not a single homogeneous strain. Since its global distribution, different BCG substrains have diverged genetically due to continuous *in vitro* passaging. Variations in genomic composition, vaccine production, and storage practices across regions, as well as host physiological factors, all contribute to the observed heterogeneity in vaccine efficacy[50]. Despite this variability, the BCG vaccine has an excellent safety record. The most common adverse reaction is regional suppurative lymphadenitis, whereas systemic BCG infection occurs rarely and almost exclusively in immunocompromised individuals[50].

The inconsistent efficacy of the BCG vaccine remains one of its major limitations. Multiple studies, particularly those that include tropical participants, suggest that frequent exposure to environmental mycobacteria enhances host antimycobacterial immunity, which can mask the immunizing effect of BCG[51]. Some clinical observations also indicate that a stronger tuberculin skin reaction is associated with an increased risk of developing active TB, possibly because an exaggerated antimycobacterial immune response promotes the transition from latent TB (LTB) to active TB[51]. Another proposed mechanism is that pre-existing immunity against environmental mycobacteria restricts BCG replication following vaccination, thereby diminishing its protective effect[51]. Furthermore, comparative studies between developed and developing countries have shown that environmental exposure to diverse microorganisms in developing regions induces a Th2-skewed immune response, which may further compromise the efficacy of BCG. Interestingly, such a Th2 response was not observed in the high-altitude country included in the study[53].

The limitations of BCG efficacy underscore the urgent need for next-generation anti-TB vaccines. Numerous novel vaccine concepts and candidates have been developed, with several

currently in clinical trials. These emerging vaccine candidates are discussed in detail in the referenced literature, which is recommended for further reading[53].

1.3.2 Treatment of TB

According to the guidelines proposed by the U.S. Centers for Disease Control and Prevention (CDC) in collaboration with other public health institutions, the most recent recommendations permit a shortened regimen for drug-sensitive pulmonary tuberculosis in adults, reducing the standard 6-month treatment to a 4-month course under specific conditions. In adults aged 12 years and older with pulmonary TB caused by organisms susceptible to isoniazid and rifampin, the 4-month regimen of isoniazid, rifapentine, pyrazinamide, and moxifloxacin (given as 2 months of isoniazid + rifapentine + pyrazinamide + moxifloxacin, followed by 2 months of isoniazid + rifapentine + moxifloxacin) is conditionally recommended[54].

For rifampin-resistant or multidrug-resistant TB (in people age 14 years and older), the guidelines now strongly recommend 6-month regimens using bedaquiline, pretomanid, and linezolid (with or without moxifloxacin) under certain criteria rather than the older 15-month or longer regimens[54].

1.4 Mtb biology

1.4.1 General biology of Mtb

Mtb belongs to the Mycobacteriaceae family, and its obligate host is the human being[55]. It forms the MTBC together with ten other mycobacterial species capable of causing tuberculosis in humans or other animals. These species share more than 99% genetic identity, and since 2018, all members of the MTBC have been regarded as synonyms of Mtb[56].

Genetically, the Mtb H37Rv strain was the first to be fully sequenced[55]. The genome is approximately 4.4 megabases in size and encodes over 4,000 genes. Comparative genomic analyses further reveal that the lack of horizontal gene transfer during Mtb evolution renders it a monomorphic species within the Mycobacteriaceae family[55]. Evidence suggests that the earliest infection of humans by Mtb dates back to around 70,000 years ago[57]. Over millennia, Mtb and its human hosts have co-evolved, leading to mutual adaptations—such as human genetic variants associated with TB susceptibility or resistance, and the phylogeographical diversification of Mtb lineages[57].

Physiologically, Mtb is a Gram-positive, acid-fast, and G + C-rich bacterium[58]. As a slow-growing mycobacterium, Mtb typically forms visible colonies on solid medium within 10–28 days, whereas *in vivo* studies in murine models have estimated its doubling time to range between 18 and 54 hours[58].

1.4.2 Mtb membrane structure

Mtb bacilli contain cytosol surrounded by a complex cell envelope that encases and protects the intracellular components. This envelope is central to bacterial physiology: it contributes to cell division, motility, molecular transport, environmental resilience, and host–pathogen interactions[59]. Electron microscopy reveals that the mycobacterial envelope is structurally atypical compared with canonical Gram-positive and Gram-negative bacteria[60].

Structurally, the Mtb cell envelope comprises four major layers. Closest to the interior is the plasma membrane, followed by the cell wall, which consists of an inner peptidoglycan layer and an outer arabinogalactan layer. Covalently attached to arabinogalactan via mycolic acids is the mycomembrane (also referred to as the outer membrane). The outermost layer is the capsule, which

is rich in neutral polysaccharides and only weakly associated with the mycomembrane. It can be readily shed into the extracellular milieu[60].

Although the mycobacterial envelope shares certain features with both Gram-positive and Gram-negative bacteria, such as a thick cell wall reminiscent of Gram-positive species and the presence of an outer membrane similar to Gram-negative species[61]. Its overall architecture is unique. The mycomembrane forms a highly hydrophobic, waxy permeability barrier that restricts the passage of large or hydrophilic molecules[61]. Mtb belongs phylogenetically to the Gram-positive phylum Actinobacteria, yet it does not reliably retain the Gram stain. Its distinct mycomembrane and lipid-rich envelope confer the characteristic acid-fast property, enabling retention of dyes during Ziehl-Neelsen (acid-fast) staining and resistance to decolorization. Thus, acid-fast staining has become the most widely used method for identifying mycobacteria.

The plasma membrane contains phospholipids and numerous proteins, including members of the MmpL family, which mediate lipid transport to the outer membrane and contribute to membrane assembly[59]. The mycomembrane also includes virulence-associated proteins. For example, mammalian cell entry (MCE) proteins facilitate bacterial uptake and modulate host immune responses[60]. Components of the capsule further shape host–pathogen interactions by influencing phagocytic uptake and inhibiting phagosome–lysosome fusion. Following entry into host cells, Mtb releases a wide array of protein and lipid virulence factors that remodel host immunity at both the cellular and tissue levels. Moreover, the capsule's polysaccharide diversity expands Mtb antigenicity, complicating clinical diagnosis and treatment[62].

A detailed understanding of the Mtb cell envelope is crucial for developing vaccines and therapeutics. Several frontline anti-TB drugs, including isoniazid and ethambutol, target key steps

in mycomembrane biosynthesis. In the face of rising MDR-Mtb prevalence, novel regimens aimed at disrupting envelope biology present a promising therapeutic direction[61].

1.4.3 Mtb virulence factors

As a highly successful human-adapted pathogen, Mtb has evolved a broad repertoire of virulence factors that modulate diverse host cell activities, including phagosomal function, cell death pathways, cytokine signaling, xenophagy, and reactive oxygen species (ROS) production[63].

Among these virulence factors, ESX-1 is one of the most critical. ESX-1 is a type VII secretion system, also known as the ESAT-6 secretion system-1, encoded by the RD1 locus—a region deleted in the attenuated M. *bovis* BCG strain. ESX-1 exports ESAT-6 (EsxA) and EsxB as a 1:1 heterodimer[63]. EsxA binds to host membranes and induces membrane rupture, a function essential for phagosomal escape and the initiation of host cell death[63].

In addition to ESX-1, numerous other protein virulence factors in Mtb modulate host cell death pathways, phagosomal biology, cytokine responses, and cellular metabolism. Functions specifically relevant to cell death modalities will be introduced in the corresponding section below. Several comprehensive reviews are recommended here for further reading[7,63,64].

Mtb lipids also function as potent virulence factors. Phosphatidylinositol mannosides (PIM), lipomannan (LM), and lipoarabinomannan (LAM) are derived from phosphatidylinositol and activate TLR2 signaling[63]. Mannose-capped LAM (ManLAM) binds to DC-SIGN and Dectin-2 to further modulate immune responses, while both PIM and LAM inhibit phagosomal maturation[63].

Trehalose-based lipids, including trehalose dimycolate (TDM), di-and poly-acyltrehaloses (DAT/PAT), and sulfoglycolipid-1 (SL-1), also contribute to virulence by inhibiting phagosomal maturation or blocking phagolysosomal fusion[63]. TDM additionally triggers Mincle-dependent

signaling and promotes bacterial cording. SL-1 functions as a TLR2 antagonist and facilitates Mtb entry into host cells[63].

Finally, phthiocerol dimycocerosates (PDIMs) and their glycosylated derivatives, PGLs, elicit anti-inflammatory responses[63]. PDIMs also promote CR3-mediated uptake of Mtb and enhance the membrane-lytic activity of EsxA[65].

1.5 General defense mechanisms of host macrophages against Mtb invasion

1.5.1 Intracellular defense mechanisms

Phagosomal maturation is one of the earliest antimicrobial mechanisms macrophages use to eliminate Mtb. Following phagocytosis, phagosomes sequester intracellular pathogens and undergo a series of membrane fusion events that enable them to acquire enzymes necessary for pathogen degradation[66,67]. This dynamic progression is tightly regulated by Rab GTPases, which orchestrate membrane fusion, protein and lipid sorting, and the transition of the phagosome from early to late stages. During maturation, phagosomes fuse with lysosomes, acquire hydrolytic enzymes, and acidify to a pH of ~5[66]. These coordinated processes are essential for intracellular control and killing of Mtb[66].

However, Mtb has evolved multiple strategies to evade destruction within phagosomes. It disrupts both phagosome biogenesis and phagosomal maturation. Mtb LAM and the secreted phosphatase SapM inhibit the production of PI3P, a critical regulator of membrane trafficking, thereby blocking phagosome–lysosome fusion[66]. As a result, Mtb-containing vacuoles retain characteristics of early phagosomes and lack key lysosomal hydrolases such as cathepsin D (Cat D)[66]. In addition, Mtb actively prevents phagosomal acidification, maintaining a near-neutral pH that restricts the activity of hydrolytic enzymes and further enhances bacterial survival[66]. Early

inhibition of phagosomal acidification is also required for subsequent Mtb escape from host phagosomes[66].

Once Mtb exits the phagosome, xenophagy becomes another major macrophage defense mechanism. Xenophagy is a selective form of autophagy in which host cells target pathogens for degradation[66]. Intracellular Mtb can be ubiquitinated directly, or its phagosomal membrane can be tagged with ubiquitin, enabling the recruitment of autophagy adaptors and the delivery of Mtb to autophagosomes[68]. This process depends on ULK1, multiple autophagy-related proteins, selective autophagy receptors, and the formation of autophagosomes, which subsequently fuse with lysosomes to kill Mtb[68,69]. Nevertheless, Mtb has also developed mechanisms to inhibit xenophagy. For example, recent evidence shows that Mtb PDIM can suppress autophagy in experimental mouse models[70]. Other inhibitory mechanisms are beyond the scope of this dissertation and will not be discussed further.

Reactive oxygen species (ROS) and reactive nitrogen species (RNS) constitute two major classes of antimicrobial effectors utilized by macrophages to eliminate intracellular Mtb[69,71,72]. Upon pathogen recognition, macrophages initiate a respiratory burst. While mitochondrial reverse electron transport and the tricarboxylic acid (TCA) cycle contribute to cytosolic ROS production[71], the primary oxidative response occurs at the phagosome. Following phagocytosis, the NADPH oxidase (NOX2) complex assembles on the phagosomal membrane and transfers electrons to oxygen, generating superoxide ($O_2^{\cdot -}$). This superoxide is subsequently converted into hydrogen peroxide (H_2O_2) and hydroxyl radicals ($HO\cdot$), agents capable of damaging mycobacterial DNA and the cell wall[69,71]. Beyond direct killing, ROS also modulate host immune signaling and contribute to the induction of cell death in infected macrophages[71]. In parallel, cytokine stimulation, particularly by IFN-γ, induces the expression of inducible nitric oxide synthase (iNOS)[72]. This

enzyme converts L-arginine into nitric oxide radicals (NO·). While NO· alone is often insufficient for bacterial killing in experimental settings, its rapid reaction with superoxide generates peroxynitrite (ONOO-). In murine models, peroxynitrite eliminates Mtb more efficiently than either ROS or RNS alone[72]. The role of RNS in human macrophages, however, remains distinct. While human macrophages likely utilize NO· as an antimicrobial effector *in vivo*, robust NOS2 expression is rarely observed under standard experimental conditions. Consequently, RNS-mediated killing has historically been difficult to demonstrate in *ex vivo* human macrophage models[72].

To survive this hostile environment, Mtb employs multiple evasion strategies. Metabolically, the bacterium can shift between aerobic and anaerobic states to minimize exposure to oxidative stress. Mtb also actively neutralizes threats by expressing antioxidant enzymes, such as superoxide dismutase (SodA) and catalase (KatG), which degrade host-derived superoxide and peroxides to prevent oxidative damage[71]. Furthermore, specific Mtb virulence factors interfere with host TLR signaling pathways to actively dampen the production of ROS[71].

When intracellular survival mechanisms fail, the host macrophage engages programmed cell death (PCD) as a final line of defense. Depending on the specific modality, cell death (apoptosis) can entrap Mtb bacilli and facilitate their uptake by neighboring cells via efferocytosis. Conversely, Mtb actively drives necrotic cell death, contributing to tissue necrosis and the progressive loss of lung function characteristic of tuberculosis. During infection, macrophages may undergo multiple forms of programmed necrosis, including necroptosis, pyroptosis, and ferroptosis. These modalities distinctively shape the immune landscape at the site of infection, with varying implications for host protection. The latter sections will first provide an overview of

PCD pathways relevant to Mtb infection, followed by a detailed discussion of how Mtb activates and manipulates these pathways across mouse, human, and zebrafish models.

1.5.2 Cytokine-mediated defense responses of macrophages

During Mtb infection, macrophages not only engulf bacilli and deploy intracellular antimicrobial pathways but also secrete a broad array of cytokines that shape the immune response at the infection site. Macrophages are major producers of TNF-α, interleukin (IL)-1α/β, IL-18, IL-12, and various chemokines that orchestrate cell recruitment and local immune activation[73–76]. How these cytokines contribute to host protection is discussed below.

The importance of TNF-α has been demonstrated in multiple *in vivo* models. TNF receptor-deficient mice exhibit markedly elevated mycobacterial burdens in the lungs and extrapulmonary tissues and succumb to infection within 2–3 weeks, highlighting their profound susceptibility to Mtb[76]. Disruption of TNF-α signaling also impairs granuloma formation, which is considered protective in early infection. In addition, TNF-α regulates diverse immune cell subsets and contributes to the organization of the inflammatory microenvironment. However, zebrafish studies showed that excessive TNF-α drives macrophage necrosis, promoting Mm dissemination[77]. Together, these findings underscore that TNF-α is protective within an optimal range, whereas excessive or insufficient TNF-α compromises host control.

IL-1α, IL-1β, and IL-18 belong to the IL-1 cytokine family and play distinct but complementary roles during TB. The protective function of IL-1β is supported by human genetic studies, which link IL1B variants to altered TB susceptibility, although population-specific differences complicate interpretation[73]. Murine studies further show that deficiency in IL-1β or IL-1 receptor signaling exacerbates TB pathology, while carefully timed inhibition of IL-1β can reduce late-stage immunopathology, illustrating the need for precise IL-1β regulation[73,78]. IL-1α,

although less extensively studied, is increasingly recognized as an important early alarmin in TB. Upon Mtb infection or macrophage membrane damage, IL-1α can be rapidly released to initiate inflammation. It has been implicated in driving IL-6 production, promoting neutrophil recruitment, and contributing to early containment of bacilli[76]. IL-18 plays a distinct role by linking inflammasome activation to adaptive immunity. Upon Mtb-induced inflammasome signaling, IL-18 is processed and secreted, contributing to IFN-γ induction in T cells and NK cells, a key cytokine for macrophage activation[76].

Macrophages also secrete IL-12, a cytokine that bridges innate and adaptive immunity. Human genetic studies have demonstrated that individuals with IL-12p40 deficiency exhibit a marked susceptibility to Mtb infection, underscoring its essential role in host defense[76]. Consistent with these observations, *in vivo* murine studies showed that local delivery of IL-12 to the infection site reduces bacterial burden, whereas IL-12 depletion increases bacterial growth during infection[76]. IL-12p40 deficiency also results in compromised antigen-specific IFN-γ production, which is attributed to impaired recruitment and activation of IFN-γ–producing memory T cells[76]. In the absence of sufficient IFN-γ, macrophage activation is weakened and deviates toward less protective states. Collectively, these findings highlight the critical protective role of macrophage-derived IL-12 in orchestrating IFN-γ–dependent immunity and controlling Mtb infection.

1.6 The roles of IFN-β in macrophage-Mtb interactions

IFN-β, a member of the Type I IFN family, has long been recognized for its antiviral functions. Canonical IFN-β signaling begins with its binding to the two subunits of the IFN-α receptor, IFNAR1 and IFNAR2[79]. Engagement of IFNARs triggers the phosphorylation and activation of JAK/STAT molecules, including STAT1, STAT2, and STAT3. These STAT proteins subsequently form homo- or heterodimers that drive the expression of IFN-stimulated genes

(ISGs)[80]. In total, Type I IFNs regulate an estimated 300–500 genes, and activation of IFNAR signaling by IFN-β leads to extensive reprogramming of the host transcriptome.

It is increasingly appreciated that IFN-β also plays a critical role in the host response to Mtb infection[81]. During Mtb infection, human and mouse macrophages and myeloid dendritic cells are the major producers that express IFN-β, which is driven by the cGAS-STING pathways[81]. In *in vivo* mouse models, IMs and plasmacytoid dendritic cells (pDCs) have been identified as the major IFN-β-responsive populations[82]. How IFN-β affects the host is context-dependent, determined not only by the virulence and genetic background of Mtb but also by the host's immune competence. Pioneering studies demonstrated that mice deficient in IFNAR signaling exhibit lower bacterial burdens and improved survival following Mtb infection[81]. Subsequent mechanistic research suggested several aspects in which IFN-β may impair host resistance. For example, Type I IFNs can suppress IL-1α and IL-1β production, reduce prostaglandin E_2 (PGE_2) synthesis, and promote IL-10 expression[83]. It shifts macrophages toward a less protective state. Type I IFNs have also been shown to inhibit the recruitment or activation of IFN-γ-producing lymphocytes, thereby weakening classical macrophage activation[84]. Together, these studies support the idea that IFN-β, or Type I IFNs more broadly, can subvert host resistance to Mtb infection, particularly in otherwise resistant hosts[81].

In many circumstances, IFN-β increases macrophage susceptibility to Mtb infection. Which specific cell death pathway is activated by IFN-β during Mtb infection remains an unanswered question. Addressing this knowledge gap may clarify how the *in vivo* IFN-β response translates into the regulation of cell fate at the single-macrophage level. Currently, the published data on this topic are limited.

One study performed a genome-wide CRISPR-Cas9 screen in Mtb-infected RAW 264.7 murine macrophages[85]. The researchers identified components of the IFN-β signaling pathway as key regulators of cell death. However, inhibitor analyses in the same study showed that many established pathways—including apoptosis, necroptosis, ferroptosis, pyroptosis, parthanatos, and autophagic cell death—were not induced under the experimental conditions[85]. Another study reported that Type I IFN decreases macrophage energy metabolism during mycobacterial infection, leading to dissipation of the mitochondrial membrane potential[86]. This finding may explain how IFN-β potentiates macrophage cell death during Mtb infection and suggests that IFN-β could be linked to a previously uncharacterized metabolic form of cell death. Nevertheless, a subsequent publication from the same group demonstrated that exogenous Type I IFN exacerbates Mtb-induced cell death in hMDMs, yet hMDMs themselves do not secrete detectable IFN-β during Mtb infection[87]. Moreover, an IFNAR-neutralizing antibody does not block Mtb-induced cell death in infected hMDMs. Together, these observations complicate the proposed association between IFN-β and *ex vivo* Mtb-induced macrophage death[87].

To date, no defined cell death pathway has been shown to mediate IFN-β-related Mtb-induced macrophage death.

1.7 General programmed cell death pathways related to Mtb infection

1.7.1 Apoptosis

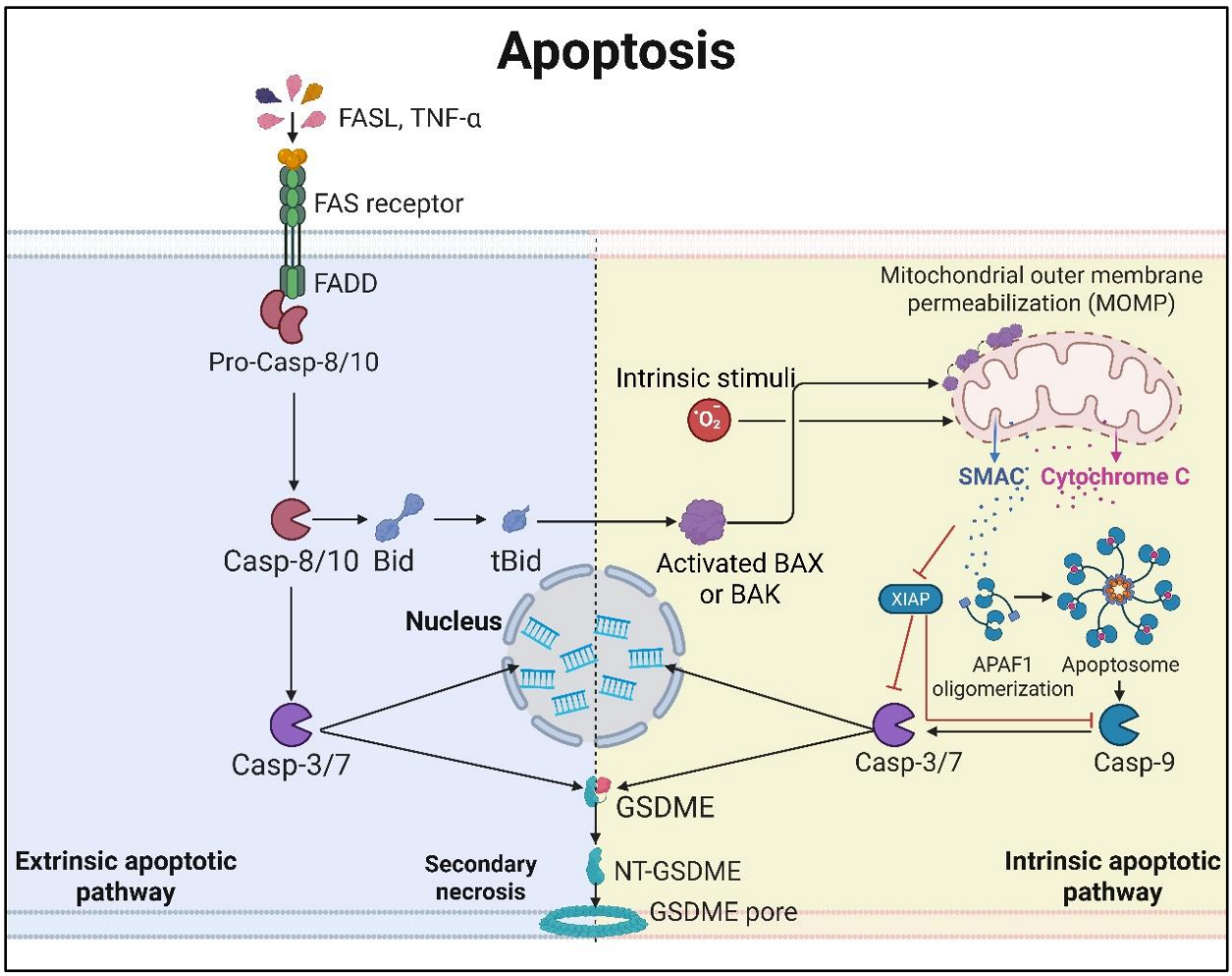

Fig. 1: Extrinsic and intrinsic apoptosis pathways and their link to secondary necrosis. Host cell apoptosis proceeds through two interconnected pathways. In the extrinsic pathway, extracellular death ligands, such as FASL or TNF-α, engage death receptors (e.g., FAS, TNFR), recruiting the adaptor proteins, e.g., FADD. FADD associates with pro-Casp-8/10, which are cleaved to their active forms, Casp-8/10. Active Casp-8/10 directly cleaves and activates executioner Casp-3/7, executing apoptosis. The intrinsic pathway regulation hub is the mitochondria. Intrinsic stimuli such as high reactive oxygen species ($^{\cdot}O_2^-$) exert stress on mitochondrial membranes, activating the pro-apoptotic BAX/BAK complex and inducing mitochondrial outer membrane permeabilization (MOMP). MOMP releases cytochrome c (cyt c) and SMAC/DIABLO. Cyt c binds APAF1 to form the apoptosome, activating Casp-9, which in turn activates Casp-3/7. SMAC antagonizes XIAP, a Casp-3/7 inhibitor, further promoting apoptosis. In crosstalk with the extrinsic pathway, activated Casp-8/10 also cleaves Bid to generate truncated Bid (tBid), which may also activate the BAX/BAK complex. If executioner caspases are activated but apoptosis remains incomplete, secondary necrosis can ensue. Casp-3/7 cleaves gasdermin E (GSDME), releasing its N-terminal fragment (NT-GSDME), which then oligomerizes and inserts into the plasma membrane to form pores, leading to membrane rupture and secondary necrosis.

Apoptosis is distinguished from necrosis by its unique morphological features[88]. The cellular changes include cytoplasmic shrinkage, nuclear fragmentation, membrane blebbing, and apoptotic body formation[88–90]. Mammalian cell apoptosis can be executed mainly via two signaling pathways: the extrinsic and intrinsic pathways (**Fig. 1**). Although initiated differently, both pathways converge on the caspase-3 (Casp-3) activation[88–91]. The extrinsic pathway is triggered when death ligands bind to their corresponding death receptors[92,93], prompting the assembly of the death-inducing signaling complex (DISC). The DISC, containing the Fas-associated death domain (FADD) and pro-Casp-8, facilitates the homodimerization and auto-cleavage of pro-Casp-8 into its active p41/p43 forms[94–96]. After further processing and dissociation from the DISC, active Casp-8 cleaves executioner caspases, such as Casp-3 and Casp-7[95]. In contrast, the intrinsic apoptosis pathway is a mitochondria-dependent process initiated by mitochondrial outer membrane permeabilization (MOMP)[89,91,97,98]. MOMP is triggered by BAX/BAK activation, or stimuli such as irradiation, toxins, or mitochondrial reactive oxygen species (mROS), and it causes the release of cytochrome c (cyt c)[97]. In the cytoplasm, cyt c and the adapter protein Apaf1 assemble to form the apoptosome. This complex serves as a scaffold for the recruitment of the initiator caspase, pro-Casp-9. Although the precise mechanism by which Apaf1 activates caspase-9 is debated, the dimerization of pro-Casp-9 on the apoptosome is a critical step that promotes the auto-cleavage of Casp-9[99,100]. The activated Casp-9 proceeds to cleave and activate executioner pro-Casp-3/7[88,90,97,101]. Activated executioner caspases, in turn, cleave crucial cellular substrates such as α-fodrin, gelsolin, and PARP, which drive the hallmark features of apoptosis, including cell shrinkage, membrane blebbing, and DNA fragmentation[94] (Fig. 1).

The Bcl-2 and IAP protein families are critical regulators that fine-tune apoptosis, which determines the cell fate[102–106]. The pro-apoptotic Bcl-2 family proteins BID, BAX, and BAK are

central to the crosstalk between the extrinsic and intrinsic apoptotic pathways[102,107–109]. Upon induction of extrinsic apoptosis, Casp-8 activation leads to cleavage of BID into its truncated form, tBID. This active fragment translocates to the mitochondria, where it binds to and activates BAX and BAK[109,110]. The activated BAX and BAK monomers then oligomerize, causing MOMP and initiating the intrinsic apoptosis pathways[108]. To counteract the induction of apoptosis, the IAP family protein XIAP acts as an inhibitor by directly binding to casp-3/7/9[105,111]. However, following MOMP, SMAC (also known as DIABLO) is released from the mitochondria and binds to XIAP, which displaces the bound caspases. This relieves their inhibition and allows the apoptotic signaling cascade to proceed[112] (**Fig. 1**).

During apoptosis, a cell exposes phosphatidylserine (PS) on its outer membrane leaflet, signaling phagocytes to engulf the apoptotic corpse in a process known as efferocytosis[113,114]. This process is crucial for maintaining tissue homeostasis and downregulating inflammatory immune responses[115,116]. When efferocytosis fails or is insufficient to remove apoptotic cells in a timely manner, apoptotic cells undergo secondary necrosis, a regulated process characterized by cell swelling and loss of structural integrity. Mechanistically, active Casp-3 cleaves the GSDME protein. The resulting N-terminal fragment, NT-GSDME, translocates to the cell membrane and forms pores, causing plasma membrane rupture (PMR) and the release of cytoplasmic components[117–119]. PMR also releases damage-associated molecular patterns (DAMPs), which typically elicit a pro-inflammatory response[117,120]. However, some evidence suggests that because secondary necrosis is preceded by apoptosis, it can have context-dependent immunosuppressive effects, thereby eliciting an immune response that more closely resembles apoptosis than primary necrosis[121].

1.7.2 Pyroptosis

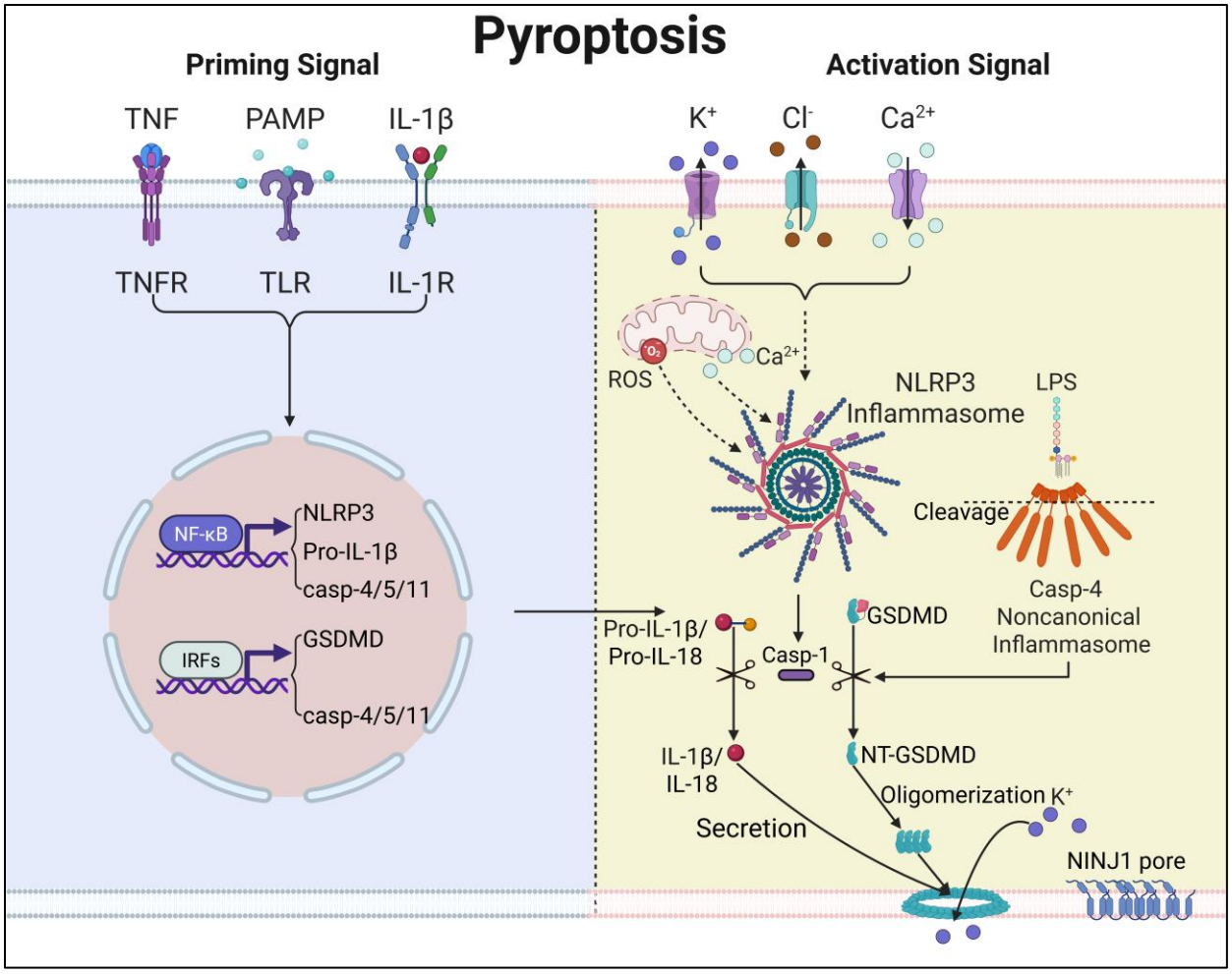

Fig. 2: Canonical and non-canonical pyroptosis pathways.
Canonical pyroptosis proceeds through two steps: priming and activation. Priming occurs via TNF-α, TLR, and IL-1β signaling, which activate NF-κB and IRFs to induce expression of inflammasome components (e.g., NLRP3, Casp-4/5/11) and downstream effectors such as GSDMD and pro-IL-1β. Activation of the NLRP3 inflammasome is triggered by inflammasome assembly in response to stimuli, including K^+ and Cl^- efflux, Ca^{2+} influx, and mitochondrial ROS (mROS). The assembled NLRP3 inflammasome (containing NLRP3/ASC/Pro-Casp1) cleaves and activates Casp-1, which in turn processes GSDMD. The N-terminal GSDMD fragments oligomerize and insert into the plasma membrane, forming pores that promote further K^+ efflux and amplify NLRP3 activity. In the non-canonical pathway, intracellular LPS directly activates Casp-4 (Casp-11 in mice), which subsequently cleaves GSDMD. The GSDMD pore drives K^+ efflux and subsequent activation of the canonical pathway NLRP3. Following GSDMD activation, NINJ1 oligomerizes to form large membrane pores, ultimately leading to plasma membrane rupture and necrotic cell death.

Pyroptosis is a regulated form of necrosis characterized by gasdermin activation and subsequent membrane pore formation[122–125] (**Fig. 2**). Pyroptosis signaling pathways are primarily classified as canonical and non-canonical pathways[122,125–127]. Canonical pyroptosis is mainly mediated by five inflammasomes: NLRP3, AIM2, NLRP1, PYRIN, and NLRC4[128,129]. The NLRP3 inflammasome is predominantly involved in detecting intracellular Mtb, and consequently, its molecular mechanism of activation and signaling will be discussed in more detail.

NLRP3 inflammasome activation requires two distinct signals. Signal I, the priming signal, is initiated by the activation of receptors such as Toll-like receptors (TLRs) or the IL-1 receptor (IL-1R). It activates the downstream NF-κB pathway, leading to the transcriptional upregulation of NLRP3 and its substrates, such as pro-IL-1β, and involves post-translational modifications that prepare the inflammasome for rapid response[129,130]. Signal II occurs when NLRP3 recognizes its activators, triggering the full assembly and activation of the NLRP3 inflammasome[131–134]. Common NLRP3 activators include cellular events such as K^+ and Cl^- efflux, Ca^{2+} flux, mitochondrial dysfunction, and lysosomal membrane permeabilization (LMP)[131,132].

The active canonical NLRP3 inflammasome is a protein complex comprising NLRP3, an adaptor protein (ASC), and recruited pro-casp-1. In primates, one additional protein, NLRP11, is recruited[135]. Upon stimulation, the inflammasome forms multiple pro-Casp-1 monomers, which then undergo proximity-driven auto-cleavage into their active form, Casp-1[129,136]. Casp-1 proceeds to cleave gasdermin D (GSDMD) into its N-terminal (NT-GSDMD) and C-terminal (CT-GSDMD) fragments. The hydrophobic NT-GSDMD fragment translocates to the plasma membrane, where it oligomerizes to form GSDMD pores. Concurrently, Casp-1 also processes pro-interleukin (IL)-1β and pro-IL-18 into their mature forms, IL-1β and IL-18, respectively. These pro-inflammatory cytokines are subsequently released through the GSDMD pores into the extracellular environment,

eliciting a robust inflammatory response[122,123] (**Fig. 2**).

The non-canonical inflammasomes, which primarily consist of human pro-CASP-4/5 or their murine homolog, pro-Casp-11. In primates, NLRP11 also participates in the non-canonical CASP-4/-5 inflammasome signaling in response to cytosolic LPS[137]. Upon binding of LPS these pro-caspases oligomerize and become activated via autocleavage to generate active CASP-4, -5, or Casp-11 proteases[128,138–140]. The active inflammatory caspases then directly cleave GSDMD, leading to the formation of GSDMD pores in the plasma membrane. GSDMD pores allow for K^+ efflux, which can activate the canonical NLRP3 inflammasome pathway[129,140].

The final step is the activation of NINJ1, which results in the generation of larger pores, leading to plasma membrane rupture[141–143]. How precisely NINJ1 is activated remains unclear, but following GSDMD pore formation, an osmotic influx of water drives cell swelling and rounding. The resulting increase in mechanical stress on the plasma membrane is an activation signal for NINJ1 monomers to assemble into pores[144]. NINJ1 is involved in PMR following pyroptosis, necroptosis, and ferroptosis[145].

1.7.3 Necroptosis

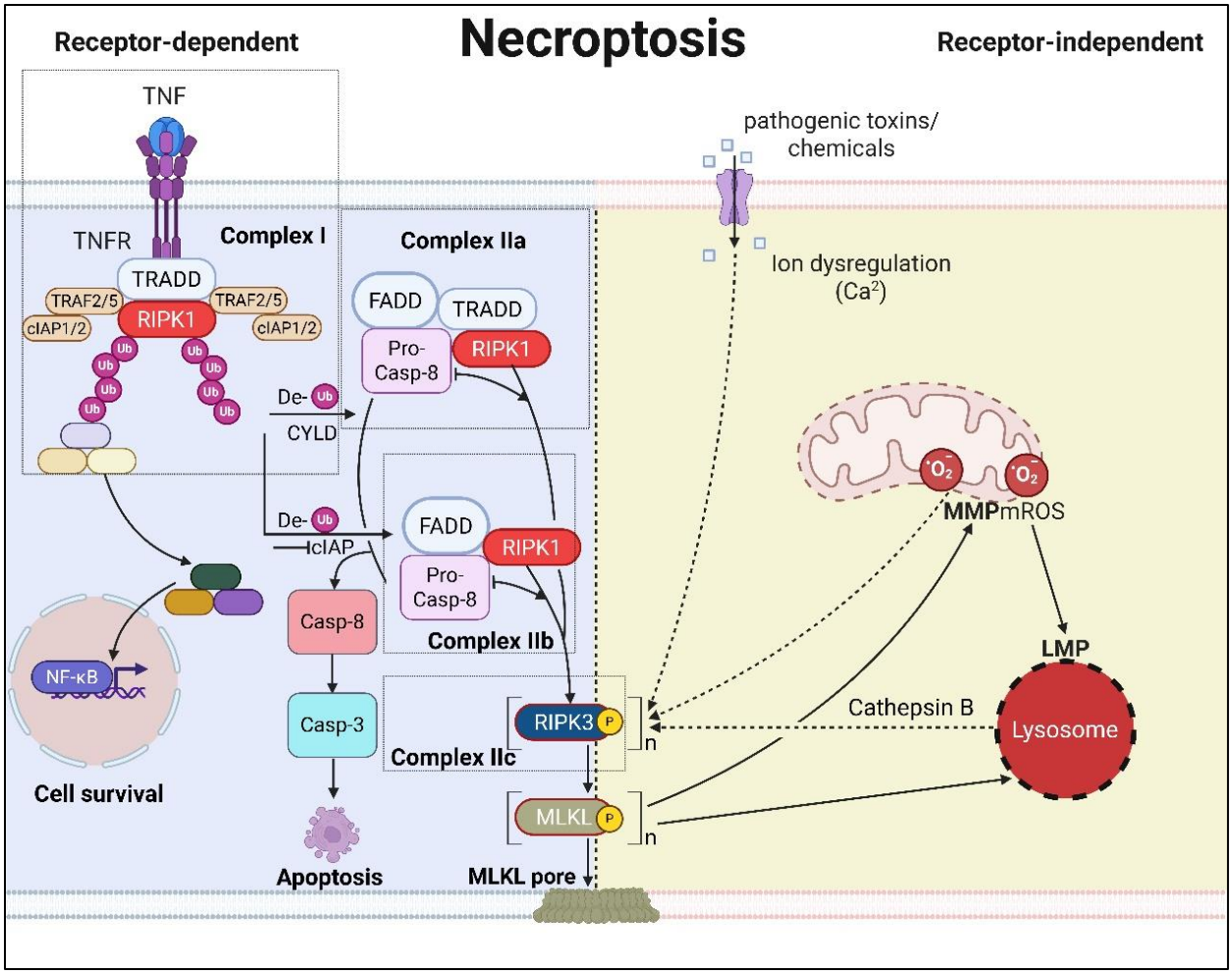

Fig. 3: Receptor-dependent and -independent necroptosis pathways.
The receptor-dependent pathway is initiated by the binding of TNF to its receptor, TNFR. This recruits TRADD and RIPK1, which then assemble Complex I by recruiting TRAF2/5 and cIAP1/2. Within Complex I, RIPK1 is ubiquitinated, which promotes cell survival by activating the NF-κB pathway. Under certain conditions, RIPK1 can be deubiquitinated by CYLD or through the inhibition of cIAPs. This deubiquitination event leads to a switch from pro-survival signaling to a pro-death cascade, resulting in the formation of the cytosolic Complex IIa or Complex IIb. These complexes contain pro-Casp-8. If active, Casp-8 cleaves Casp-3 and other executioner caspases to trigger apoptosis. However, if Casp-8 is inhibited, RIPK1 kinase activity is unleashed, leading to the phosphorylation of RIPK3. Activated RIPK3 then phosphorylates MLKL. Phosphorylated MLKL oligomerizes, translocates to the plasma membrane, and forms pores, ultimately causing membrane permeabilization and necroptotic cell death. The receptor-independent pathway can be triggered by various stimuli that are not receptor-dependent. Pathogenic toxins or chemicals can induce ion dysregulation (e.g., Ca^{2+} influx), leading to the activation of RIPK3. Furthermore, mitochondrial membrane permeabilization (MMP) and lysosomal membrane permeabilization (LMP) cause the release of mitochondrial reactive oxygen species (mROS) and cathepsin B (Cat B), respectively. These factors can also indirectly activate the RIPK3-MLKL axis. A positive

feedback loop may exist where phosphorylated MLKL exacerbates MMP and LMP, thus amplifying the signal to ensure the execution of necroptosis.

Necroptosis is a regulated form of necrosis mediated by receptor-interacting serine/threonine kinase 3 (RIPK3) and its substrate, mixed lineage kinase domain-like pseudokinase (MLKL)[146,147] (**Fig. 3**). Although early studies revealed that necroptosis is triggered by the activation of specific receptors[147,148], subsequent research has identified other regulators that mediate necroptosis independently of this mechanism, such as Z-RNA binding protein 1 (ZBP-1)[149]. This receptor-independent induction is often described as non-canonical or non-classical[146,150]. As no single term is universally accepted for these pathways, this article will use the terms "receptor-independent necroptosis" and "receptor-dependent necroptosis" (**Fig. 3**).

The TNF-TNFR signaling pathway plays a central role in immunologic processes and has been used to delineate the mechanism of receptor-dependent necroptosis[151,152]. Upon binding its ligand, TNF, TNFR trimerizes. This conformational change allows its intracellular death domain (DD) to recruit TNFR1-associated death domain (TRADD), which then forms a larger complex by recruiting TNF receptor-associated factor (TRAF) 2/5, RIPK1, and cellular inhibitor of apoptosis (cIAP) 1/2. Functioning as ubiquitin E3 ligases, TRAF and cIAP ubiquitinate the recruited RIPK1. This modification facilitates the recruitment of additional signaling molecules and leads to the activation of the NF-κB pathway, which eventually promotes cell survival and proliferation[146,150,152,153].

Complex I serves as a checkpoint between cell survival and regulated cell death. When RIPK1 ubiquitination is compromised, for instance by the deubiquitinase CYLD or through the inhibition of cIAPs, RIPK1 dissociates from Complex I to form a secondary pro-apoptotic assembly, Complex II[152–154]. The composition of this complex depends on the specific trigger. The first scenario is initiated by the deubiquitinase CYLD. It deubiquitinates multiple substrates, including TRAFs and RIPK1, causing RIPK1 to be released into the cytosol[155]. RIPK1 then

assembles Complex IIa with TRADD, Fas-associated death domain (FADD), FLICE-like inhibitory protein ($FLIP_L$), and pro-Casp-8[152,153]. Within this complex, pro-Casp-8 heterodimerizes with $FLIP_L$, promoting its cleavage and activation, which in turn activates downstream pro-Casp-3 to induce extrinsic apoptosis[156]. In the second scenario, the absence or inhibition of cIAPs leads to the formation of Complex IIb, which is distinguished from Complex IIa by the absence of TRADD. This complex, which can also be triggered by other receptors such as Fas, DR4/5, and TLR4, similarly functions as Complex IIa as a platform for pro-Casp-8 activation to induce extrinsic apoptosis [152,153].

Activated Casp-8 also cleaves RIPK1 and RIPK3, a mechanism that inhibits necroptosis and promotes apoptosis[156]. When Casp-8 is absent or inhibited, this suppression of RIPK1/3 is removed. This allows RIPK3 to oligomerize with RIPK1, forming Complex IIc (also known as necrosome) that recruits MLKL[157]. Within this complex, a phosphorylation cascade activates RIPK1, RIPK3, and MLKL[150,152]. Finally, the activated and oligomerized MLKL translocates to the cell membrane, binding to phosphoinositides and causing PMR[150,152,158].

Receptor-independent necroptosis may bypass the formation of Complex I, IIa, and IIb, but it converges with receptor-dependent necroptosis at Complex IIc[150]. A key mediator of receptor-independent necroptosis is ZBP-1, an intracellular sensor of viral Z-RNA and endogenous Z-DNA[149,159,160]. When activated, ZBP-1 undergoes a conformational change that allows it to bind RIPK3, forming a unique Complex IIc sufficient to activate the necroptosis executioner, MLKL[149]. In addition, there are other factors known to modulate the necroptosis signaling pathway. Calcium ions (Ca^{2+}) can promote necrosome assembly, while reactive oxygen species (ROS/mROS) enhance RIPK1 and MLKL activity[161,162]. A recent study has also shown that MLKL polymerization can induce LMP, which in turn creates a positive feedback loop that amplifies

necroptosis[163].

Necroptotic cells undergo morphological changes characteristic of necrosis, including cell and organelle swelling, and ultimately, membrane rupture. This loss of membrane integrity leads to the release of intracellular contents, including damage-associated molecular patterns (DAMPs), inflammatory cytokines, and chemokines, which in turn elicit a profound inflammatory response[148,153].

1.7.4 Ferropotosis

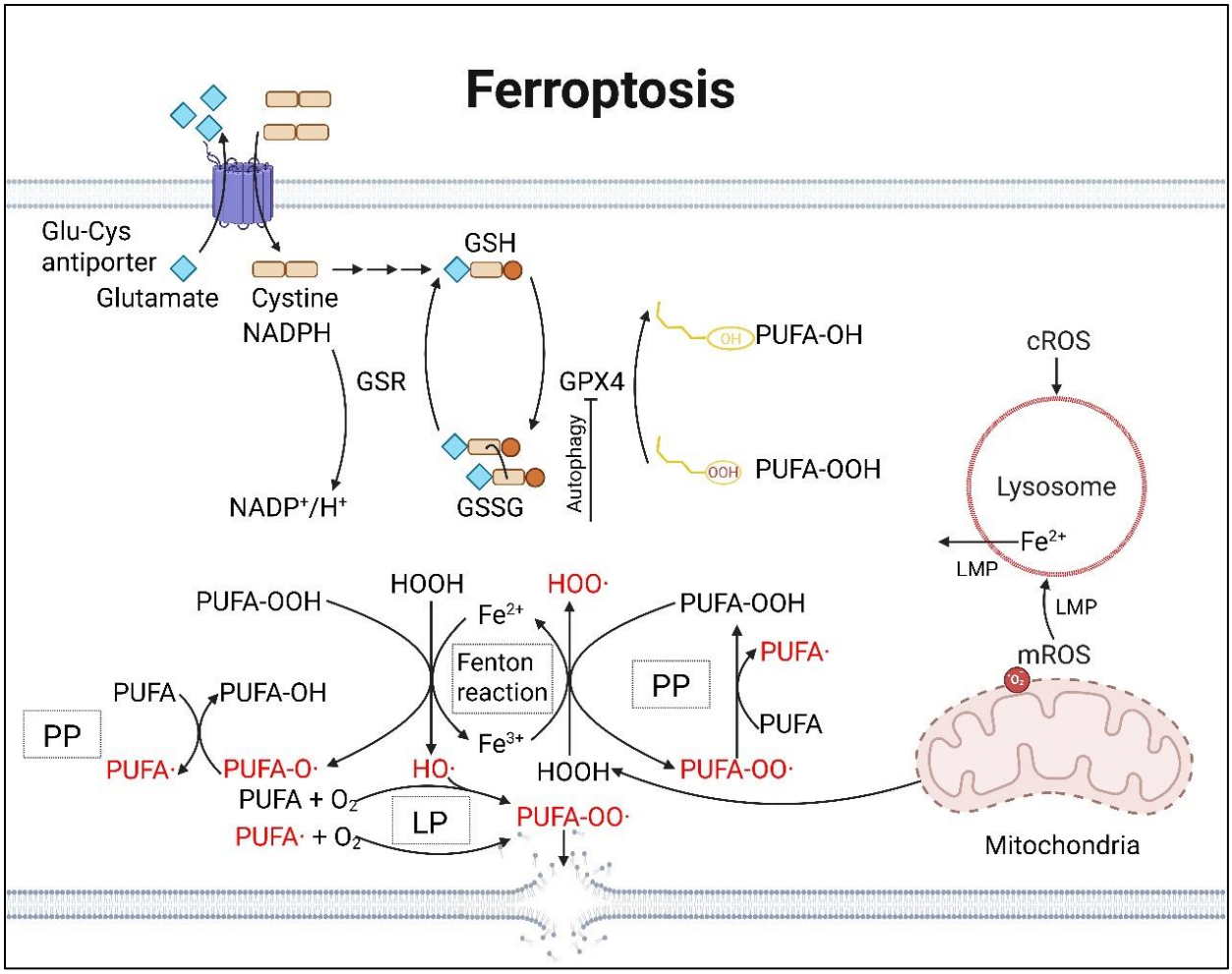

Fig. 4: The ferroptosis signaling pathway.
Ferroptosis is initiated by the accumulation of lipid peroxides, particularly peroxidized polyunsaturated fatty acids (PUFA-OOH). The enzyme glutathione peroxidase 4 (GPX4) is the central regulator of this process, preventing cell death by reducing PUFA-OOH to its non-toxic alcohol form (PUFA-OH). This protective reaction consumes reduced glutathione (GSH), oxidizing it to glutathione disulfide (GSSG). Cellular GSH levels are maintained through two key mechanisms. First, the glutamine-cystine (Glu-Cys) antiporter (system Xc^-) imports cystine, a precursor for GSH synthesis. Second, glutathione reductase (GSR) catalyzes the regeneration of GSH from GSSG in an NADPH-consuming manner. Lipid peroxidation is accelerated by the Fenton reaction, where ferrous (Fe^{2+}) and ferric (Fe^{3+}) ions react with peroxides to generate highly reactive hydroxyl (HO•) and hydroperoxyl (HOO•) radicals. These radicals attack PUFAs, creating lipid radicals that propagate a chain reaction, leading to the accumulation of PUFA-OOH and other lipid peroxides. This widespread lipid peroxidation is believed to disrupt membrane integrity, ultimately causing necrotic cell death. Destabilization of organelles, such as lysosomes and mitochondria, can occur through membrane permeabilization, which releases ferrous iron (Fe^{2+}) and reactive oxygen species (ROS). If cellular antioxidant defenses are insufficient to counteract this release, the cell will undergo ferroptosis. LP = lipid peroxidation; PP = peroxidation propagation.

Ferroptosis is a form of regulated necrosis defined by iron-dependent lipid peroxidation[164–168] (**Fig. 4**). Ferroptosis is an outcome of the imbalance between cellular oxidation and antioxidant mechanisms, by which oxidative stress leads to cell death rather than peroxide clearance. The induction of ferroptosis is driven by two interconnected mechanisms: the iron-mediated Fenton reaction and the subsequent propagated lipid peroxidation[166]. The process begins with the Fenton reaction, in which labile ferrous iron (Fe^{2+}) is oxidized by hydrogen peroxide (H_2O_2) to generate ferric iron (Fe^{3+}) and highly reactive hydroxyl radicals (HO•)[169,170]. These radicals initiate a chain reaction by attacking polyunsaturated fatty acids (PUFAs) to create PUFA radicals (PUFA•), which then react with molecular oxygen to form PUFA peroxyl radicals (PUFA-OO•). The resulting lipid hydroperoxides (PUFA-OOH) can also undergo a Fenton-like reaction with ferrous iron, producing lipid alkoxyl radicals (PUFA-O•) and lipid peroxyl radicals (PUFA-OO•). These reactive species, in turn, attack adjacent lipid molecules, thereby propagating and amplifying the lipid peroxidation cascade[168,170].

The antioxidant mechanism mediated by glutathione peroxidase 4 (GPX4) is a crucial defense against the induction and propagation of lipid peroxidation[171]. GPX4 detoxifies PUFA peroxides by converting them to their non-toxic alcohol forms. This reaction is coupled with the GPX4-catalyzed oxidation of reduced glutathione (GSH) to glutathione disulfide (GSSG). To maintain this protective cycle, GSSG is reduced back to GSH by glutathione-disulfide reductase (GSR) in a reaction that consumes NADPH and produces $NADP^+$[164]. GSH, an antioxidant thiol abundant in all mammalian tissues, is supplied through *de novo* synthesis, which begins with the import of cystine via the SLC7A11 transporter[172,173]. Consequently, inhibiting key steps in the antioxidant mechanisms, including SLC7A11 transportation, GSH synthesis, and GPX4, is known to favor the induction of ferroptosis[167].

Ferroptosis can be directly fueled by several other cellular processes. For instance, the mitochondrial TCA cycle can deplete cysteine, thereby sensitizing cells to this form of cell death. Mitochondria also contribute by generating reactive oxygen species (ROS) through the electron transport chain (ETC), which drives the production of hydroxyl radicals HO• via the Fenton reaction[164]. Furthermore, lysosomal dysfunction or rupture can cause Fe^{2+} release, significantly amplifying the Fenton reaction and exacerbating ferroptosis[174,175].

At the point of ferroptosis execution, the accumulation of lipid peroxides at the plasma membrane increases its tension, a process that culminates in ionic dysregulation, osmotic cell swelling, and eventual PMR mediated by NINJ1[164,176]. While the initial study suggested ferroptosis was morphologically distinct from some forms of necrosis based on electron microscopic data, subsequent findings reveal clear necrotic phenotypes, including cell and organelle swelling and moderate nuclear condensation[177,178]. Following PMR, dying cells release DAMPs. These molecules can then shape the immune response at both the cellular and systemic levels, critically affecting outcomes in various contexts, such as infectious disease[179,180].

1.8 Manipulation of host cell death pathways in infected macrophages by Mtb

1.8.1 Mtb and apoptosis

Mtb modulates host cell death pathways, directing the infected cell toward either apoptosis or necrosis to its own advantage[181]. Several review articles provide detailed summaries on the interaction of Mtb with host cell apoptosis[181–183], and consequently, this aspect of Mtb-host cell death interaction will be discussed in less detail. Initial studies in *ex vivo* human alveolar macrophages (hAMs) found that both virulent Mtb H37Rv and the attenuated strain H37Ra induce the production of TNF-α, a cytokine that promotes both host cell death and survival depending on

the context (**Fig. 1** and **2**)[184]. Subsequent work using the same host cell model revealed that avirulent mycobacterial strains, such as *M. kansasii* (Mka), and attenuated Mtb strains, including *M. bovis* (Mbo)-derived BCG and Mtb H37Ra, induce significantly higher levels of apoptosis compared to virulent strains such as Mtb H37Rv, Mtb BMC 96.1, and Mbo [185]. The induction of macrophage apoptosis by Mtb and other mycobacteria is a well-documented phenomenon, observed across various models, including human *ex vivo* cells, murine *ex vivo* and *in vivo* models, and the *in vivo* zebrafish model[184–188].

The induction of extrinsic apoptosis by mycobacteria in host macrophages is linked to the TNF-α production[184,185,189]. The downstream mechanisms were further elucidated in studies using murine RAW 264.7 cells and BMDMs[189]. In RAW 264.7 cells stimulated with TNF-α, the E3 ubiquitin ligase c-Cbl phosphorylates and ubiquitinates the short form of cellular FLICE-like inhibitory protein ($cFLIP_S$), triggering its degradation. This degradation liberates pro-Casp-8, allowing for its activation[189]. Infection of BMDMs with Mtb H37Rv confirmed that the induction of apoptosis is significantly dependent on c-Cbl[189]. Extrinsic apoptosis can also be induced through an ER stress pathway triggered by the Mtb virulence factor Rv0297. When expressed in RAW 264.7 cells, Rv0297 accumulates in the ER, activating the UPR and inducing stress that results in caspase-8-dependent apoptosis[190]. However, it remains unclear whether these specific signaling pathways are involved in human cell models.

In addition to extrinsic pathways, Mtb is also known to induce intrinsic apoptosis in hMDMs and murine macrophages[191–194]. In hMDMs, Mtb infection can trigger both mitochondrial outer membrane permeabilization (MOMP) and mitochondrial permeability transition (MPT)[194]. The attenuated Mtb H37Ra and virulent H37Rv induce MOMP-dependent intrinsic apoptosis; only the virulent H37Rv strain significantly induces MPT-driven necrosis[194]. Further research has

explored the molecular regulatory mechanism of this pathway. For instance, the BH3-only protein Bim was found to be significantly upregulated in J774 macrophages during Mtb infection, where it was shown to be a critical factor in driving intrinsic apoptosis[195].

Specific Mtb virulence factors have also been shown to mediate the intrinsic apoptosis[196]. The essential Mtb virulence lipid, phthiocerol dimycocerosate (PDIM/DIM), modulates ESX-1-dependent intrinsic apoptosis in hMDMs[192]. Similarly, a study using recombinant heparin-binding hemagglutinin (HBHA) in RAW 264.7 cells showed that this virulence factor can translocate to the mitochondrial outer membrane, inducing MPT, BAX-mediated MOMP, and subsequent cytochrome *c* (cyt c)-dependent apoptosis[193]. Furthermore, several virulence factors from the PE_PGRS family have been implicated in apoptosis induction[190,191]. Among these, PE_PGRS30 has been shown to bind to host prohibitin 2 (PHB2)[191], a protein that normally inhibits intrinsic apoptosis[197]. Ectopic expression of PE_PGRS30 in RAW 264.7 cells and murine alveolar macrophages (mAMs) induced apoptosis, an effect linked to the binding of PE_PGRS30 to PHB2 on the mitochondria[191] .

Mtb virulence factors also inhibit apoptosis, thereby mitigating potential bactericidal effects[181,198]. This inhibitory effect is frequently demonstrated in studies using mycobacterial knockout (KO) mutants and their complemented counterparts. Typically, in corresponding research contexts, a KO mutant induces a higher level of apoptosis, whereas the wild-type (WT) and complemented strains induce a comparably lower level[186,199–203].

The apoptosis inhibitor from Mtb, NuoG, is a subunit of the type I NADH dehydrogenase and was discovered through a gain-of-function (GOF) screen using *M. smegmatis* (Msm) clones containing Mtb genomic fragments[186]. The Mtb Δ*nuoG* mutant induces significantly higher levels of apoptosis compared to Mtb. The absence of *nuoG* was shown to promote a ROS- and TNF-α-

dependent extrinsic apoptosis pathway in THP-1 cells and human alveolar macrophages (hAMs)[199]. Similarly, Danelishvili *et al*. demonstrated that the putative proteins Rv3654c and Rv3655c inhibit extrinsic apoptosis in human U937 cells. Pull-down assays and mass spectrometry (MS) analysis suggested that Rv3654c and Rv3655c may interact with host proteins PSF and ALO17 to achieve this inhibition[200]. Another study indicates that the Mtb protein tyrosine phosphatase PtpA phosphorylates the host[201]. Since GSK3α is a known regulator of extrinsic apoptosis[204], this interaction may represent another mechanism by which Mtb inhibits this pathway.

Mtb virulence factors also interact with and impede mitochondria to inhibit intrinsic apoptosis. For example, Mtb Cpn60.2 (GroEL2) can be exported into the macrophage cytosol, translocate to host mitochondria, and interact with the anti-apoptotic protein mortalin, thereby impeding intrinsic apoptosis[202]. In another study, RAW 264.7 cells transfected with Mtb *Rv3033* showed reduced apoptosis when infected with Mtb H37Ra or *M. bovis* BCG. Mechanistically, Rv3033 was found to inhibit caspase-9, but not caspase-8, cleavage and the PERK pathway of the ER-stress response[203]. Furthermore, some factors may inhibit both pathways. The Mtb SecA2 secretion system and superoxide dismutase A (SodA) play important roles in inhibiting apoptosis in THP-1 cells[205].

Despite this growing list of virulence factors that inhibit host apoptosis, very few studies have extended these findings to *in vivo* infection models. The *nuoG* deletion mutant shows increased apoptosis in the lungs of infected mice and is attenuated for growth[186]. While one study showed that *M. marinum* (Mm) induces apoptosis in zebrafish macrophages *in vivo*[188], the specific signaling pathways involved in apoptosis induction or manipulation by Mtb in the zebrafish model remain unknown.

The cell death modality affects the host immune response, which in turn shapes the

pathogenesis of tuberculosis[121,206]. It is well-established that Mtb manipulates this apoptosis-necrosis switch to modulate the local immune environment and advance its pathogenesis. One example of this manipulation is the antagonistic relationship between two lipid mediators: Prostaglandin E2 (PGE_2) and Lipoxin A4 (LXA_4). Research by Chen et al. demonstrated that these eicosanoids function as a regulatory switch governing host cell fate during Mtb infection. The study revealed that the virulent Mtb strain H37Rv significantly induces LXA_4 in hMDMs, whereas the avirulent H37Ra strain primarily stimulates the production of PGE_2[207]. LXA_4, produced during virulent infection, promotes necrosis by suppressing the host-protective PGE_2 pathway through the inhibition of cyclooxygenase-2 (COX-2) and by inducing mitochondrial inner membrane perturbation. Conversely, the high levels of PGE_2 generated during avirulent H37Ra infection were shown to inhibit LXA_4 production, favoring apoptosis. In summary, virulent Mtb exploits this lipid signaling axis by inducing LXA_4, which in turn suppresses the pro-apoptotic PGE_2 pathway and promotes necrotic cell death, thereby creating a microenvironment favorable for its survival and proliferation[207].

1.8.2 Mtb and pyroptosis

While pyroptosis can be a host-protective response during bacterial infections[208], the interaction between Mtb and the host cell inflammasomes is complex[208,209]. Initial studies using Mm established that its RD1 region and ESX-1 secretion system were essential for triggering the release of the cytokines IL-1β and IL-18 in murine BMDMs[210,211]. This inflammasome activation was specifically shown to require the host sensor NLRP3[210]. Subsequent research extended these findings to Mtb, demonstrating that its RD1 region was also necessary for Casp-1 activation and the secretion of IL-1β and IL-18 in murine peritoneal macrophages, a process dependent on host

potassium^{+} efflux[212]. In murine models, the production of IL-1β has long been recognized as a protective mechanism against the progression of Mtb infection[213]. Studies utilizing BMDMs from *Casp1/11*$^{-/-}$, *Asc*$^{-/-}$, and *Nlrp3*$^{-/-}$ mice established a critical role for the canonical Nlrp3 inflammasome pathway in mediating IL-1β secretion in response to Mtb during *ex vivo* infections[214]. Similarly, Dorhoi *et al.* reported that Mtb activates NLRP3 via the ESX-1 secretion system in BMDMs, and that LPS priming further enhances NLRP3-dependent IL-1β secretion[215]. Cat B activity and LMP might be required for ESAT-6-dependent NLRP3 inflammasome activation during Mtb infection in BMDMs[216] . Beyond NLRP3, other inflammasome pathways have been implicated. Studies using *Aim2*$^{-/-}$ mice revealed their increased susceptibility to Mtb infection, with peritoneal macrophages from these mice showing significantly reduced Casp-1 activation and diminished secretion of both IL-1β and IL-18 [217]. This suggests that the AIM2 inflammasome, potentially activated by cytosolic Mtb genomic DNA, is also a key player in the murine anti-TB response.

The host cell inflammasome detects Mtb, but the bacteria strive to inhibit this detection[208,209]. For instance, the Mtb serine/threonine protein kinase, PknF, suppresses NLRP3 inflammasome activation stimulated by LPS/ATP treatment[218]. Consistently, murine and human macrophages infected with the Mtb Δ*pknF* Mtb strain exhibit significantly higher levels of IL-1β release in a manner dependent on the ESX-1 secretion system, NLRP3, ROS, and K^{+}/Cl^{-} efflux[218]. The tyrosine phosphatase (PtpB) of Mtb interacts with ubiquitin (Ub) and directly interferes with the execution of pyroptosis by dephosphorylating host PI4P and PI(4,5)P_2, which in turn impairs the translocation of the pore-forming NT-GSDMD to the plasma membrane[219] . A screen of secreted Mtb proteins that are able to inhibit NLRP3 or AIM2 inflammasome identified Mtb Protein Kinase G as an inhibitor of NLRP3 inflammasome assembly [220]. In the absence of Nlrp3,

Mtb can inhibit the AIM2 inflammasome activation triggered by cytosolic DNA in BMDMs and bone-marrow-derived dendritic cells (BMDCs)[218,221].

The occurrence of pyroptosis in *in vivo* murine models was also suggested. Interestingly, significant discrepancies exist between *ex vivo* and *in vivo* murine studies. While *ex vivo* findings highlight the importance of the inflammasomes, Casp-1, and ASC, *in vivo* Mtb infection models have shown that IL-1β secretion can occur independently of Casp-1/11, ASC, and even NLRP3[214,215]. These findings, coupled with evidence that other proteases can process pro-IL-1β into its mature form[222], suggest that in the more complex *in vivo* environment, other cell types or alternative proteolytic pathways may contribute to the processing and release of IL-1β[214,215]. The best evidence to date that the inflammasome activation may provide a protective host immune response was provided by infecting wild-type and *Gsdmd*$^{-/-}$ mice with the *PtpB* deletion mutant of Mtb, which induces an increase in inflammasome activation[219]. The study shows that the *PtpB* mutant is attenuated compared to wild-type Mtb in the wild-type mice but that this phenotype is rescued in the *Gsdmd*$^{-/-}$ mice[219]. The result that *Aim2*-deficient mice are more susceptible to Mtb infection is somewhat inconclusive, since AIM2 has inflammasome-independent functions[217].

In human macrophage models, using the THP-1 macrophage-like cell line, it was established that both Mtb and Mm trigger IL-1β secretion through a CASP-1 and NLRP3-dependent mechanism[223–225]. More recent work using electron microscopy (EM) and live-cell imaging has visually confirmed the execution of pyroptosis in THP-1 cells during Mtb infection[226]. Further complexity in human cells has been revealed by the discovery of roles for non-canonical inflammasomes. The primate-specific protein NLRP11 was found to be essential for NLRP3 activation during Mtb infection in THP-1 cells[227]. The non-canonical inflammasome sensor CASP-4/5 has also been implicated in IL−1β secretion in this context[227]. The current model suggests that

NLRP11/CASP4/5 is involved in the initial sensing of a putative cytosolic Mtb molecule to activate the CASP4/5 proteolytic activity, which will result in GSDMD cleavage and pore formation. The GSDMD pore will result in K^+ efflux, which will activate the canonical NLRP3 inflammasome[227]. Studies using primary human cells, including hMDMs and hAMs, show that Mtb upregulates AIM2 expression in a PPARγ-dependent manner[228]. Nevertheless it was PPARγ and Nlrp3 rather than AIM2 that are responsible for the induction of IL-1β secretion[217,228]. This is consistent with many studies in BMDMs, which demonstrate the complete abolition of IL-1β production and cell death after the deletion of Nlrp3[215,218].

1.8.3 Mtb and necroptosis

Mtb-mediated host cell necrosis induction seems to be context-dependent. The zebrafish model, using Mm, shows that in a high TNF-α environment, host macrophages activate a TNF-αR-RIPK1-RIPK3 signaling cascade that mediates mitochondrial membrane potential dissipation through mitochondrial mROS production. This pathway also involves cyclophilin D (CYPD) and partially overlaps with the upstream components of the mammal necroptosis signaling[229,230]. Further studies using zebrafish and THP-1 cells revealed that Mm triggers a high-TNF-α-driven signaling pathway beginning with mitochondrial ROS generation, followed by LMP, Ca^{2+} release by the endoplasmic reticulum (ER), mitochondrial Ca^{2+} uptake, and subsequent CYPD activation. This signaling circuit ultimately leads to MPT-driven necrosis[231]. While ATP depletion was suggested as a downstream consequence of MPT, the terminal execution mechanism remains unclear, since zebrafish lack an ortholog of human MLKL[232].

In hMDMs, Mtb H37Rv but not Mtb H37Ra induces MPT[194]. RIPK3 is shown to be involved in both mitochondrial regulation and necroptosis in Mtb-infected hMDMs[233]. During Mtb infection, Bcl-x_L facilitates the translocation of pro-CASP-8 and RIPK3 to the mitochondria,

where they form a complex with RIPK1. Interestingly, RIPK1 was found to be dispensable, as its inhibition did not impact complex formation or cell death[233]. RIPK3 was shown to promote CYPD-ANT binding and MPT pore (MPTP) opening, leading to mROS-dependent necrosis[233]. Notably, silencing MLKL significantly reduced cell death, highlighting a potential role for MLKL in this context [233]. These findings suggest that Mtb may induce a hybrid form of necroptosis in which both MPT and MLKL are essential. In the human THP-1 cell line, the Mtb virulence factor TNT (tuberculosis necrotizing toxin) was shown to drive necroptosis by depleting cytosolic NAD^+ through its glycohydrolase activity during Mtb infection[234]. This NAD^+ depletion triggers RIPK3 and MLKL activation, leading to necroptosis. Furthermore, cytosolic NAD^+ depletion was found to propagate to mitochondrial NAD^+ pools, leading to MPT, mitochondrial membrane potential loss, and ATP depletion[234].

A recent study investigated a human disease-associated mutation, *Lrrk2*^{G2019S} [235]. It reveals that in *Lrrk2*^{G2019S} BMDMs, Mtb-induced cell death occurs via initial activation of the pyroptosis signaling pathway, but ultimately culminates in GSDMD-mediated necroptosis. Following AIM2 activation, GSDMD forms pores on mitochondria, releasing mROS into the cytosol, which activates RIPK1, RIPK3, and MLKL. SiRNA-mediated knockdown of ZBP-1 and TRIF did not inhibit this process, indicating that this GSDMD-linked necroptotic pathway diverges from both known receptor-dependent and -independent necroptosis models[235]. It remains unclear how *Lrrk2*^{G2019S} correlates with mROS production and RIPK1/RIPK3 activation. Stutz et al. observed that Mtb infection upregulates MLKL, ZBP-1, TNFR1, and other necroptosis-related genes in mAMs and BMDMs, yet no MLKL phosphorylation or Casp-3/8 activation was detected. Moreover, MLKL knockout did not alter TB progression *in vivo*[236], suggesting that necroptosis is not universally engaged during infection.

In summary, necroptosis induction during mycobacterial infection is highly context-dependent and remains a subject of debate. Across studies reporting necroptosis in human and murine macrophages, mitochondria consistently play a central role, often involving MPT as a pivotal event[233–235]. However, findings such as the dispensability of MLKL in BMDMs[236] challenge the observed necroptosis induction in Mtb pathogenesis. In zebrafish, where no MLKL ortholog has been identified, canonical necroptosis models do not apply. Thus, how the Mm-induced MPT-driven cell death observed in zebrafish translates to human macrophage death modalities remains unresolved.

1.8.4 Induction of ferroptosis by Mtb

In murine models, Mtb has been shown to induce ferroptosis, a form of iron-dependent cell death[237–239]. Initial studies of BMDMs revealed that Mtb infection triggers necrosis by increasing intracellular labile iron, mitochondrial superoxide, and lipid peroxidation[237]. This necrotic cell death was significantly inhibited by Ferrostatin-1, a scavenger of lipid peroxyl radicals, confirming the central role of ferroptosis. This process was also associated with reduced levels of glutathione (GSH) and glutathione peroxidase 4 (GPX4), directly linking GPX4-regulated ferroptosis to Mtb infection [237]. $Gpx4^{-/-}$ BMDMS show enhanced, lipid peroxidation-dependent ferroptosis after Mtb infection [238]. *Bach1* regulates the expression of genes associated with the inhibition/suppression of ferroptosis during Mtb infection *in vivo*. The pulmonary cells from Mtb-infected w.t. and $Bach1^{-/-}$ mice were used to perform scRNA-seq, identifying a cluster of genes associated with inhibition/suppression of ferroptosis[240]. An Mbo strain expressing the Mtb virulence factor, Mb3523c, induces ferroptosis in RAW 264.7 macrophages. Mb3523c was found to interact with host HSP90, promoting the lysosomal degradation of GPX4 through chaperone-mediated autophagy[239].

Parallel findings have been observed in human macrophage models. An early study showed that Ferrostatin-1 rescues hMDMs from necrosis during Mtb infection (Supplementary data)[237]. Although it is still not clear how Mtb induces ferroptosis in human macrophages, with human U937 cell lines, Qiang et al. identify that the Mtb virulence factor, PtpA, can enter the host cell nucleus and bind to the host methyltransferase PRMT6[241]. This interaction inhibits PRMT6, reducing H3R2me2a levels and subsequently decreasing the transcription of *GPX4*[241]. Furthermore, analyses of clinical and autopsy samples show a strong correlation between pulmonary tuberculosis and global changes in GSH, GPX4, lipid peroxidation, and BACH1 levels in TB patients. However, this clinical data is not definitive proof that macrophages undergo ferroptosis during Mtb infection *in vivo* in humans[237,238,240].

In summary, ferroptosis is a critical form of necrosis induced in both murine and human macrophages during Mtb infection. Current evidence consistently supports a model where Mtb actively triggers ferroptosis. The depletion of GPX4 is a convergent point in both human and murine models, though the exact mechanisms driving this reduction are still being explored[237–241]. Two distinct pathways have been proposed based on *ex vivo* studies: transcriptional repression of GPX4 by the Mtb virulence factor PtpA, and post-translational degradation of GPX4 mediated by the Mb3523c-HSP90 interaction[239,241].

1.8.5 Induction of other programmed necrosis by Mtb

Lysosomal-dependent cell death (LDCD) is a form of regulated necrosis initiated by LMP and depends on cathepsin activity[125]. However, LMP is also known to be associated with apoptosis, pyroptosis, necroptosis, and ferroptosis[242,243]. This overlap makes it unclear whether LDCD is a distinct pathway with unique executioners and, crucially, how it leads to final plasma membrane rupture (PMR).

The induction of LDCD in murine macrophages infected with Mtb is studied, with conflicting findings from *ex vivo* macrophage models[244,245]. One study demonstrated that Mtb induces LMP, and an atypical, cathepsin-independent necrosis that requires the Mtb PhoPR virulence factor and host lysosomal lipases, but not BAX/BAK or Casp-1[244]. Morphologically, this cell death involves nuclear deformation resembling macrophage extracellular trap cell death (METosis), although a direct mechanistic link was not established[244]. In contrast, a more recent study concluded that Mtb triggers LMP and a following cathepsin-dependent necrosis in BMDMs and RAW 264.7 cells. Mechanistically, this study proposed that cytosolic ACOD1 depletes HSP70, leading to lysosomal destabilization. It remains unknown whether either of these proposed mechanisms is relevant to human macrophages or translates to an *in vivo* context[245].

"METosis" was proposed as another form of regulated necrosis, in which macrophages release extracellular trap structures as they die, similar to the well-established NETosis pathway in neutrophils [246]. Although several molecular hallmarks of "METosis" have been identified, their necessity appears to be context-dependent, and none have been proven essential for its induction[247]. Consequently, it remains unclear whether this pathway is analogous to NETosis. Hence, we prefer the term DNA-release-associated necrosis (DRAN). To date, no signaling pathway has been identified that directly connects the process of DNA release to the lytic event of PMR. Mtb infection induces DNA release that is associated with cell death in human monocyte-derived macrophages (hMDMs). The DNA expulsion involves peptidyl arginine deiminase 4 (PAD4) and is associated with citrullinated Histone 4 (CitH4), a process amplified by IFN-γ [248]. Another study found that Mtb strains exhibiting a "cording" phenotype induce greater DNA release [249]. Many questions remain regarding the host cell signaling pathway that mediates DRAN. The extracellular DNA (eDNA) of neutrophils generated by NETosis traps and inhibits bacterial growth of some

human pathogens, but seems not to affect Mtb[250]. It is unclear if the extruded DNA of macrophages binds to Mtb and has bactericidal effects[248,249]. Secondly, it remains to be shown whether the DNA release is a marker for a novel cell death signaling pathway in macrophages or merely a consequence of necrotic cell death, which is also associated with DNA release[248,249].

1.9 Importance of cell death pathways for Mtb virulence in vivo

Granulomas are a hallmark of tuberculosis[251,252]. Clinical observations of human lungs over a long time have established that as TB progresses, the granulomas undergo liquefactive and caseous necrosis, leading to tissue destruction and inflammatory pneumonia[251,253]. This macroscopic histological evidence also demonstrates that granuloma necrosis is associated with the exit of Mtb and a significant inflammatory response, providing a clear link between TB progression and necrosis at the cellular level[254].

Mtb induces both apoptosis and necrosis *in vivo*. Early evidence from mouse models revealed that the extent of apoptosis varies depending on the specific Mtb and mouse strains used[255,256]. This variability in apoptosis level was linked to the bacterial burden in the lungs and correlates with the apoptosis induction to TB development[256]. A more recent study solidified this concept, showing that intrinsic apoptosis in mouse myeloid cells is crucial for restricting TB progression[257]. To demonstrate this, researchers used *Casp8*$^{-/-}$;*Mlkl*$^{-/-}$ and *Bax*$^{Lyz2\text{-}Cre}$;*Bak*$^{-/-}$ mice with impaired intrinsic apoptosis pathways[257]. Compared to control mice, these mutants exhibited a higher Mtb load (CFU) in their lungs, indicating a failure to control the infection[257]. Consistently, a mutant of Mtb that is deficient in inhibiting host cell apoptosis is attenuated in the mouse model[186].

Pyroptosis, a form of necrotic cell death, appears to play a partially protective role in mouse models of TB. Mice deficient in key pyroptotic components Asc and Casp-1/11 showed decreased survival during TB, and *Asc*$^{-/-}$ mice also had an increased bacterial burden[214]. Mtb mutants deficient in the inhibition of pyroptosis are attenuated in the mouse model[219,220]. In contrast, ferroptosis exacerbates TB progression *in vivo*[237,238]. Mice deficient in Gpx4, a key negative regulator of ferroptosis, displayed increased tissue necrosis following Mtb infection, while mice overexpressing Gpx4 exhibited reduced lung pathology[238]. Furthermore, Gpx4 deficiency specifically in the myeloid compartment resulted in decreased host resistance and increased tissue necrosis[238]. This data strongly suggests that Mtb induces ferroptosis *in vivo*, which leads to worse TB outcomes.

1.10 Targeting cell death pathways for host-directed therapy (HDT)

Host-directed therapies for TB are proposed to alter the fate of infected cells toward a cell death pathway that initiates a protective immune response[258,259]. For instance, clofazimine, a widely used drug to treat drug-resistant TB[260], has been shown to induce CASP-3-mediated apoptosis in THP-1 cells, which might synergize with its direct bactericidal activity[261,262]. A more direct way to induce host cell apoptosis was successful by using compounds that antagonize inhibitors of apoptosis mediator proteins in order to achieve increased resistance to Mtb infection in mice [257]. Navitoclax, a small-molecule Bcl-2 inhibitor, significantly induces apoptosis in lung immune cells and improves bacterial clearance in the mouse model of tuberculosis[263] . In contrast, some therapies aim to inhibit host-detrimental forms of cell death to increase resistance to Mtb infections. Drugs inhibiting voltage-gated L-type $Ca2^{+}$ channels suppress necrosis under high-TNF-α conditions in the zebrafish model, but their effect on host resistance was not assessed[231] . Alisporivir and desipramine synergize to suppress necrosis under high-TNF-α conditions and

improve zebrafish resistance to Mm infections[229]. During Mtb infection, PGE_2 and LXA_4 levels regulate the induction of host cell apoptosis versus necrosis, respectively[181]. Zileuiton is a clinically approved medication that decreases the level of LXA_4 by inhibiting the activity of 5-lipoxygenase. Mayer-Barber *et al.* reported that zileuton, combined with PGE_2, significantly improves host survival and decreases lung CFUs of Mtb in *in vivo* mouse models[264]. A similar approach using lipoxygenase inhibitors to decrease levels of the necrosis-inducing eicosanoid LTB_4 was successful in increasing zebrafish resistance to Mm infections[230] . These findings show that inhibiting host cell necrosis regulated by eicosanoids is a promising approach to restricting TB progression. The ferroptosis inhibitor ferrostatin-1 protects mice against Mtb infection by inhibiting macrophage ferroptosis[237,238], suggesting that targeting the ferroptosis pathway might also be a promising HDT strategy.

1.11 Summary

Mtb, the causative agent of TB, remains one of the most serious threats to global health among infectious diseases. A defining pathological hallmark of TB is the formation of granulomas accompanied by extensive tissue necrosis in the lungs. This destruction of lung tissue reflects the substantial levels of host cell death triggered during Mtb infection.

Alveolar macrophages serve as the first line of defense against inhaled Mtb, whereas interstitial macrophages play a critical role during the early phase of infection. These macrophage populations employ a range of bactericidal mechanisms to restrict Mtb growth and also present antigens to T cells, thereby initiating the adaptive immune responses that culminate in granuloma formation. However, if Mtb is not effectively eliminated and replicates beyond a certain threshold, it can induce macrophage death. The lysis of infected macrophages facilitates bacterial

dissemination to previously uninfected lung regions and even to extrapulmonary sites. Understanding how Mtb kills host macrophages is essential for elucidating the molecular strategies the pathogen uses to subvert host defenses. Mapping the specific cell death pathways and identifying the host targets manipulated by Mtb may ultimately inform the development of immunoprophylactic approaches and HDTs for TB.

This dissertation summarizes my primary research project, titled "Characterization of Programmed Cell Death Pathways Activated in Mycobacterium tuberculosis-Infected THP-1 Cells and Human Monocyte-Derived Macrophages." My work centers on determining how the Mtb strain H37Rv induces necrotic cell death in THP-1 cells and hMDMs. Although numerous studies have examined Mtb-induced cell death in various macrophage models, the mechanisms underlying this process, specifically in human macrophages, remain poorly understood. My research aims to define the programmed cell death pathways activated in THP-1 cells and hMDMs and to identify potential host targets exploited by Mtb during infection. Such targets, if validated, may offer promising entry points for HDT development.

Chapter 2 examines the induction of apoptosis in both macrophage models upon Mtb infection. Chapter 3 evaluates the activation of pyroptosis and necroptosis, while Chapter 4 investigates whether Mtb triggers ferroptosis, another form of regulated necrosis. Chapter 5 assesses LMP in Mtb-infected THP-1 cells using time-lapse live-cell imaging. Chapter 6 characterizes a phenomenon of cell-death-associated DNA release, quantifies its occurrence, and discusses its potential consequences for both the host and the pathogen, including an exploratory analysis of the signaling pathways that may drive this process. Finally, Chapter 7 summarizes and integrates the key findings, discusses their implications, and outlines future research directions.

Chapter 2: Assessment of the role Type I IFN plays in cell death induced by Mtb H37Rv in THP-1 cells

2.1 Abstract

Type I IFNs are generally regarded as host-protective during viral infections. However, in the context of tuberculosis, accumulating evidence indicates that Type I IFN signaling does not confer host protection. Instead, it may exacerbate disease progression and contribute to increased pathology and tissue damage. Despite these observations, it remains unclear at the cellular level whether Type I IFN enhances specific forms of cell death in Mtb-infected macrophages.

In this chapter, two kinetic assays were performed to define the optimal time points for sample collection and downstream analyses for the THP-1 and hMDM infection models, respectively. Then, the IFN-β-IFNAR signaling axis is investigated. To demonstrate activation of this pathway during Mtb infection, a Western blot (WB) for phosphorylated STAT1 was performed. Complementary Enzyme-Linked Immunosorbent Assay (ELISA) data show that *ex vivo* THP-1 cells secrete only marginal levels of IFN-β following Mtb infection. Finally, IFNAR neutralization assays reveal that blockade of this pathway does not alter the extent of Mtb-induced cell death. Together with published findings in hMDMs, these results indicate that IFN-β and IFNAR signaling do not play a significant role in the cell death modalities examined in this study.

2.2 Materials and Methods

Cell cultures and differentiation

Wild-type (w.t.) THP-1 cells (TIB-202) were obtained from ATCC (American Type Culture Collection; VA, USA). Monocytic THP-1 cells were cultured in RPMI 1640 medium (ATCC, 30-2001) supplemented with 10% heat-inactivated fetal bovine serum (FBS) (Gibco, NY, USA; A52567-01). The culture medium was refreshed every 2–3 days to maintain a cell density between 2×10^5 and 1×10^6 cells/mL prior to differentiation. THP-1 cells were pelleted and resuspended in complete medium containing 50 ng/mL phorbol 12-myristate 13-acetate (PMA) (Sigma, MA, USA; P1585), adjusted to a final density of 1×10^6 cells/mL. Cells were seeded at 5×10^5/well in non-treated 24-well plates (ThermoFisher, MD, USA; 144530). Cells were treated with PMA for 2 days, after which they were washed twice with Dulbecco's phosphate-buffered saline (DPBS; ThermoFisher, 14190144) and incubated for an additional 2 days in fresh PMA-free medium before treatment or infection. All cell lines were stored in freezing medium composed of 10% dimethyl sulfoxide (DMSO) in 90% FBS for cryopreservation.

ELISA

The Human IFN-β DuoSet ELISA kit (Bio-techne, DY814-05) was used to quantify secreted IFN-β in THP-1 cell supernatants, following the manufacturer's protocols. Supernatants were pooled and aliquoted for analysis, with each condition assessed in four parallel wells. Absorbance was measured at 450 and 540 nm (background), and final cytokine concentrations were calculated using linear regression in GraphPad Prism.

SDS-PAGE and Western Blotting

THP-1 cells or hMDMs were lysed in 1% NP-40 lysis buffer (1% NP-40, 0.4 mM EDTA, 10 mM Tris-HCl, 150 mM NaCl) supplemented with Halt™ Protease and Phosphatase Inhibitor

Cocktail (Thermo Scientific, 78442). Lysates were centrifuged, and the supernatants were collected. Cell lysates were mixed with 4× Laemmli buffer (Thermo Scientific, J60015.AD) and denatured for 30 minutes before gel-loading.

Total protein concentrations were determined using the Pierce™ BCA Protein Assay Kit (Thermo Scientific, 23227). For SDS-PAGE, 20 µg of protein per sample was loaded onto SurePAGE Bis-Tris 12% gels (GenScript, M00668). Electrophoresis was performed at 50 V for 20 minutes, followed by 150 V for 50 minutes. Proteins were transferred to PVDF membranes (Thermo Scientific, 88585) using the eBlot™ L1 transfer system (GenScript, L00686).

Membranes were blocked with SuperBlock™ Blocking Buffer (Thermo Scientific, 37580) for 20 minutes and incubated with primary antibodies diluted in TBS-T (2.4 g/L Tris-base, 8.8 g/L NaCl, 0.1% Tween-20; pH 7.6) for 2 hours or overnight. After six 2-minute washes with TBS-T, membranes were incubated with HRP-conjugated secondary antibodies in TBS-T for 1 hour, followed by another series of six 2-minute washes. Signal detection was carried out using SuperSignal™ West Pico PLUS Chemiluminescent Substrate (Thermo Scientific, 34580), and membranes were imaged with the iBright™ FL1500 Imaging System (Invitrogen, A44241). The information on antibodies is provided in the Appendix Table 1.

Band intensities were quantified using ImageLab software. Target protein intensities were normalized to β-actin levels from the same experiment, and these values were further normalized to the untreated or uninfected day 1 control for statistical analysis.

$$Relative\ band\ intensity = \frac{\frac{BI_{Mtb,target}}{BI_{Mtb,\beta act}}}{\frac{BI_{coun,target}}{BI_{coun,\beta act}}}, BI = Band\ intensity$$

2.3 Results

2.3.1 Kinetics of cell death induced by Mtb H37Rv in THP-1 cells and hMDMs

To systematically investigate the activation of established cell death pathways following Mtb infection in human macrophages, we first performed a kinetic analysis of host cell death induction (**Fig. 5A** and **B**). Adenylate kinase (AK) and lactate dehydrogenase (LDH) release assays were used as quantitative readouts of cell lysis after infection with Mtb at MOI:5 for the indicated durations. We observed a significant increase in cell death in Mtb-infected THP-1 cells and hMDMs beginning at day 1 post-infection, with levels continuing to rise and reaching a peak around day 3. Approximately 50–60% of infected THP-1 cells died by day 3, whereas ~30% of uninfected (UI) THP-1 cells exhibited cell death at or after day 3. In contrast, UI hMDMs showed <10% cell death at most time points, reflecting their overall healthy status without Mtb infection. No further increase in AK or LDH release was observed in the Mtb-infected groups at days 4 or 5 compared with day 3, likely due to degradation of released enzymes at later time points. In addition, the presence of gentamicin in the chase medium kills extracellular Mtb and helps mitigate any additional cell death resulting from secondary infection events. Accordingly, subsequent analyses in this study focused on days 1–3 post-infection for both THP-1 cells and hMDMs. Earlier time points may also be prioritized to minimize interference from background cell death resulting from natural aging or reduced healthiness following PMA differentiation.

The AK release assay and the LDH release assay both measure the level of plasma membrane rupture and can therefore be used interchangeably, with comparable data quality. However, the AK release assay exhibited a high background signal due to the presence of FBS in the culture medium (data not shown). To mitigate this issue, we subsequently transitioned entirely

to the LDH release assay. Representative LDH release data from infected and uninfected THP-1 cells at 1–3 d post-infection are shown in **Fig. 16K**.

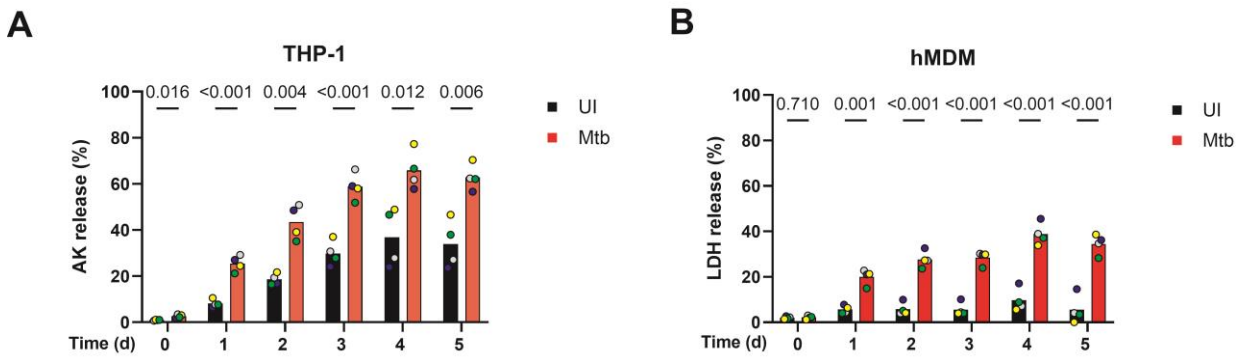

Fig. 5: Kinetics of Mtb-mediated cell death induction.
THP-1 cells (**A**) and hMDMs (**B**) were infected with H37Rv Mtb at an MOI of 5 for 4 h. **A** Mean percentages of AK release relative to the lysis control. Each colored dot represents an independent experiment (N = 4). **B** Mean percentages of LDH release relative to the lysis control. Each dot represents an independent experiment, with colors indicating distinct human monocyte donors (N = 4).

Previous work suggested that Mtb infection induces a cell death pathway dependent upon type I IFN signaling [265]. To test the correlation between the IFNAR signaling pathway and cell death, we performed an IFNAR neutralization assay to determine whether IFNAR inhibition could rescue THP-1 cells from Mtb infection. Control experiments assessed the efficacy and duration of IFNAR neutralization by stimulating THP-1 cells with IFN-β in the presence or absence of the IFNAR-neutralizing antibody (Ab), followed by immunoblotting for phosphorylated STAT1 (pSTAT1) and total STAT1 (**Fig. 6A–D**). With the addition of 100 ng/mL IFNAR neutralizing antibody, the relative STAT1 phosphorylation level was decreased by 55%–90% at different time points in a representative experiment. A dose-response experiment further showed that STAT1 phosphorylation was reduced by ~70% when the Ab was used at 100 ng/mL. Considering both the efficacy and antibody availability, 100 ng/mL was used for the following infection experiments.

The optimized experimental conditions were then applied to Mtb-infected THP-1 cells. THP-1 cells were infected with w.t. H37Rv Mtb at MOI:5, followed by IFNAR neutralization. pSTAT1 and total STAT1 (tSTAT1) were immunoblotted to confirm the effective IFNAR blockade. The results confirmed that STAT1 is activated during Mtb infection in THP-1 cells and that IFNAR neutralization effectively inhibits STAT1 phosphorylation (**Fig. 7A–D**). Across four independent experiments, the ratio of pSTAT1 to total STAT1 did not significantly change (**Fig. 7C**), while a significant decrease in the ratio of STAT1 to β-actin (β-act) was observed (**Fig. 7D**) (one outlier was identified and excluded by Grubbs' test at $\alpha = 0.05$). This may reflect a concomitant reduction in both pSTAT1 and tSTAT1 levels, leading to an unchanged ratio. Despite effective IFNAR blockade, no significant decrease in LDH release was observed in Mtb-infected THP-1 cells (**Fig. 7E**), indicating that IFNAR inhibition does not attenuate cell death in them. Furthermore, the ELISA result revealed that while IFN-β is produced during Mtb infection (**Fig.**

7F), the absolute levels are low. These findings collectively suggest that type I IFNs are not actively involved in THP-1 cell death during *ex vivo* Mtb infection.

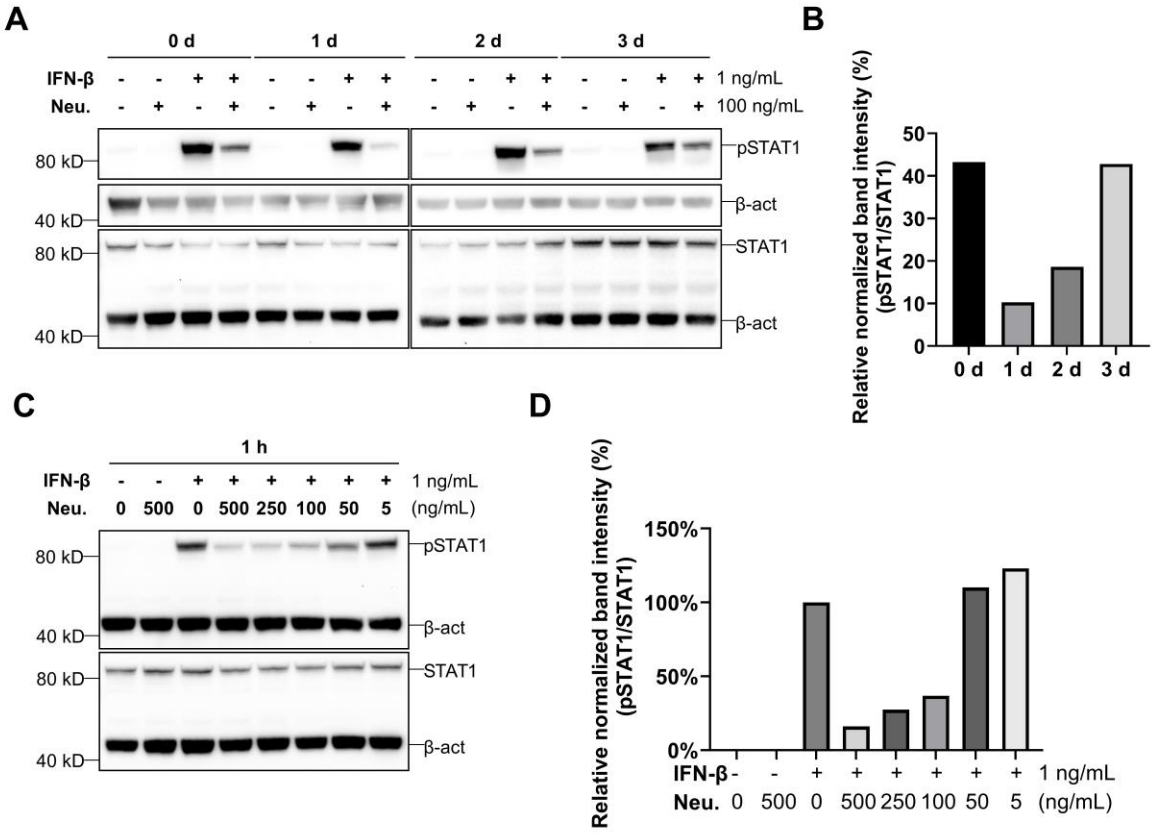

Fig. 6: Optimization of the Interferon-alpha/beta receptor (IFNAR) neutralizing assay.
A Immunoblot images showing STAT1 expression and phosphorylation in THP-1 cells following IFN-β treatment and IFNAR neutralization at various time points. Images are from a single experiment (N = 1). **B** Quantification of band intensities shown in **A**. **C,** Western blot images showing STAT1 expression and phosphorylation in response to increasing concentrations of IFN-β and IFNAR neutralization. Images are from a single experiment (N = 1). **D** Quantification of band intensities shown in **C**.

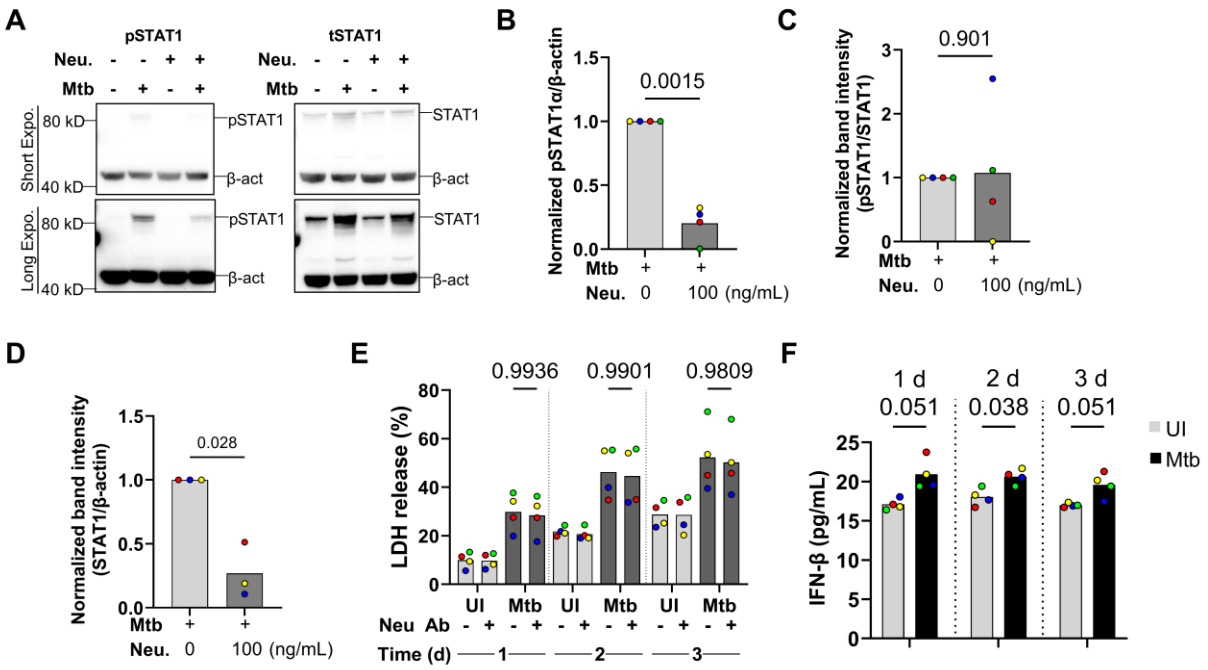

Fig. 7: Evaluation of the involvement of IFN-β in Mtb-induced cell death.
A Representative western blot images showing STAT1 expression and phosphorylation following Mtb infection and IFNAR neutralization. Data are representative of four independent experiments. **B–D** Quantification corresponding to **A**, showing the relative ratio of p-STAT1α to β-actin (**B**), p-STAT1α to STAT1 (**C**), and the normalized STAT1/β-actin ratio (**D**). For **B–D**, each colored dot represents an independent experiment (N = 4). Welch's t-tests were used for statistical analysis, and *p*-values are shown on the graphs. For **D**, Grubb's test identifies and excludes an outlier at α = 0.05. **E** THP-1 cells were infected with H37Rv Mtb at MOI:5 for 1–3 days. IFN-β secretion was measured by ELISA. **F** Percentages of LDH release relative to the positive control. Each colored dot represents an independent experiment (N = 4). Two-way ANOVA was performed for panel **F**, with *p*-values presented accordingly.

2.4 Discussion

In this chapter, *ex vivo* infection models of THP-1 cells and hMDMs are first established. Our methods for differentiating THP-1 cells and hMDMs are based on a previous study in which the authors demonstrated that THP-1 cells differentiated by PMA (50 ng/mL) for 2 days and rested for an additional 2 days transcriptionally resemble hMDMs[266]. We used THP-1 cells and hMDMs to investigate the modalities of cell death associated with Mtb infection. Kinetic assays were performed to determine the time window in which an adequate amount of cell death could be observed while the extent of material degradation remained limited. THP-1 cells and hMDMs undergo significant necrosis within the first 3 days post-infection (**Fig. 5A** and **B**). The duration of subsequent infection experiments was determined by these kinetic assays, based on the extent of cell death induction and material degradation. The first 3 days were therefore selected as the time window for harvesting samples for cell death-related analyses.

Previous work in murine macrophages showed that type I IFN signaling is involved in Mtb-mediated cell death induction[265]. Nevertheless, work by the same group demonstrated that Mtb infection of hMDMs and THP-1 cells did not induce substantial secretion of type I IFNs, and that blocking type I IFN signaling did not affect cell death induction[267]. Consistent with this study, we show that IFN-β signaling is not involved in cell death signaling during the first three days of Mtb infection in THP-1 cells (**Fig. 7E**) and that Mtb infection results in only a minimal increase in IFN-β production (**Fig. 7F**), as we also previously showed for hMDM[268]. Our studies highlight differences between murine and human macrophages in the cell death pathways activated following Mtb infection.

Chapter 3: Analysis of apoptosis induction after Mtb infection

3.1 Abstract

Mtb can induce apoptosis in human macrophage models *ex vivo*. In general, apoptotic cell death is considered host-beneficial, whereas necrotic forms of cell death can exacerbate tuberculosis (TB) pathology and tissue damage. The cell death modalities associated with *Mtb* infection are highly context-dependent. Early studies demonstrated that human macrophages exposed to specific cytokines, such as TNF-α, exhibit enhanced apoptosis during *Mtb* infection. However, Mtb also employs virulence factors to inhibit apoptosis. For example, our previous work identified nuoG as an Mtb virulence factor that suppresses apoptosis in human macrophages.

In Chapter 2, kinetic assays revealed substantial cell lysis (necrosis) during *Mtb* infection. Chapter 3 builds upon these findings by determining the extent of apoptosis induced in THP-1 cells and hMDMs under the same experimental conditions established in Chapter 2. In this chapter, YO-PRO-1 and Draq7 staining were used to distinguish early apoptosis from necrotic cell death. In parallel, activation of the canonical apoptotic signaling pathway was assessed by WB. Our results show that *Mtb* induces only minor levels of apoptosis in THP-1 cells and hMDMs during the first 3 days of infection. Secondary necrosis following apoptosis was detected in THP-1 cells but not in hMDMs. Collectively, these findings indicate that apoptosis is not a significant form of cell death induced by *Mtb* in human macrophages.

3.2 Materials and Methods

Cell cultures and differentiation

Human peripheral blood mononuclear cells (PBMCs) were isolated from LeukoPak according to the protocol as previously described[269]. CD14+ monocytes were purified using CD14 MicroBeads (Miltenyi Biotech, CA, USA; 130-050-201), with the bead volume reduced to one-third of the manufacturer's recommended amount. All other steps were performed according to Miltenyi Biotech's instructions. To obtain human monocyte-derived macrophages (hMDMs), monocytes were pelleted and resuspended at 1×106 cells/mL in hMDM growth medium consisting of RPMI 1640, 10% FBS, 5% human AB serum (GeminiBio, CA, USA; 100-318-100), and 10 ng/mL human M-CSF (Bio-Techne, MN, USA; 216-MCC-010). Monocytes were seeded in uncoated 24-well plates at the same density as THP-1 cells. On day 3 post-seeding, additional growth medium was added, and the medium was replaced every 3 days thereafter. hMDMs were used for the following experiments on day 7 or 9 post-differentiation.

YO-PRO-1 and DRAQ7 staining and analysis

THP-1 cells or hMDMs were seeded in 8-well chamber slides and infected with dsred H37Rv *Mtb* at an MOI of 5 for pulse-chase experiments or left uninfected. At the indicated time points, the culture medium was replaced with 200 µL of staining solution containing 0.5 µM YO-PRO-1 (Biotium) and 0.3 µM DRAQ7™ (Invitrogen, D15106). Cells were stained at 37 °C for 15 min and immediately imaged. For each condition and experimental repeat, more than 200 cells were analyzed.

Confocal microscopy

Cells were imaged using a Zeiss LSM 800 laser scanning confocal microscope equipped with two gallium arsenide phosphide photomultiplier tube (GaAsP-PMT) detectors and one transmitted light photomultiplier tube (T-PMT) detector. A 40×/NA 1.2 water immersion objective was used for all imaging experiments.

For time-lapse live-cell imaging, the observation chamber was maintained at 37°C with 5% CO_2 supplied via a humidified incubator. Z-stacks spanning 10 µm with 1 µm intervals were acquired every 10 minutes for up to 20 hours. Each field consisted of 11 optical slices. A total of four fields were imaged, with a maximum of two experimental conditions per experiment. Each image spanned an area of 319.45 × 319.45 µm, corresponding to 2048 × 2048 pixels. For immunofluorescence microscopy, 3-4 fields were imaged with Z-stacks spanning 20 µm with 1 µm interval. 1 slice with proper signals was selected for MFI quantification. Airyscan confocal microscopy and 3D volume rendering were performed using a Zeiss LSM 980 microscope with the same 40×/NA 1.2 water objective.

3.3 Data availability (applied throughout this dissertation)

Datasets generated from time-lapse live-cell imaging experiments, along with files used for image analysis, are publicly available via Mendeley Data[270] at **DOI: 10.17632/rkbw676zf2.3** (https://data.mendeley.com/datasets/rkbw676zf2/3).

3.4 Results

3.3.1 Analysis of apoptosis induction in THP-1 cells and hMDMs during the first three days of Mtb infection

To ensure that YO/Draq7 double staining accurately distinguishes early apoptotic from late apoptotic or necrotic cells, a control experiment was performed. THP-1 cells were treated with MG132, an inducer of apoptosis, and then stained and subjected to time-lapse live-cell imaging to validate that YO and Draq7 reliably discriminate early apoptotic and necrotic cells (**Fig. 8A**, also see **supplementary video (SV) 1**).

After validating this method, the same staining protocol was applied to THP-1 cells or hMDMs infected with dsRed H37Rv Mtb at MOI:5. Fluorescence microscopy showed that more than 90% of cells were infected at 1, 2, and 3 d post-infection (**Fig. 9B** and **D**), whereas fewer than 6% of total cells exhibited an early apoptotic phenotype in THP-1 cells and less than 2 % in hMDMs (**Fig. 9A** and **C**; **Fig. 10A** and **B**).

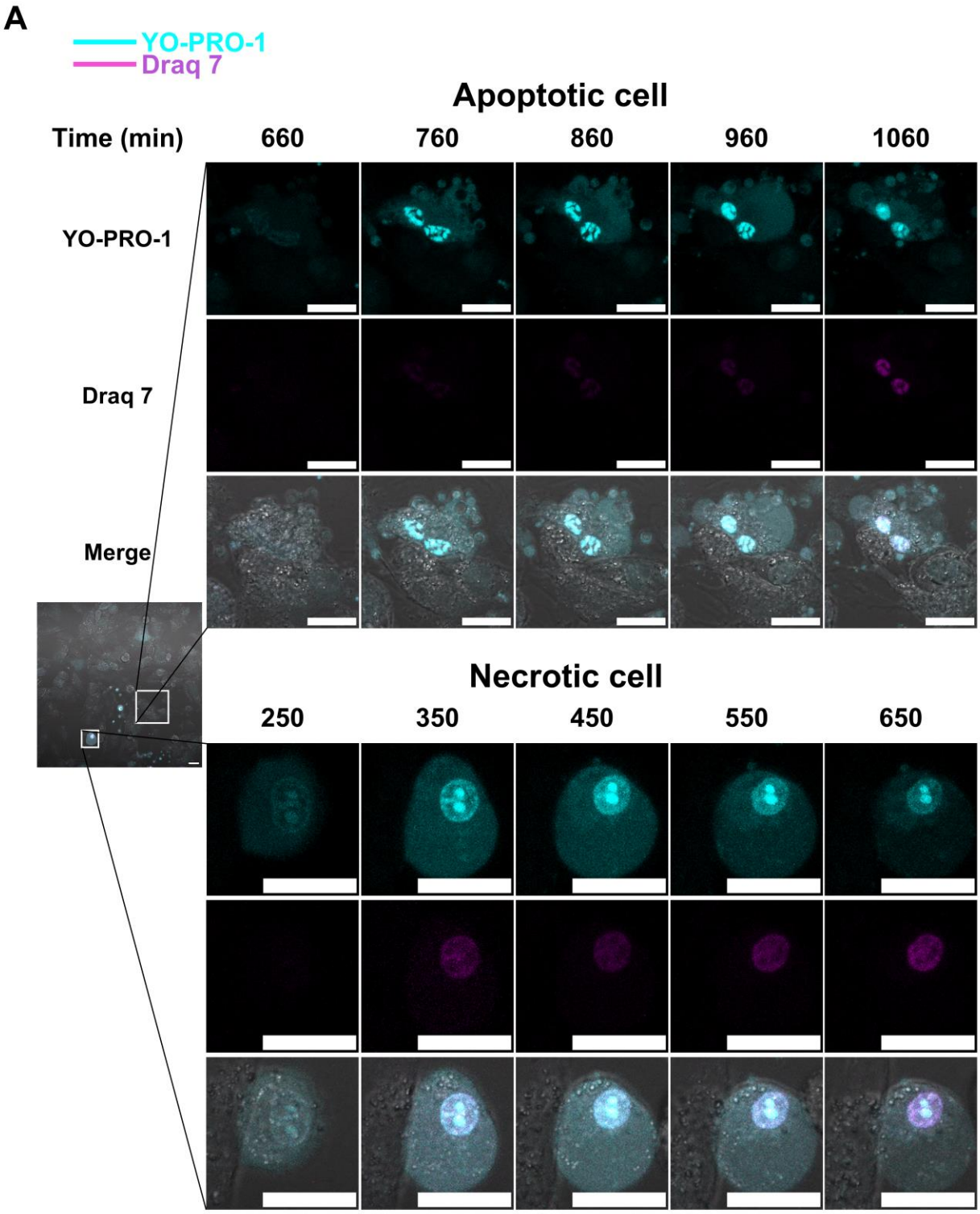

Fig. 8: Validation of YO-PRO-1 and Draq7 staining in distinct cell death modalities.
A Representative confocal fluorescence images of THP-1 cells treated with 10 µM MG132 (N = 1). Following MG132 addition, cells were stained with YO-PRO-1 (100 nM) and Draq7 (300 nM)

for 15 min before initiating time-lapse live-cell imaging. Cells were maintained at 37 °C and 5% CO_2 and imaged continuously for 20 h. Z-stack images (11 slices at 1 μm intervals) were captured every 10 min. Regions containing cells exhibiting characteristic apoptotic or necrotic morphology were selected and enlarged. Fluorescence signals for YO-PRO-1 (cyan), Draq7 (magenta), and merged images with transmitted-light overlays are shown. Five representative time points are displayed for each condition. The necrotic-cell image layout is identical to that of the apoptotic-cell panel. Scale bars: 20 μm.

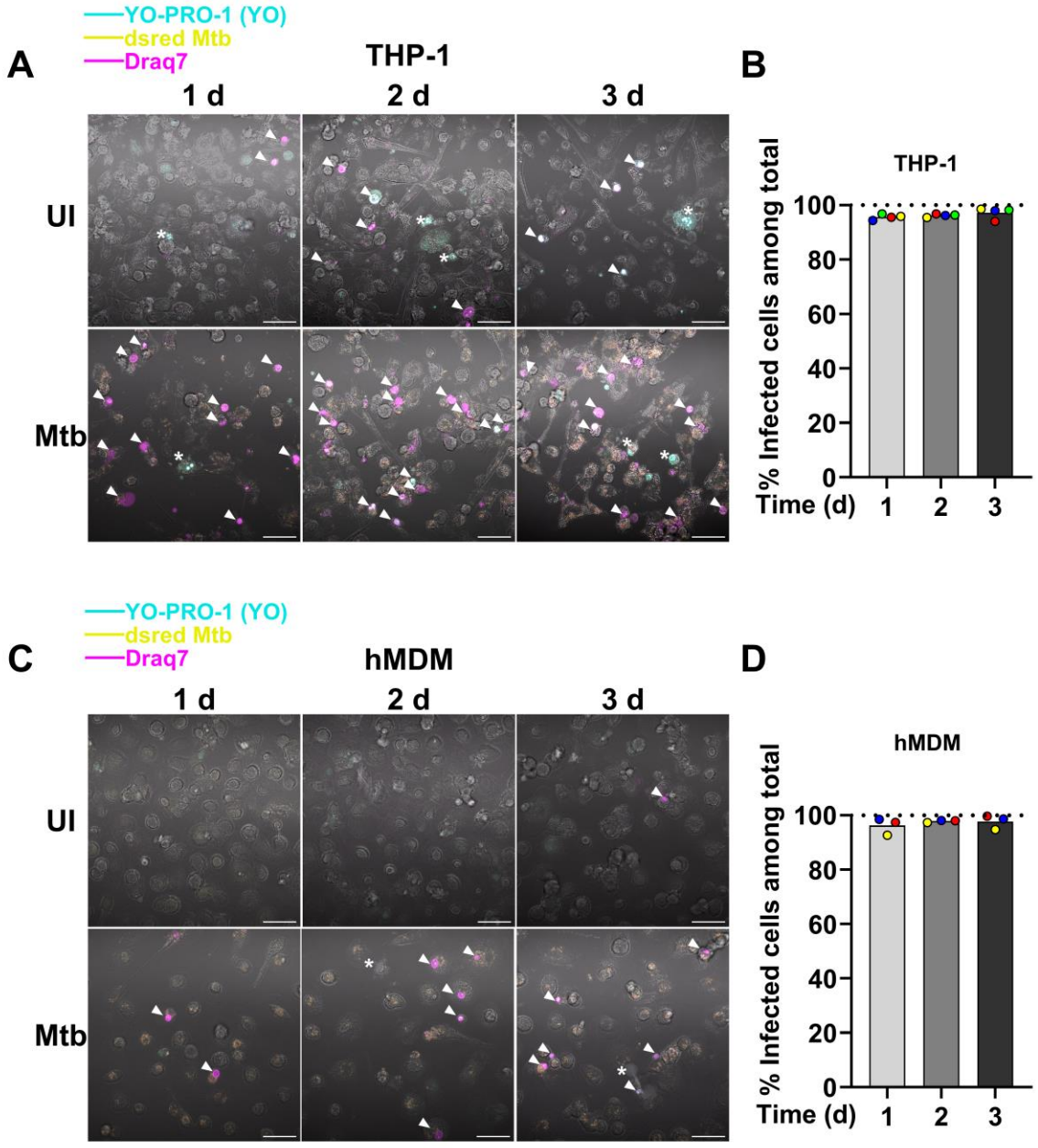

Fig. 9: Assessing early apoptosis by YO-PRO-1 and Draq7 staining in Mtb-infected THP-1 cells.

A, C Representative confocal fluorescence images of THP-1 (**A**) or hMDMs (**C**). THP-1 cells (N = 4) or hMDMs (N = 3) were infected with dsred H37Rv Mtb at MOI:5 for 1, 2, or 3 d. Cells were stained with YO-PRO-1 and Draq 7 for 15 min at 37 °C prior to imaging. Z-stack images (11 slices at 1 µm intervals) were captured for each field of view (FoV). White triangles indicate necrotic cells, while asterisks indicate early apoptotic cells. Fluorescence signals for YO-PRO-1 (cyan), Draq7 (magenta), dsred (yellow), and transmitted-light signals are merged. Scale bars: 50 µm. **B,**

D Quantification of percentages of infected cells among total cells for THP-1 cells (**B**) or hMDMs (**D**).

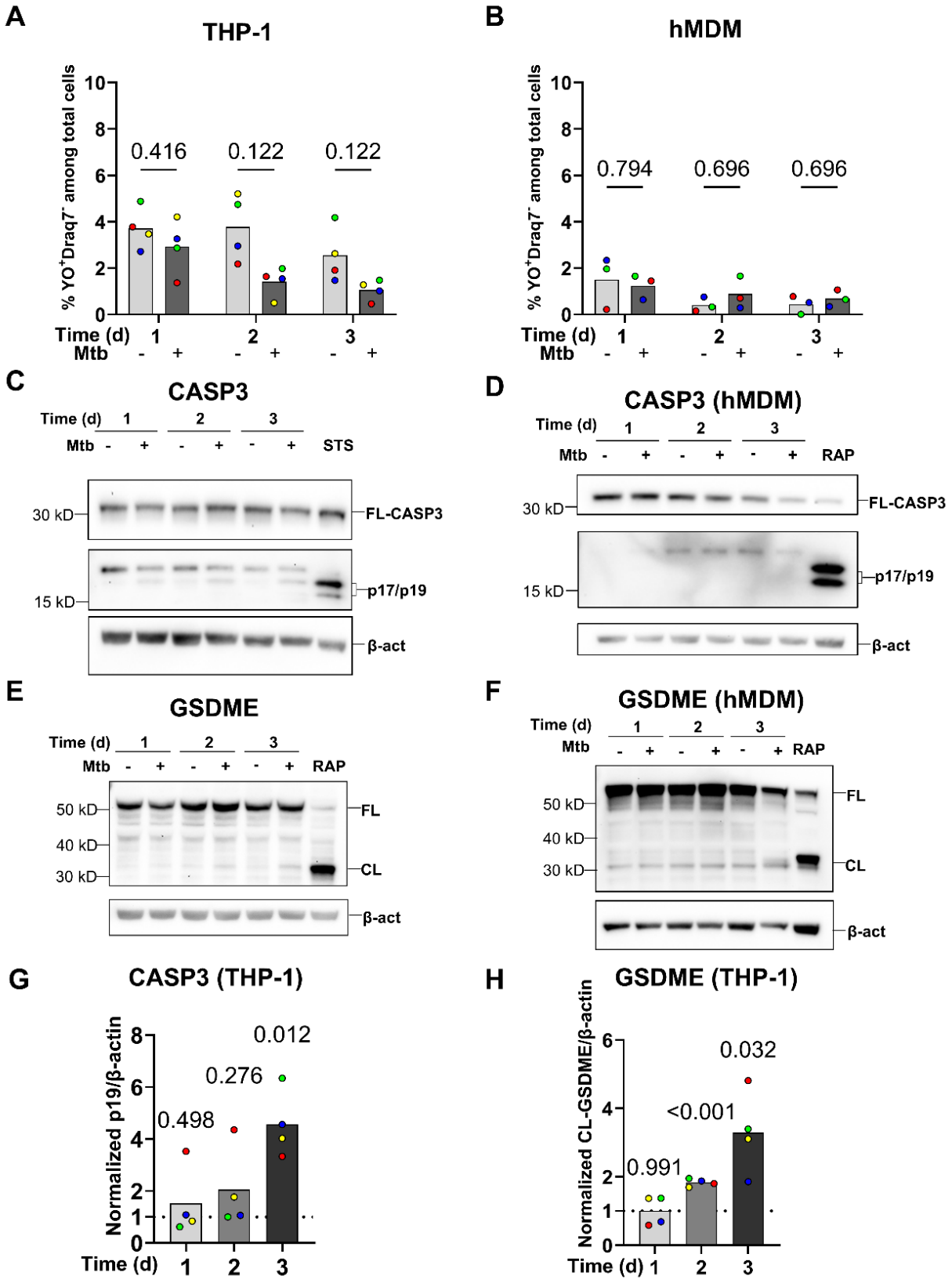
A
THP-1
% YO+Draq7- among total cells
0.416
0.122
0.122
Time (d) 1 2 3
Mtb - + - + - +
B
hMDM
% YO+Draq7- among total cells
0.794
0.696
0.696
Time (d) 1 2 3
Mtb - + - + - +
C
CASP3
Time (d) 1 2 3
Mtb - + - + - + STS
30 kD
FL-CASP3
15 kD
p17/p19
β-act
D
CASP3 (hMDM)
Time (d) 1 2 3
Mtb - + - + - + RAP
30 kD
FL-CASP3
15 kD
p17/p19
β-act
E
GSDME
Time (d) 1 2 3
Mtb - + - + - + RAP
50 kD
40 kD
30 kD
FL
CL
β-act
F
GSDME (hMDM)
Time (d) 1 2 3
Mtb - + - + - + RAP
50 kD
40 kD
30 kD
FL
CL
β-act
G
CASP3 (THP-1)
Normalized p19/β-actin
0.012
0.276
0.498
Time (d) 1 2 3
H
GSDME (THP-1)
Normalized CL-GSDME/β-actin
0.032
<0.001
0.991
Time (d) 1 2 3

Fig. 10: Mtb H37Rv induces marginal CASP3 activation in THP-1 cells but not in hMDMs. **A, B** Percentage of early apoptotic cells among total cells assessed by fluorescence microscopy. THP-1 cells were infected with dsRed-expressing H37Rv Mtb at MOI:5 for 4 h, stained with YO and Draq7, and imaged at 1, 2, or 3 d post-infection. More than 200 cells were analyzed per time point in each replicate (N = 3). Multiple paired t-tests were performed to compare infected groups with uninfected groups. and p-values are shown in the graphs. Each colored data point represents an independent experiment (**A**, THP-1, N = 4) or a distinct donor (**B**, hMDM, N = 3). **C**–**H** THP-1 cells were infected with H37Rv Mtb at MOI:5 for 4 h or left uninfected. Cells were lysed after 1-3 d. C–F, Representative western blot images showing the cleavage of CASP3 (**C** and **D**) and GSDME (**E** and **F**) in THP-1 cells (**C** and **E**) or hMDMs (**D** and **F**), respectively. FL: full-length target protein. CL: cleaved target protein. STS: Staurosporine (1 μM, 6 h). RAP: Raptinal (10 μM, 6 h). **G** and **H**, bar graphs showing the quantification of normalized band intensities corresponding to THP-1 cleaved CASP3 (**G**), and GSDME (**H**). Each value in the infected groups was normalized to its uninfected counterpart from the same experiment. Band intensities were quantified using ImageLab software. One-sample t-tests were performed to compare the normalized values to 1, and p-values are shown in the graphs. Each colored data point represents an independent experiment (N = 4).

To further assess activation of apoptotic signaling pathways during Mtb infection, CASP3 and GSDME activation were examined by immunoblotting, as they are critical executioners of apoptosis and secondary necrosis. In THP-1 cells, cleaved (activated) CASP-3 and GSDME were readily detected, indicating significant activation (**Fig. 9C, E, G,** and **H**). In contrast, activated CASP3 or GSDME bands were not detected in hMDMs (**Fig. 10D** and **F**). Given that a significant level of CASP-3 activation was observed, the next question was whether the apoptotic signaling pathway is fully activated. We therefore analyzed the activation of the upstream initiator caspases CASP8 and CASP9 by immunoblotting (**Fig. 11A**–**D**), which revealed no detectable activation during Mtb infection. Collectively, these data indicate that, in Mtb-infected THP-1 cells, a subset of cells undergoes secondary necrosis, whereas early apoptotic events are infrequent and difficult to capture. In hMDMs, apoptotic cells are rare (~2%) during Mtb infection and are detectable only by single-cell microscopic analysis.

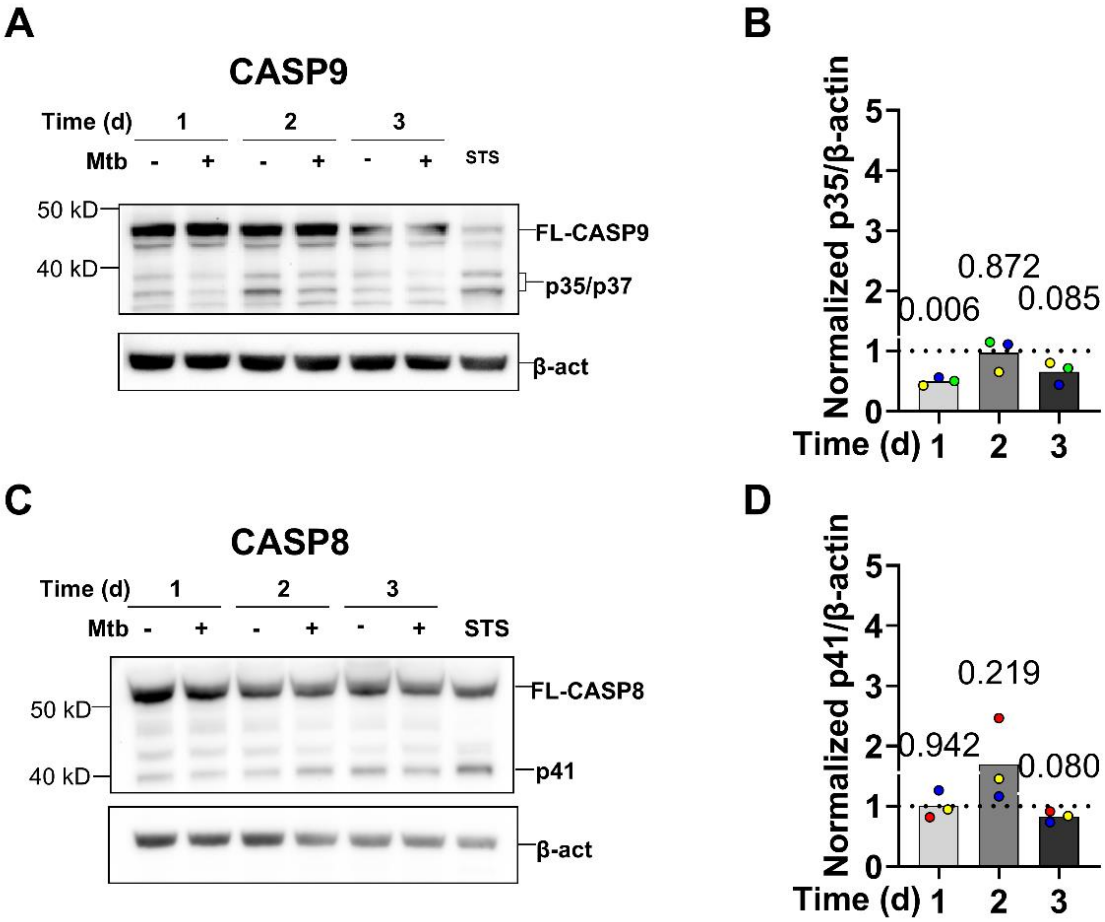

Fig. 11: Mtb H37Rv does not induce CASP8 or 9 activation in THP-1 cells.
A, C Representative western blot images showing the cleavage of CASP9 and CASP8, respectively. THP-1 cells were infected with H37Rv Mtb (+) at MOI 5 for 4 h or left uninfected (-). Cells were lysed after 1-3 d. STS: Staurosporine (1 μM, 6 h). **B, D** Bar graphs showing the quantification of normalized band intensities corresponding to THP-1 cleaved CASP9 (**B**), and CASP8 (**D**). Each value in the infected groups was normalized to its uninfected counterpart from the same experiment. Band intensities were quantified using ImageLab software. One-sample t-tests were performed to compare the normalized values to 1, and p-values are shown in the graphs. Each colored data point represents an independent experiment (N = 3).

3.5 Discussion

Mtb limits the induction of host cell apoptosis to increase its virulence[181,182,271]. Consistently, the attenuated Mtb strain H37Ra induced an increased level of apoptosis compared to its virulent isogenic counterpart H37Rv[185,272]. Several Mtb proteins have been described to mediate the inhibition of host cell apoptosis[182,271]. For example, NuoG is a subunit of the type 1 NADH dehydrogenase of Mtb and a virulence factor involved in Mtb's capacity to inhibit apoptotic cell death[186]. Mtb-infected THP-1 cells showed less than a 10% increase in apoptosis compared to uninfected controls, even after 5 days of infection[185,186,199].

Consistent with these findings, our YO-PRO-1 and Draq7 staining revealed that fewer than 6% of THP-1 cells underwent apoptosis during *Mtb* infection, whereas only ~2% of hMDMs exhibited an apoptotic phenotype. Accordingly, our observation of minimal (THP-1 cells) to undetectable (hMDMs) CASP3 activation (**Fig. 10C, D,** and **G**) aligns well with previous reports[185,186,199]. Notably, substantial GSDME activation was detected in THP-1 cells but was not observed in hMDMs. Given that neither CASP8 nor CASP9 activation was detected during Mtb infection, as assessed by WB analysis (**Fig. 11**), THP-1 cells do not appear to engage a canonical apoptotic program. Instead, the CASP-3 and GSDME activation observed in THP-1 cells may represent a secondary consequence of other cell death pathways. In hMDMs, apoptotic events during Mtb infection were rare and detectable only by microscopy at the single-cell level. Collectively, these results indicate that apoptosis is not a major form of cell death in *ex vivo* human macrophage models during Mtb infection.

Chapter 4: Analysis of pyroptosis and necroptosis after Mtb infection

4.1 Abstract

Previous studies have demonstrated that IL-1β and ASC are host-protective in *in vivo* murine models, suggesting that pyroptosis—whether it occurs in macrophages—may limit TB pathology. Subsequent studies reported that *ex vivo* murine and human macrophage models undergo pyroptosis during Mtb infection. However, data directly addressing whether Mtb induces pyroptosis in hMDMs remain limited. In addition, our previous work demonstrated that Mtb attenuates pyroptosis in BMDMs via the virulence factor PknF. In line with our conclusion that Mtb can dampen pyroptosis, another group approached this question from a different angle and showed that Mtb inhibits pyroptosis through an ubiquitin-dependent mechanism involving the secreted phosphatase PtpB, which ultimately restrains GSDMD pore-forming activity at the plasma membrane.

Dr. Robert Watson's work further identified an interconnection between pyroptotic and necroptotic signaling pathways. In murine macrophage models, GSDMD activation precedes and is required for necroptosis induction. Thus, if human macrophages undergo pyroptosis during Mtb infection, it is plausible that necroptosis may be concurrently engaged.

In this chapter, we show that Mtb induces a significant increase in GSDMD cleavage in THP-1 cells, but not in hMDMs, indicating differential engagement of pyroptotic signaling between these two human macrophage models. In contrast, phosphorylation of MLKL was not detected in either THP-1 cells or hMDMs during Mtb infection, indicating that necroptosis is not induced during Mtb infection in THP-1 cells or hMDMs.

4.2 Materials and Methods

HT-29 cell culture

The HT-29 cell line (ATCC, HTB-38; LOT: 70061450) was cultured in the same growth medium as THP-1 cells. Accutase (Millipore-Sigma, A6964) was used at 10 mL per 75 cm^2 flask to detach HT-29 cells for passaging or seeding. Cells were seeded at the same density as THP-1 cells 1 d prior to necroptosis induction. HT-29 cells were passaged every 3–4 d upon reaching approximately 80% confluence.

Cell treatments and experimental controls

For necroptosis induction, THP-1 cells, hMDMs, and HT-29 cells were pretreated with z-VAD-FMK (Cell Signaling Technology, 60332S) at 20 μM for 1 h, followed by treatment with 100 ng/mL human TNF-α (R&D Systems, 10291-TA-020) in combination with 10 μM SM-164 (Cell signaling Technology, 56003S). All treatments were conducted at 37 °C in a humidified atmosphere with 5% CO_2.

Other experimental methods used in this chapter were performed as previously described.

4.3 Results

4.3.1 Analysis of pyroptosis induction in THP-1 cells and hMDMs during Mtb infection

Given that previous studies have demonstrated pyroptosis induction in various models during Mtb infection[226,227], we investigated whether pyroptosis constitutes a major form of Mtb-induced cell death in macrophages. THP-1 cells and hMDMs were infected with H37Rv Mtb at MOI:5 for 4 h, and cell lysates were collected at 1, 2, and 3 d post-infection. Western blot analysis

revealed significant GSDMD cleavage in THP-1 cells following Mtb infection, whereas no detectable cleavage was observed in hMDMs (**Fig. 12A–D**). Quantification showed that, at 1 d post-infection, cleaved GSDMD (CL-GSDMD) levels increased by approximately 2-fold compared with the uninfected counterpart. There is no indication that later time points will show higher levels of GSDMD cleavage. The limited magnitude and lack of temporal amplification of GSDMD cleavage suggest that pyroptosis is not a predominant form of cell death during Mtb infection under these conditions. In addition, the rapid collapse of pyroptotic cells and the potential for increased inhibition of pyroptosis at later stages of infection may explain the limited detectability of this pathway over time.

Notably, the blots show two bands in the 30–32 kD region (**Fig. 12A**). We investigated whether these two bands represent specific cleaved (activated) forms of GSDMD and whether they are associated with Mtb virulence. As shown in **Fig. 13A**, both bands were detected using two independent anti-GSDMD antibodies. Infections with multiple mycobacterial strains showed that all tested strains induced GSDMD cleavage and cell lysis, resulting in the same two bands (**Fig. 13B–E**). The positive control confirmed that the upper band corresponds to the cytotoxic, cleaved form of GSDMD, which is the primary focus of this study. Quantitative analyses suggest that different mycobacterial strains may induce alternative forms of GSDMD cleavage (**Fig. 15C**, **D**). However, since the lower band was consistently present across all infected conditions, it is unlikely to be specifically associated with Mtb virulence.

Another hallmark of pyroptosis induction is the secretion of IL-1β. The ELISA (**Fig. 15F**) results also demonstrated that THP-1 cells secreted significant amounts of IL-1β during Mtb infection, reaching approximately 100 pg/mL at days 1 and 3 post-infection. It is well-established that the secretion of IL-1β from Mtb-infected cells *ex vivo* is dependent on inflammasome

components and activity[215,223,224], although one study showed that the secretion of IL-1β from Mtb-infected cells *ex vivo* is independent of GSDMD[273]. Both our previous findings[227] and the data presented in this study (**Fig. 26E**) indicate that IL-1β secretion from infected THP-1 cells is mediated by the non-canonical inflammasome CASP4/5. Therefore, the detected IL-1β secretion indicates pyroptosis induction in Mtb-infected THP-1 cells.

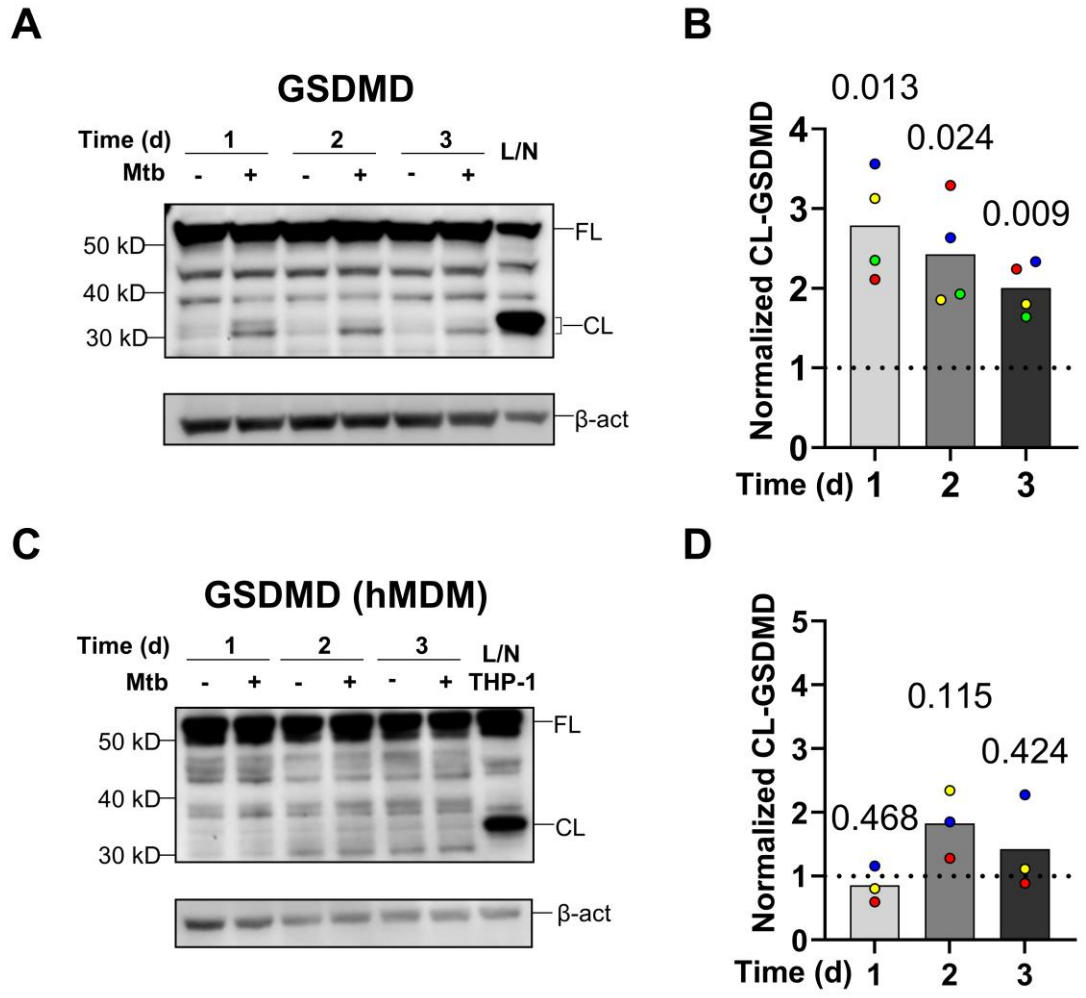

Fig. 12: H37Rv Mtb induces GSDMD cleavage in THP-1 cells but not in hMDMs.
THP-1 cells (**A** and **B**) or hMDMs (**C** and **D**) were infected with w.t. H37Rv Mtb at MOI:5 for 4 h or left uninfected. Cells were lysed after 1-3 d. **A, C** Representative western blot images showing GSDMD cleavage in THP-1 cells (**A**) and hMDMs (**C**). FL: full-length target protein. CL: cleaved target protein. L/N indicates LPS (100 ng/mL, 4.5 h) plus nigericin (20 μM, 30 min) treatment as a positive control. **B, D** Quantification of band intensities corresponding to cleaved GSDMD (**B** and **D**), as indicated next to each Western blot. Band intensities were quantified using ImageLab software, normalized to the corresponding β-actin bands, and then expressed relative to the uninfected counterparts from the same experiment. Bar graphs display the normalized band intensities of the infected groups. One-sample t-tests were used to compare normalized values to 1, and *p*-values are shown in the graphs. Each colored data point represents an independent experiment (N = 4) for THP-1 cells (**B**) or an individual human donor (N = 3) for hMDMs (**D**).

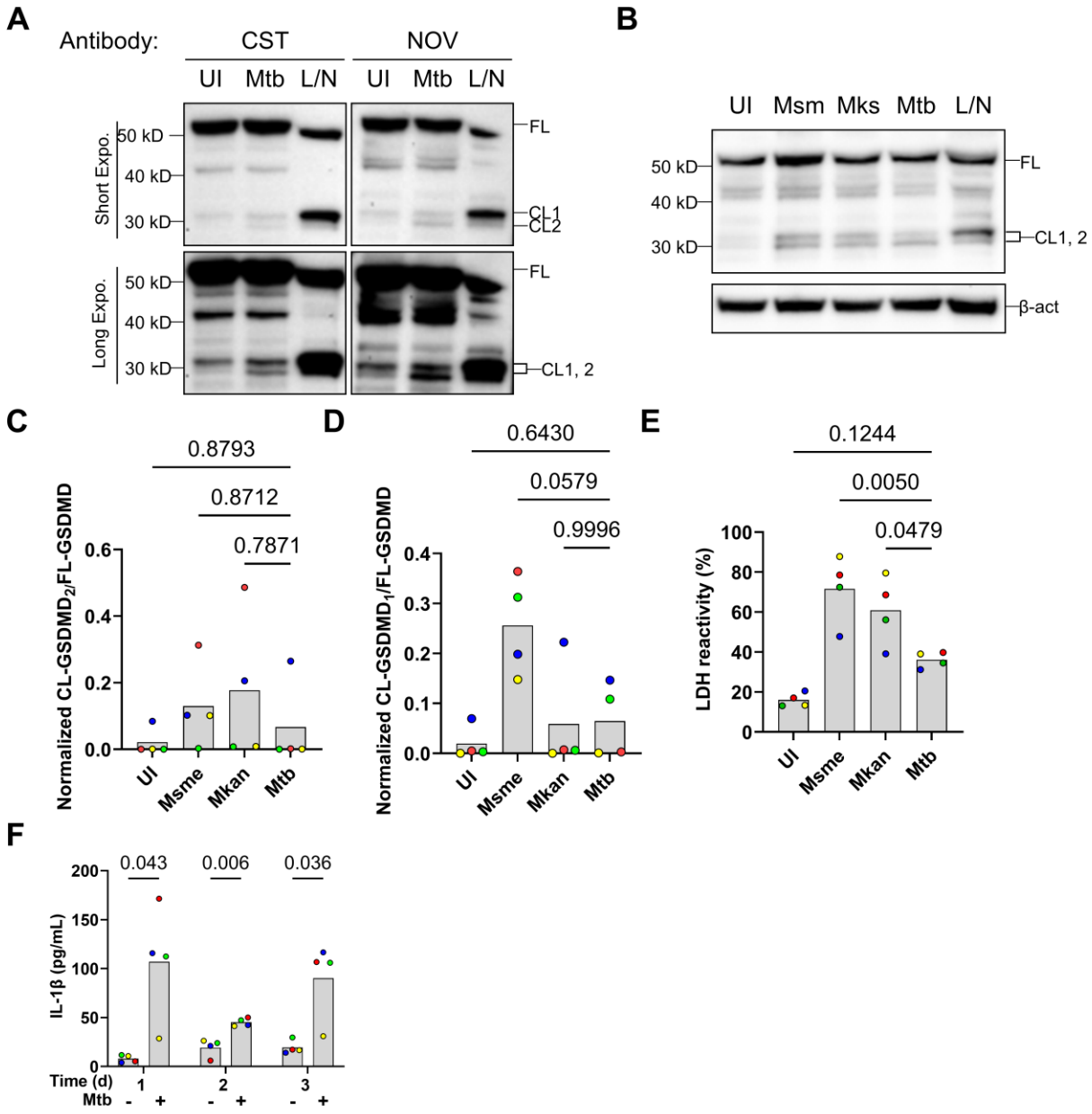

Fig. 13: Mycobacterial species induce variable GSDMD cleavage, and different cell types have distinct sensitivity to necroptosis induction.

A Immunoblot images showing GSDMD cleavage in THP-1 cells infected with Mtb H37Rv at MOI:5 for 4 h and harvested at 1 d or treated with LPS and Nigericin (L/N) or left uninfected (UI). Blots were probed using CST and NOV antibodies. Images are from one experiment (N = 1). **B** THP-1 cells were uninfected or infected with *Mycobacterium smegmatis* (Msm), *Mycobacterium kansasii* (Mkan), and Mtb, all at MOI:5 or treated with L/N. Representative western blot images showing GSDMD cleavage induced by different mycobacterial strains in THP-1 cells (N = 4). **C, D** Quantification of normalized GSDMD cleavage band intensities corresponding to **B**. **E** quantification of LDH release as a percentage of the lysis control, corresponding to **B**. Each colored data point represents an independent experiment (N = 4) for **C–E**. One-way ANOVA with

Brown-Forsythe correction was performed, and *p*-values are shown in the graphs. **F** ELISA measurement of IL-1β secretion from Mtb-infected THP-1 cells (MOI:5) at 1, 2, and 3 d. Multiple unpaired t-tests with Welch's correction were performed (N = 4). The ELISA was performed by Akshaya Ganesh (ORCID: 0000-0002-5432-118X)

4.3.2 Analysis of necroptosis induction in THP-1 cells and hMDMs during Mtb infection

GSDMD can permeabilize mitochondria, triggering ROS release and subsequent necroptosis marked by MLKL phosphorylation[235]. We next investigated whether necroptosis is induced in our cell models as a result of GSDMD activation (THP-1 cells). Despite clear GSDMD activation in THP-1 cells, we failed to detect MLKL phosphorylation at any time point (**Fig. 14A** and **B**), as shown by the pMLKL/β-actin ratio. Ratios of pMLKL to total MLKL (tMLKL) also support this statement (**Fig. 15E** and **F**). Similarly, in hMDMs, neither pyroptosis (**Fig. 12C** and **D** nor necroptosis (**Fig. 14C** and **D**) was detected under the experimental conditions.

The control experiments validate the anti-pMLKL antibody using HT-29 cells, which are highly sensitive to necroptosis induction (**Fig. 15A**). Cells treated with TNF-α, SM-164, and z-VAD-FMK (TSZ) exhibited at least a 9-fold increase in MLKL phosphorylation compared to the untreated control. Inhibition of RIPK1 by necrostatin-1 completely abrogated MLKL phosphorylation (N = 1), which further validates the pMLKL band on the WB image. While necroptosis inducers robustly activated necroptotic signaling and induced MLKL phosphorylation in HT-29 cells, no changes in MLKL phosphorylation were detected in THP-1 cells or hMDMs (**Fig. 15B–D**). To date, we have not identified optimized, practical conditions that induce robust necroptosis in THP-1 cells or hMDMs.

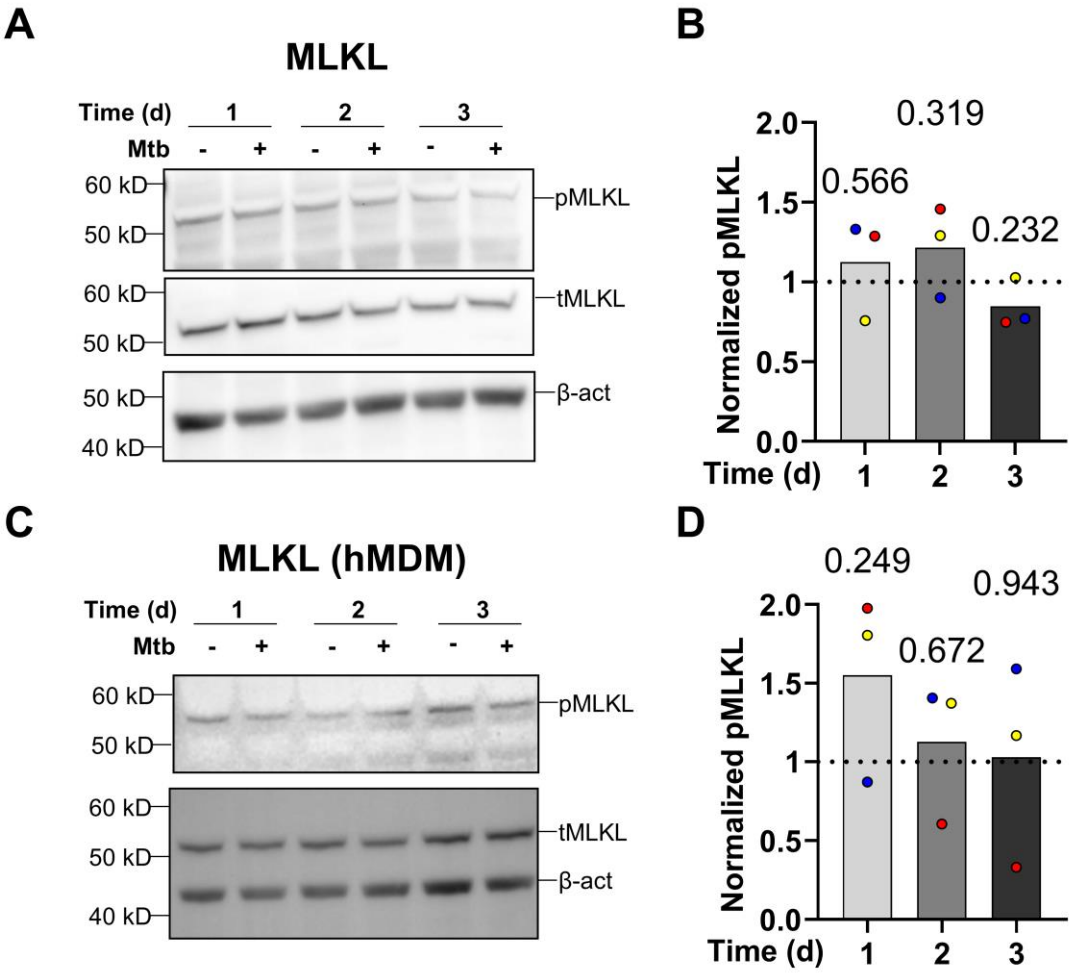

Fig. 14: H37Rv Mtb does not induce MLKL phosphorylation in THP-1 cells or hMDMs. THP-1 cells (**A** and **B**) or hMDMs (**C** and **D**) were infected with w.t. H37Rv Mtb at MOI:5 for 4 h or left uninfected. Cells were lysed after 1-3 d. **A, C** Representative WB images showing MLKL phosphorylation in THP-1 cells (**A**) and hMDMs (**C**). **B, D** Quantification of band intensities corresponding to phosphorylated MLKL (**A** and **C**), as indicated next to each Western blot. Band intensities were quantified using ImageLab software, normalized to the corresponding β-actin bands, and then expressed relative to the uninfected counterparts from the same experiment. Bar graphs display the normalized band intensities of the infected groups. One-sample t-tests were used to compare normalized values to 1, and *p*-values are shown in the graphs. Each colored data point represents an independent experiment (N = 3) for THP-1 cells (**A**) or an individual human donor (N = 3) for hMDMs (**C**).

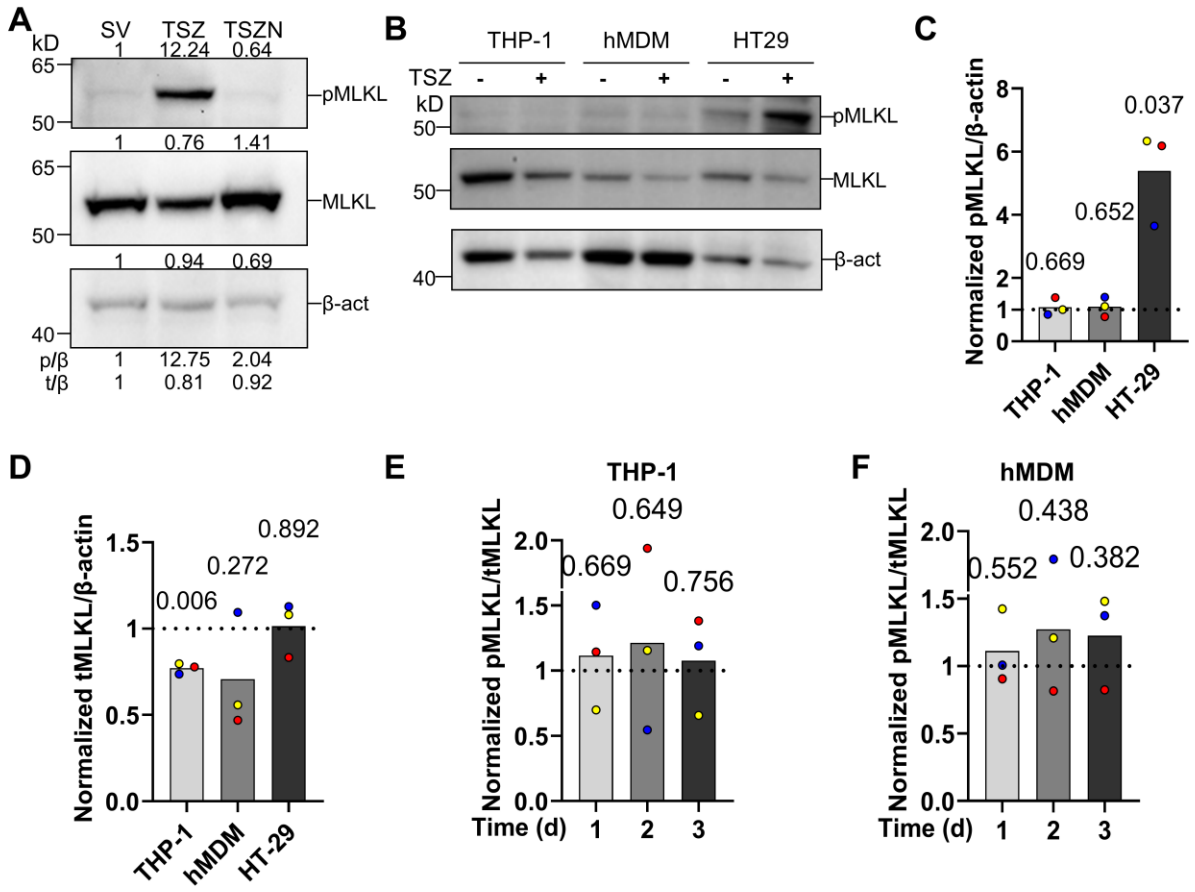

Fig. 15: Validation of anti-pMLKL antibody and quantifications supplement previous WB analysis.

A Western blot analysis of MLKL phosphorylation during necroptosis induction or inhibition in different cell types. SV, solvent control (0.3% DMSO); TSZ, TNF-α (100 ng/mL, O/N), SM-164 (10 µM, O/N), and zVAD-FMK (20 µM, O/N); TSZN, TSZ plus necrostatin-1 (10 µM, O/N). G, HT-29 cells were treated with SV, TSZ, or TSZN (N = 1). Band intensities were quantified using ImageLab software and normalized to SV for each target protein; normalized values are shown above the corresponding bands. **B** THP-1 cells, hMDMs, or HT-29 cells were treated with SV or TSZ. **C, D** Quantification of normalized band intensities corresponding to phosphorylated MLKL is shown. Values from TSZ-treated samples were normalized to their SV-treated counterparts from the same experiment. Band intensities were quantified using ImageLab software. One-sample t-tests were performed to compare normalized values to 1, and p-values are shown in the graphs. Each colored data point represents an independent experiment using THP-1 cells or a distinct human donor for hMDMs (N = 3). **E, F** Quantification of normalized band intensities corresponding to phosphorylated MLKL from **Fig. 12B** or **D,** respectively. One-sample t-tests were performed to compare normalized values to 1, and p-values are shown in the graphs. Each colored data point represents an independent experiment (N = 3) for THP-1 cells (**Fig. 15E**) or distinct human donors (N = 3) for hMDMs (**Fig. 15F**).

4.4 Discussion

Our data reveal a divergence in inflammasome activation: while we observe GSDMD induction in THP-1 cells (**Fig. 12A** and **B**), we detect none in hMDMs (**Fig. 12C** and **D**). The IL-1β secretion from Mtb-infected THP-1 cells was detected (**Fig. 13F**). However, the concentration is substantially lower than that reported in other studies[224,273]. This induction of pyroptosis is consistent with Dr. Trude Flo's previous study[274]. While differences in cell culture and differentiation conditions, as well as infection protocols, may contribute to this discrepancy, our findings suggest that pyroptosis is only modestly induced in THP-1 cells during Mtb infection. PMA, a standard agent for differentiating THP-1 cells, induces calcium influx. This increase in intracellular Ca^{2+} may potentiate inflammasome activation in THP-1 cells upon Mtb infection. Nevertheless, we let PMA-treated THP-1 cells rest for 2 days before infection, so it is unlikely that PMA treatment is the primary factor driving increased inflammasome activation. Alternatively, THP-1 cells do not express the protein Sterile Alpha And TIR Motif Containing 1 (SARM1), a global inhibitor of inflammasomes present in human macrophages, which renders THP-1 cells more sensitive to inflammasome activation compared to hMDMs[275]. Interestingly, while there is some GSDMD activation in THP-1 cells (**Fig. 12A** and **B**), this does not seem to result in overt pyroptosis since there was no effect of CASP4/5 deletion on cell death (**Fig. 26**). This result is consistent with our published data showing that the non-canonical inflammasome pathway is essential for inflammasome activation in THP-1 cells but does not affect cell death and lysis as measured by LDH release assay and Syt G staining[227].

In addition, MLKL phosphorylation was not detected in either THP-1 cells or hMDMs during Mtb infection (**Fig. 14A–D**), indicating that necroptosis is not induced under our

experimental conditions and that GSDMD cleavage does not lead to downstream MLKL phosphorylation.

Chapter 5: Analysis of GPX-4-regulated ferroptosis after Mtb infection

5.1 Abstract

Ferroptosis is a metabolic form of cell death that depends on the accumulation of peroxidized PUFAs. GPX4 removes accumulated oxidized phospholipids by reducing them to their corresponding alcoholic forms. Extensive studies using *in vivo* mouse and macaque models have demonstrated that ferroptosis plays an essential role in tissue damage during TB progression. In *ex vivo* murine BMDM and human MDM models, work from Dr. Eduardo Amaral's group showed that ferroptosis is the predominant form of cell death induced by Mtb during infection. However, data from human *ex vivo* macrophage models remain limited. Given that murine and human cells exhibit distinct oxidative responses and metabolic programs, there is currently no consensus on whether Mtb induces ferroptosis consistently in human macrophages.

In this chapter, GPX4 expression levels were assessed by WB in THP-1 cells and hMDMs during Mtb infection. We further stained THP-1 cells with Liperfluo (LF), a probe that reports lipid peroxidation levels. Our work demonstrates that ferroptosis is not a predominant form of cell death induced by Mtb in these two human macrophage models during the time window assessed.

5.2 Materials and Methods

Cell treatments and experimental controls

For the Liperfluo (LF) assay, THP-1 cells were treated with cumene hydroperoxide (CuPx) at 100 µM for 2 h. For ferroptosis induction, THP-1 cells were treated with 10 µM RSL-3 (MedChemExpress, HY-100218A) for 24 h. Where indicated, ferroptosis was inhibited by co-treatment with 10 µM ferrostatin-1 (MedChemExpress, HY-100579).

Liperfluo Assay

Liperfluo (Dojindo Molecular Technologies, MD, USA; L248-10) was added to THP-1 cells at a final concentration of 10 µM, 30 minutes prior to infection. Following incubation, cells were washed twice with DPBS to remove excess dye. DRAQ7™ (Invitrogen, D15106) was added to the infection medium at a 1:1000 dilution to monitor cell death. As a positive control for lipid peroxidation, 100 µM cumyl hydroperoxide (Thermo Scientific, T06I072) was added to uninfected cells 2 hours before imaging.

$$Normalized\ LF\ intensity = \frac{LF(RawIntDen)_{single\ cell}}{\overline{LF(RawIntDen)}_{UI}}$$

Image analysis

For the LF assays, LF fluorescence intensities were quantified across 11 frames. Single-cell segmentation was conducted using the method and code adapted from "da_tracker."[276] FIJI and Cellpose 2.0 were combined to quantify the fluorescent intensities. These modules were run in the Python environment.

Cells were classified as "infected" if z-projection images consistently showed dsRed-labeled Mtb within the same cell across multiple consecutive frames. For uninfected cells,

5.3 Results

5.3.1 Analysis of the involvement of GPX-4 regulated ferroptosis in THP-1 cells and hMDMs during Mtb infection

Ferroptosis is a programmed cell death pathway that is activated after Mtb infection in BMDMs and during *in vivo* infections[237,238,240]. However, as most supporting studies are derived from murine *in vivo* or *ex vivo* models, we sought to determine whether ferroptosis is similarly

induced in human macrophage models. GPX4 reduction and lipid peroxidation are two key events that lead to ferroptosis induction. Immunoblotting analysis of GPX4 revealed that Mtb infection did not reduce GPX4 levels in either THP-1 cells or hMDMs at 1–3 days post-infection (**Fig. 16A–D**).

Lipid peroxidation is a defining hallmark of ferroptosis[277]. To assess lipid peroxidation, we performed Liperfluo (LF) staining followed by fluorescence microscopy in Mtb-infected THP-1 cells. The membrane impermeability dye Draq7 indicated that approximately 15–20% of Mtb-infected cells were dead at 4 and 24 h post-infection. Despite this level of cell death, LF fluorescence intensity remained unchanged, indicating no detectable increase in lipid peroxidation during Mtb-induced cell death (**Fig. 16E–I**). In contrast, THP-1 cells treated with cumene hydroperoxide (CuPx) exhibited an approximately fourfold increase in the raw integrated density (RawIntDen) of LF fluorescence compared with untreated, uninfected controls, validating both the functionality of the LF probe and the Cellpose-FIJI-based image analysis workflow.

To further evaluate the potential contribution of lipid peroxidation to cell death, we treated Mtb-infected THP-1 cells with ferrostatin-1 (Fer-1), a well-characterized ROS scavenger. The control LDH assay shows that at 10 μM, Fer-1 significantly reduced cell lysis induced by RSL-3, a canonical ferroptosis inducer (**Fig. 16J**), confirming the inhibitor's efficacy. We then assessed whether Fer-1 could attenuate Mtb-induced cell death at early time points using LDH assays (**Fig. 16K**). However, Fer-1 treatment at the same concentration did not reduce LDH release from Mtb-infected cells. Collectively, these data indicate that ferroptosis does not contribute substantially to Mtb-induced cell death in THP-1 cells and hMDMs at the time points examined (**Fig. 16E–I**).

Corresponding nested plots of LF RawIntDen are shown in **Fig. 17A** and **B**. The same dataset was further analyzed at the single-cell level using nested one-way ANOVA, which revealed

no significant difference between infected and uninfected cells at either time point. This conclusion is consistent with that obtained from the bulk population analysis.

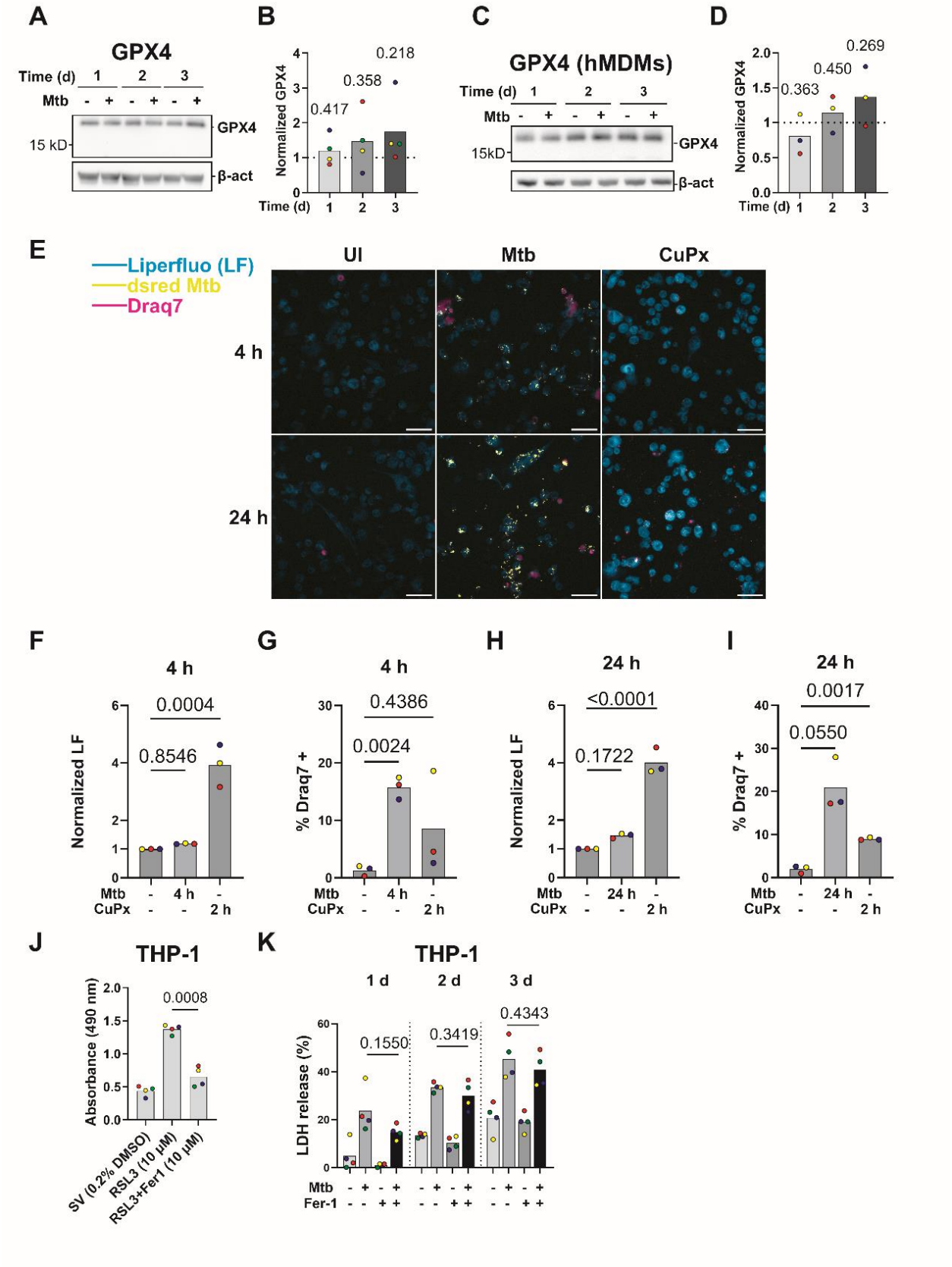
A
GPX4
Time (d) 1 2 3
Mtb - + - + - +
15 kD
GPX4
β-act
B
Normalized GPX4
0.218
0.358
0.417
Time (d) 1 2 3
C
GPX4 (hMDMs)
Time (d) 1 2 3
Mtb - + - + - +
15kD
GPX4
β-act
D
Normalized GPX4
0.269
0.450
0.363
Time (d) 1 2 3
E
Liperfluo (LF)
dsred Mtb
Draq7
UI
Mtb
CuPx
4 h
24 h
F
4 h
Normalized LF
0.0004
0.8546
Mtb - 4 h -
CuPx - - 2 h
G
4 h
% Draq7 +
0.4386
0.0024
Mtb - 4 h -
CuPx - - 2 h
H
24 h
Normalized LF
<0.0001
0.1722
Mtb - 24 h -
CuPx - - 2 h
I
24 h
% Draq7 +
0.0017
0.0550
Mtb - 24 h -
CuPx - - 2 h
J
THP-1
Absorbance (490 nm)
0.0008
SV (0.2% DMSO)
RSL3 (10 μM)
RSL3+Fer1 (10 μM)
K
THP-1
1 d
2 d
3 d
LDH release (%)
0.1550
0.3419
0.4343
Mtb - + - + - + - + - + - +
Fer-1 - - + + - - + + - - + +

Fig. 16: Mtb does not induce GPX4-regulated ferroptosis in THP-1 cells or hMDMs at the examined time points.

A, C THP-1 cells or hMDMs were infected with H37Rv Mtb at MOI:5 for 4 h or left uninfected. Cells were lysed after 1-3 d. Representative western blot images show the GPX4 levels in THP-1 cells (**A**) (N = 4) or hMDMs (**C**) (N = 6). **B,D** Band intensities of GPX4 were quantified using ImageLab software, normalized to the corresponding β-actin bands, and then expressed relative to the uninfected counterparts from the same experiment. Bar graphs display the normalized band intensities of the infected groups. One-sample t-tests were performed to compare normalized values to 1, and *p*-values are shown in the graphs. Each colored data point represents an independent experiment (N = 4) for THP-1 cells (**B**) or an individual human donor (N = 3) for hMDMs (**D**). **E** Representative confocal microscopic images showing the level of lipid peroxidation in THP-1 cells (N = 3). Cells were infected with dsRed H37Rv Mtb (yellow) at MOI:5 for 4 or 24 h, respectively. The control group was treated with cumene hydroperoxide (CuPx) at 100 µM for 2 h, or left uninfected and untreated. Staining was performed with Liperfluo (cyan) and Draq7 (magenta). Scale bars: 50 µm. **F–I** Quantification of normalized Liperfluo fluorescence intensities (**F** and **H**), or the percentage of Draq7-positive cells relative to the total cells in each field (**G** and **I**). Each dot represents the mean measurement from an independent experiment (N = 3), with 6 fields imaged per condition. Regions of interest (ROIs) were defined using Cellpose 2.0, and Raw Integrated Densities (RawIntDen) were calculated using FIJI. Nested One-way ANOVA (**F** and **H**) or One-way ANOVA with Brown-Forsythe correction (**G** and **I**) was performed; *p*-values are presented in decimal format. **J** LDH assay validating the efficacy of Ferrostatin-1. THP-1 cells were treated with solvent control (SV), RSL-3, or a combination of RSL-3 and Ferrostatin-1 (Fer-1) at the indicated concentrations. Background-corrected absorbance values for each group are shown. **K** LDH assay measuring cell lysis in infected and uninfected THP-1 cells in the presence or absence of Fer-1. THP-1 cells were infected with w.t. H37Rv Mtb at MOI:5 for 1–3 d with or without Fer-1 (10 µM) (N = 4). The percentage of LDH release was calculated by normalizing background-corrected absorbance values to the lysis control.

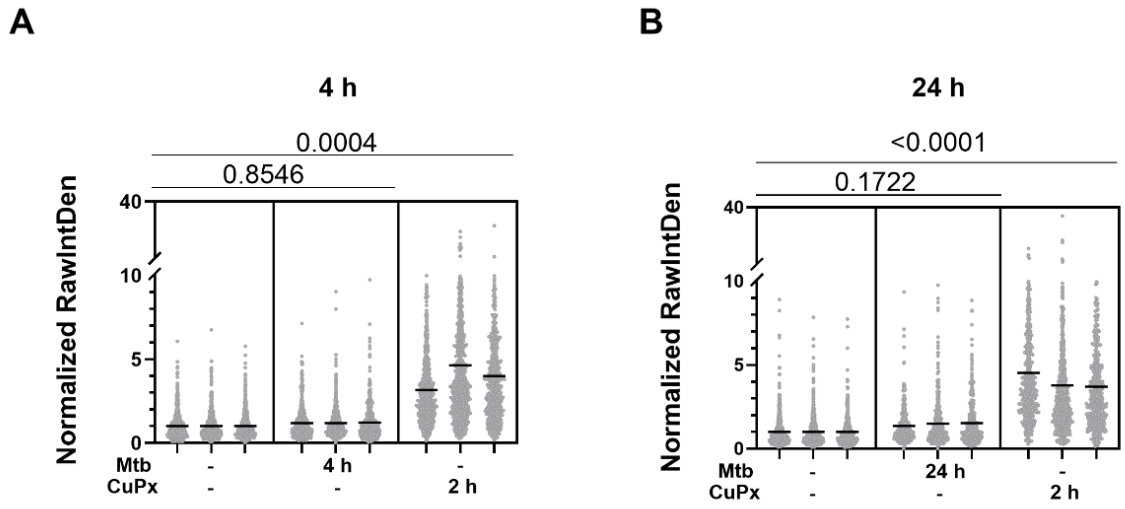

Fig. 17: Nested plot showing normalized Liperfluo fluorescence intensities in THP-1 cells. **A, B** Corresponding to **Fig. 16F** and **H**, Nested plots displaying Liperfluo RawIntDen quantification in individual THP-1 cells. Each dot represents a single cell, and each column corresponds to an independent experiment (N = 3). The number of cells per experiment ranges from 339 to 656. Black bars indicate the mean fluorescence intensity for each experiment. Statistical comparisons were performed using nested one-way ANOVA, and *p*-values are presented in the graphs.

5.4 Discussion

Previous studies have reported extensive ferroptosis in Mtb-infected murine BMDMs (MOI:10, 1 d post-infection) and *in vivo* animal models[237,240]. Ferroptosis has also been observed in Mtb-infected hMDMs (MOI:10, 4 d post-infection), U937 cells[278], and human clinical samples[238,240]. In contrast, our data show that GPX4 levels are not reduced during the first 3 days of Mtb infection in THP-1 cells or hMDMs, and that no significant elevation in lipid peroxidation is detectable in the infected THP-1 cells (**Fig. 16**). Importantly, the RSL-3/Fer-1 treatment and the LDH release assay (**Fig. 16J**) confirmed that THP-1 cells exhibit the expected lipid peroxidation response and ferroptosis induction, indicating that ferroptosis is regulated and inducible in this model.

These findings suggest that prolonged host–pathogen interactions or more advanced stages of TB disease progression may be required to elicit detectable ferroptosis in human macrophages. Alternatively, the discrepancy between murine BMDM and human macrophage data may reflect underlying biological differences that remain incompletely understood. First, the kinetics of lipid peroxidation and its resolution may differ between species. Second, human and murine macrophages may vary in their tolerance to lipid peroxidation accumulation. Third, species-specific metabolic responses to Mtb infection may affect susceptibility to ferroptosis. Collectively, these factors may shape the overall cell death phenotype observed in macrophages during Mtb infection.

Taken together with previously published findings, our data suggest that ferroptosis is not a predominant early response in human macrophages under the conditions examined, whereas it may represent an early cell death pathway in murine macrophages during Mtb infection.

Chapter 6: Analysis of Lysosomal Membrane Permeabilization during Mtb Infection in THP-1 Cells

6.1 Abstract

Lysosomes are membrane-bound cellular organelles that contain a broad spectrum of hydrolytic enzymes responsible for degrading proteins, lipids, and other macromolecules. They maintain an acidic lumen and frequently fuse with endosomes and phagosomes to degrade internalized cargo. Lysosomal enzymes, such as cathepsins and lipases, are sequestered within the lysosomal compartment and segregated from the cytosol. Upon LMP, these enzymes, together with protons, can be released into the cytosol, where they may cause irreversible cellular damage. It is well established that LMP is detrimental to cells and can contribute to multiple forms of cell death, including, but not limited to, apoptosis, pyroptosis, and ferroptosis.

Early studies demonstrated that Mtb induces mitochondrial membrane permeabilization in zebrafish macrophage models, and the consequential release of mROS is proposed to permeabilize adjacent lysosomes, thereby inducing LMP. In murine BMDMs, published work shows that Mtb infection leads to LMP, followed by Cat B release, NLRP3 inflammasome activation, and subsequent cell death.

In this chapter, we investigated whether Mtb infection induces LMP in THP-1 cells. Time-lapse live-cell confocal microscopy was performed to monitor lysosomal pH and track individual Mtb-infected cells during the final two hours preceding plasma membrane rupture (PMR). Cellpose-TrackMate combo was used to automate single-cell tracking, enabling continuous cell death monitoring and lysosomal integrity analysis. Using this approach, no detectable LMP was observed at the bulk-population level.

6.2 Materials and Methods

Cell treatments and experimental controls

For LMP induction, THP-1 cells were treated with L-leucyl-L-leucine methyl ester (LLoMe; BACHEM, 4000725) at 1 μM for at least 1 hour. All treatments were conducted at 37 ℃ in a humidified atmosphere with 5% CO_2. LMP induced by Mtb was assessed using LysoView™ 633 (LV; Biotium, CA, USA; 70058) in combination with time-lapse live-cell imaging. LV (concentration unknown) was reconstituted in 100 μL dH_2O following the manufacturer's instructions and used at a 1:2000 dilution. SYTOX™ Green Nucleic Acid Stain (Syt G; Invitrogen; S7020) was added at 0.5 μM (1:10,000 dilution) to detect plasma membrane rupture.

Image analysis

For infection experiments, time 0 was defined as the frame in which a cell first became positive for Syt G. LV fluorescence intensities were quantified across 12 frames preceding this event for each cell. The interval between two consecutive frames is set to be 10 min. For control experiments, time 0 corresponded to the first frame of image acquisition. Single-cell segmentation and tracking were conducted using the method and code adapted from "da_tracker."[276] FIJI and TrackMate-Cellpose combo were combined to quantify the fluorescent intensities.

Cells were classified as "infected" if z-projection images consistently showed dsRed-labeled Mtb within the same cell across multiple consecutive frames. For uninfected cells, 12 consecutive data points were randomly selected from each trackable single cell to establish a baseline. Curves showing more than 4 data points below the baseline, with statistically significant deviation, were considered indicative of LMP.

$$Log_2(FC) = Log_2\left(\frac{\sum_z RawIntDen|_t}{\sum_z RawIntDen|_{t0}}\right),$$

$$FC = Fold\ change;\ z = z - stack;\ t0 = the\ first\ time\ point$$

Statistics

The modified Chi-square test was used to compare two curves with known or assumed means and standard deviations (SDs), and was performed either with the Excel spreadsheet provided in a previous publication[279] or automated by Python programming for batch analyses.

6.3 Results

6.3.1 Analysis of LMP induction in THP-1 cells 2 hours prior to cell death

LMP is a well-characterized event that contributes to lysosome-dependent cell death (LDCD)[280]. Recent studies have reported LMP induction during Mtb-induced cell death in various experimental models[231,245,281]. In this study, time-lapse live-cell imaging was employed to monitor single Mtb-infected cells shortly before cell death.

The LV staining method was combined with dynamic imaging to study LMP induction during the 2-hour period preceding PMR. LV enters and accumulates within intracellular compartments, exhibiting maximal fluorescence at acidic pH and decreasing fluorescence intensity as pH increases. To validate the LV staining and the following quantification methods, THP-1 cells were treated with LLoMe, a known LMP inducer, and continuously imaged. LV fluorescence intensity was quantified using the published "da_tracker" pipeline, which integrates the Cellpose-TrackMate workflow with Fiji and a Python-based analysis environment (**Fig. 18A** and **C**; **SVs 2** and **3**).

At the single-cell level, a modified Chi-square test was applied to compare each cell's LV fluorescence intensity array with the population mean. If an array contained at least four data points below the mean and the array (curve) was significantly different from the calculated mean, the cell was classified as undergoing LMP. This analysis revealed a significant reduction in LV signal in LLoMe-treated cells compared with solvent-treated or untreated controls. Specifically, 81.25% of LLoMe-treated cells exhibited LMP, whereas only 10.25% of DPBS-treated cells met the LMP criteria (**Fig. 19A–D**), validating both the experimental design and analytical approach.

Following validation, the same procedure was applied to Mtb-infected THP-1 cells (MOI:2), which were imaged continuously for 20 hours. Infected cells that became Syt G-positive during imaging and could be continuously tracked for 2 h (12 consecutive frames) were selected for LV fluorescence quantification. Cell outlines generated by Cellpose and the tracking order produced by TrackMate were used to verify tracking accuracy. These cells were used to assess LV fluorescence intensity during the 2 h preceding PMR. The modified Chi-square analysis indicated no significant difference in relative LV fluorescence intensity between infected cells and either bystander (Bys) or uninfected (UI) cells (**Fig. 18B** and **D**, **SVs 4–6**). Interestingly, bystander cells showed increased LV intensity, potentially reflecting lysosomal biogenesis or lysosomal acidification. At the single-cell level, LMP was observed in 8.57% of infected cells, 8.45% of UI cells, and 2.44% of bystander cells (**Fig. 19E–J**). Collectively, these findings indicate that Mtb does not significantly induce LMP in THP-1 cells within 2 hours prior to PMR.

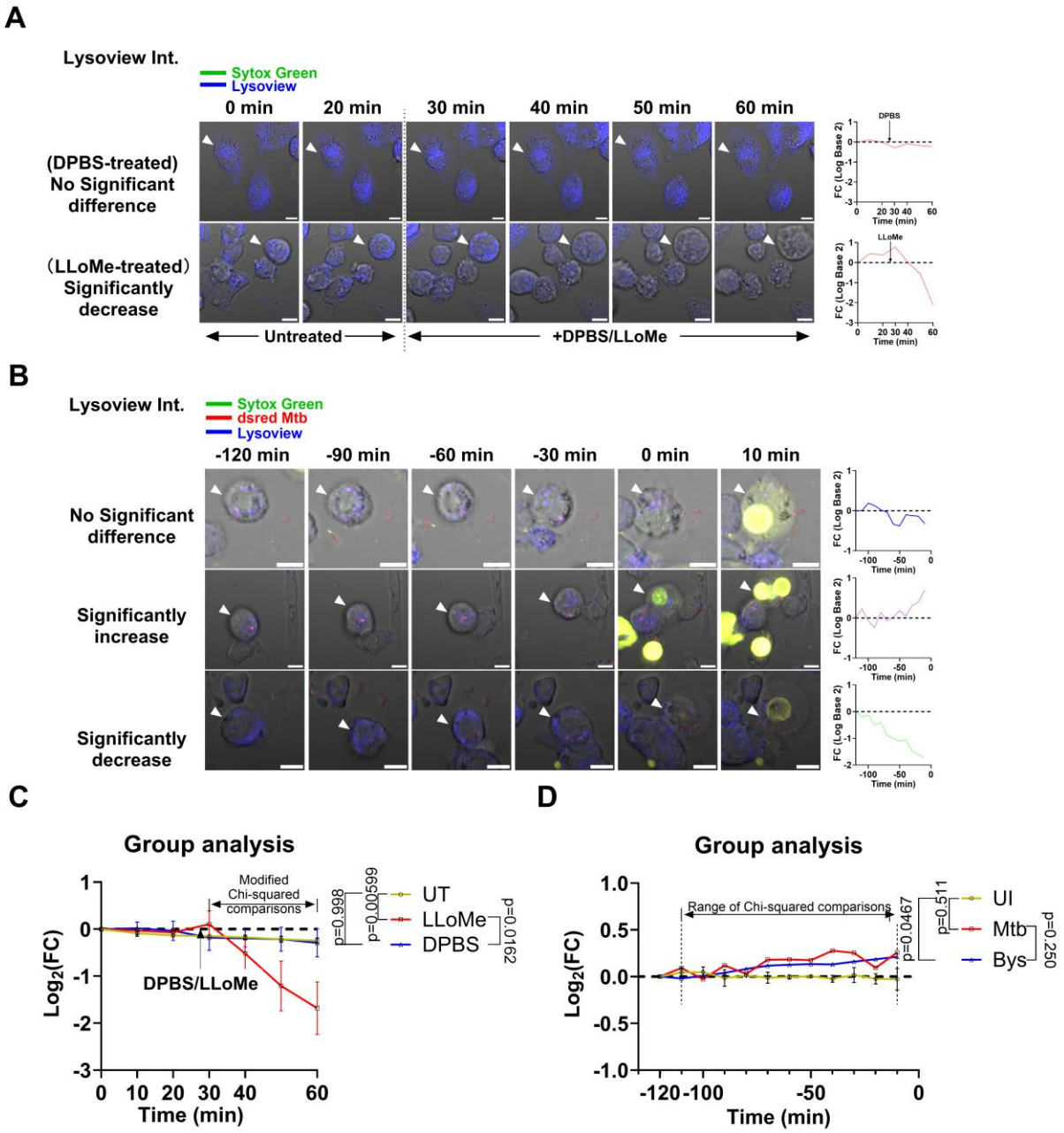

Fig. 18: Mtb does not induce detectable LMP in THP-1 cells 2 hours prior to cell death.
A Representative time-lapse live-cell imaging of THP-1 cells showing changes in Lysoview (LV, blue) fluorescence intensity over time. Cells were stained with LV and Sytox Green (Syt G, green), then treated with LLoMe or DPBS approximately 25 minutes after imaging began. White arrowheads indicate tracked cells. **B** THP-1 cells were infected with dsRed H37Rv Mtb at MOI:2 then stained with LV and Syt G. Representative time-lapse live-cell imaging of THP-1 cells shows changes in LV fluorescence intensity over time. 0 min is defined as the time when a cell first becomes Syt G^+. Negative time points indicate the duration (up to 120 min) before time point 0, during which LV intensities were quantified. The line graphs next to the confocal microscopic

images display the logarithm (log) (base 2) of fold change (FC) over time (**A** and **B**). **C, D** Corresponding to **A** or **B**, the line graphs show the log2 FC changing over time. In each independent experiment, 2 scenes were imaged for each condition, and 4 for the untreated (UT) (uninfected) condition. A total of 3 independent experiments were performed (N = 3). The UT dataset is the same as the UI from the infection experiments. 39, 48, and 71 cells were tracked and included in the statistical analysis for the DPBS, LLoMe-treated, and UT groups. For **D**, 4 biological replicates were conducted for the Mtb and bystander (Bys) conditions (N = 4), and 3 for the UI condition (N = 3). 35, 41, and 71 cells were tracked and analyzed for the Mtb, Bys, and UI groups. In **C** and **D**, each line represents the mean; error bars indicate the SD. Modified Chi-squared analyses were performed. *p*-values are shown in graphs.

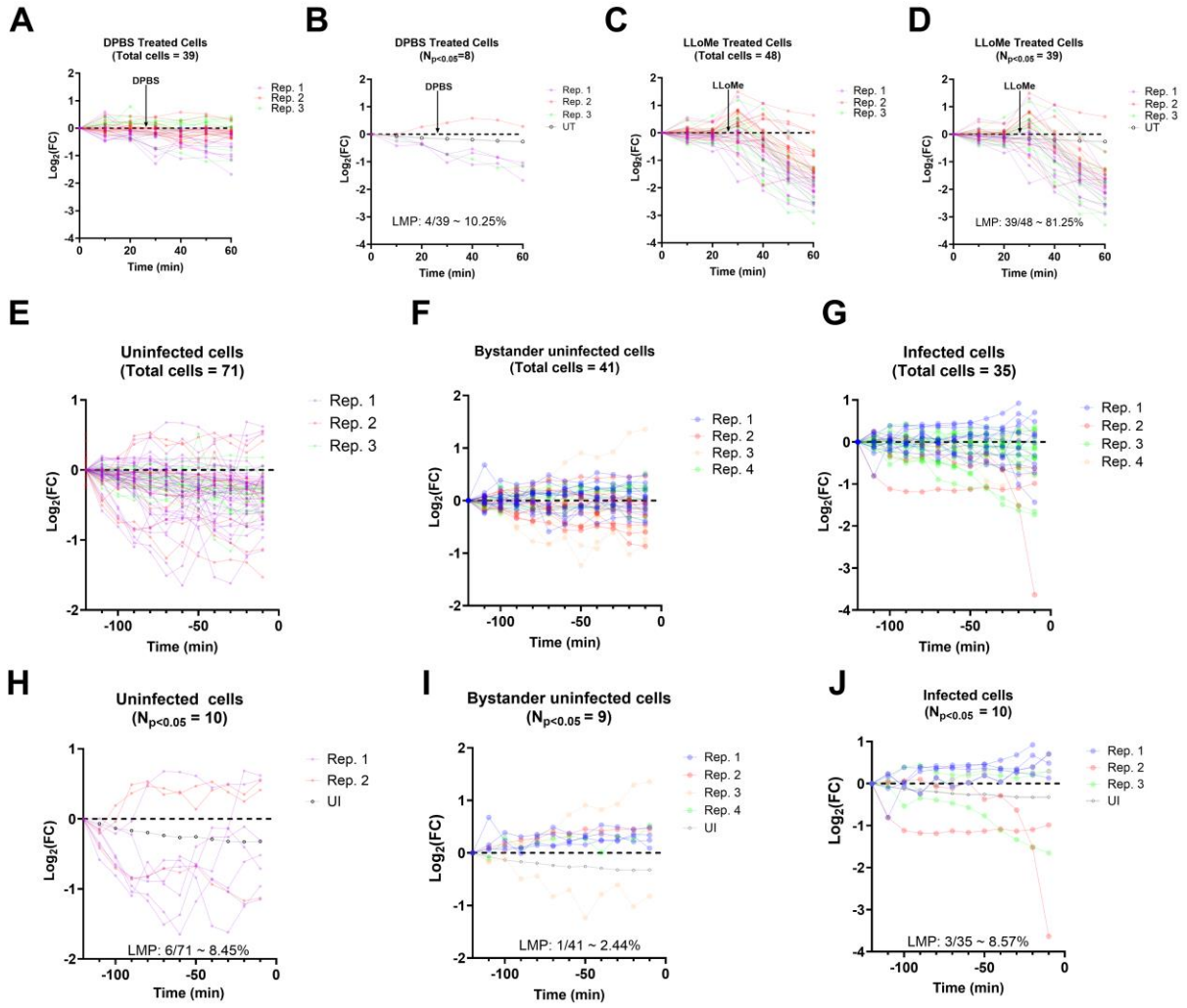

Fig. 19: Single-cell analysis of lysosomal membrane integrity in THP-1 cells during Mtb infection.

A-J The log (base 2) of normalized LV fluorescence intensity was plotted against time. The grey curves represent the mean of the UI/UT condition, which served as a baseline for comparison. Each data point indicates the fluorescence value at a specific time point for a single cell, with each color representing an independent experiment (N = 3). Each curve represents the time course of a single cell. The black arrow marks the time of DPBS or LLoMe addition. The number of total individual cells tracked in each experiment is shown in the title of each graph. **B, D, H, I, and J,** subsets of the datasets shown in **A**, **C**, **E**, **F**, or **G**, respectively, highlighting individual curves exhibiting significant differences compared with the baseline. The proportion of descending curves relative to the total number in each category was calculated and reported as the percentage of LMP.

6.4 Discussion

Several studies have reported LMP induction during Mtb infection[231,245,281]. In contrast, our live-cell imaging data revealed no evidence of LMP within the final two hours preceding plasma membrane rupture (PMR) in THP-1 cells (**Figs. 18** and **19**). Importantly, these findings also validate the robustness of our experimental design and analytical workflow, which enable high-resolution, time-resolved analysis of lysosomal pH dynamics at the single-cell level during cell death progression.

Discrepancies between our observations and previously published studies[231,245,281] may arise from differences in the timing of analysis, host cell species, and/or multiplicity of infection (MOI). Notably, many prior studies assessed LMP at earlier stages of infection or relied on population-level readouts that may obscure transient or heterogeneous events. In other cellular contexts, LMP has been linked to apoptosis, pyroptosis, and ferroptosis[174,242,282]. However, our data suggest that LDCD does not contribute to necrotic cell death in THP-1 cells during early Mtb infection, particularly during the terminal phase immediately preceding PMR.

Chapter 7: Analysis of DNA-Release-Associated Necrosis (DRAN) in THP-1 Cells and hMDMs During Mtb Infection

7.1 Abstract

Neutrophil extracellular trap (NET) formation, commonly referred to as NETosis, is a well-characterized form of neutrophil cell death associated with the release of eDNA-based structures. Neutrophil extracellular traps (NETs) are web-like networks composed primarily of nuclear or mitochondrial DNA decorated with histones and neutrophil granule proteins. Among these, myeloperoxidase (MPO) and citrullinated histone H3 (CitH3) are widely used markers of NET formation. CitH3 reflects PAD4-dependent histone citrullination and chromatin decondensation, a key step in NET release, whereas MPO contributes to the antimicrobial activity of NETs and participates in reactive oxygen species (ROS)-dependent NET formation. NETs have been shown to exert immunomodulatory functions *in vivo* and *ex vivo*, physically entangle pathogens, and promote microbial killing through the localized concentration of antimicrobial peptides and ROS-generating enzymes.

Extracellular trap-like DNA release has also been reported in macrophages. By analogy to NETosis, the term macrophage extracellular trap cell death (METosis) was introduced and proposed as a distinct form of macrophage cell death. However, the molecular mechanisms underlying METosis remain poorly defined and highly controversial. While proteins such as CitH3, MPO, and elastase have been suggested as METosis markers, there is currently no consensus regarding their necessity or universality across experimental systems. Moreover, the identity of the terminal execution mechanism leading to plasma membrane rupture during METosis has not been clearly established. The lack of a defined signaling cascade and the presence of contradictory

findings across studies challenge the classification of METosis as a discrete, independent cell death pathway.

Previous studies have reported that Mtb infection can induce the release of extracellular trap-like structures from human macrophages *ex vivo* under specific conditions[283,284]. However, these observations were limited in scope, and the phenomenon was not comprehensively characterized. Consequently, it remains unclear whether macrophage DNA release during Mtb infection represents a novel cell death pathway or reflects a morphological manifestation of an established necrotic process.

Time-lapse live-cell imaging performed during LMP analysis (Chapter 6) revealed frequent DNA release events associated with necrotic PMR. Building on this observation, the present chapter demonstrates that DNA release occurs during Mtb infection in both THP-1 cells and human monocyte-derived macrophages (hMDMs). We introduce the term DNA-release-associated necrosis (DRAN) to describe this phenotype, which morphologically resembles previously reported METosis. In THP-1 cells, DRAN accounted for approximately 60% of total necrotic cell death, whereas only ~30% of necrotic hMDMs exhibited detectable DNA release, suggesting that the dominant early necrotic death pathway in hMDMs remains mechanistically unresolved. We further show that the released DNA can associate with extracellular Mtb. Genetic ablation of CASP4/5 or ninjurin-1 (NINJ1), as well as pharmacological inhibition of GSDMD, did not reduce DNA release or necrotic cell death in Mtb-infected THP-1 cells. Collectively, these findings establish a strong correlation between DNA release and necrotic cell death during Mtb infection in human macrophage models, while indicating that pyroptotic signaling pathways are not required for DRAN execution.

7.2 Materials and Methods

Cell cultures and neutrophil acquisition

THP-1 *ninj1*$^{-/-}$ mutant cells were generated by Dr. Liron David as described[285]. The THP-1 *casp4/5*$^{-/-}$ strain and its corresponding w.t. control were kind gifts from Dr. Clare Bryant (University of Cambridge, UK)[286].

Human neutrophils were isolated from whole blood using the EasySep™ Direct Human Neutrophil Isolation Kit (Stemcell Technologies, Van, CA; 19666). After isolation, neutrophils were washed once with THP-1 growth medium to remove residual EDTA and seeded into 8-well collagen I-coated imaging chambers (ibidi, 80829). Cells were seeded for at least 1 hour to allow adherence before Mtb infection. Refer to Appendix Table 2 for detailed information on materials, kits, and reagents.

Image analysis

Cells exhibiting DNA release were distinguished from cells without DNA release based on the z-projection of the Syt G signal. A "sum" projection was generated from the original 11 z-slices using the Z-Project function in Fiji. If the Syt G signal from an analyzed cell extended beyond the cellular outline, the cell was classified as exhibiting DNA release. For clarity of data presentation, only the z-projection generated using the "max" method is shown, rather than the "sum" projection.

ZEN 3.6 software was used for 3D volume rendering, image generation, and video creation. For 3D visualization, the rendered model was rotated 360° along the Z-axis (as defined by the microscope), with one frame captured per degree of rotation.

Immunofluorescence microscopy

Cells cultured in 8-well chambers were first washed once with phosphate-buffered saline (PBS), then fixed with 4% paraformaldehyde (PFA) in PBS (Thermo Scientific, J61899.AK) for 1 hour at room temperature (RT) or overnight at 4°C. After fixation, cells were washed three times with 0.1 M glycine in PBS (PBS-G), with each wash lasting 5 minutes. To block Fc receptors, Human TruStain FcX™ (BioLegend, CA, USA; 422302) was diluted 1:1000 in 3% BSA, 0.2% Tween-20 in PBS (PBS-BT) and applied to the cells for 1 h. Primary antibodies were diluted in 1% BSA in PBS (PBS-B) and incubated with the cells for 2 hours at RT or overnight at 4° C. After three washes with PBS, secondary antibodies and 1 μg/mL 4′,6-diamidino-2-phenylindole (DAPI; Thermo Scientific; 62248), also diluted in PBS-B, were added. Cells were washed three additional times with PBS after the staining. Information on the antibodies used is listed in Appendix Table 1. The DAPI and T-PMT channels were used as references to manually define regions of interest (ROIs) for mean fluorescence intensity (MFI) quantification in FIJI.

$$Relative\ ratio\ of\ FI = \frac{\frac{MFI_{Ab,target}}{MFI_{DAPI,target}}}{\frac{MFI_{Ab,Iso}}{MFI_{DAPI,Iso}}},$$

$$FI = fluorescence\ intensity;\ Ab = Antibody; Iso = Isotype\ antibody$$

Confocal microscopy

Cells were imaged using a Zeiss LSM 800 laser scanning confocal microscope equipped with two gallium arsenide phosphide photomultiplier tube (GaAsP-PMT) detectors and one transmitted light photomultiplier tube (T-PMT) detector. A 40×/NA 1.2 water immersion objective was used for all imaging experiments.

For time-lapse live-cell imaging, the observation chamber was maintained at 37°C with 5% CO_2 supplied via a humidified incubator. Z-stacks spanning 10 μm with 1 μm intervals were acquired every 10 minutes for up to 20 hours. Each field consisted of 11 optical slices. A total of four fields were imaged, with a maximum of two experimental conditions per experiment. Each image spanned an area of 319.45 × 319.45 μm, corresponding to 2048 × 2048 pixels.

For immunofluorescence microscopy, 3-4 fields were imaged with Z-stacks spanning 20 μm with 1 μm interval. 1 slice with proper signals was selected for MFI quantification. Airyscan confocal microscopy and 3D volume rendering were performed using a Zeiss LSM 980 microscope with the same 40×/NA 1.2 water objective.

CFU analysis

THP-1 cells were infected with w.t. H37Rv Mtb at an MOI of 5 for 4 h, after which the infection medium was replaced with fresh growth medium without gentamycin. DNase I (100 U/mL) was added to the wells either immediately after infection (0 h post-infection) or 1 h prior to supernatant collection at 2 or 3 d post-infection. Supernatants were diluted in DPBS at 1:10 and 1:100, and 100 μL of each dilution was plated in triplicate on 7H11 agar plates. Plates were monitored daily to ensure the absence of contamination, and CFUs were enumerated at 24 d post-inoculation. Only plates containing more than 20 countable colonies were included in the analysis. For each experimental condition, the mean CFU value of all technical replicates was used as the representative CFU.

7.3 Results

7.3.1 Frequency and kinetics of DNA release induced by Mtb H37Rv in THP-1 cells and hMDMs

Time-lapse live-cell imaging performed for LMP analysis also revealed extensive DNA release following PMR (**Fig. 20A**, **SVs 7** and **8**). The morphology of the observed DNA release resembles that of the previously described METosis[246,287]. To characterize the frequency and dynamics of DNA release, in both Mtb-infected and uninfected conditions, we quantified the proportion of DNA-releasing cells among all dying cells within the imaging frame. Approximately 60% of dead, Mtb-infected THP-1 cells exhibited DNA release, compared with ~20% of dead uninfected cells (**Fig. 20B**). Notably, the overall percentage of necrotic cells relative to total cells did not differ significantly between infected and uninfected groups (**Fig. 20C**). On average, DNA release occurred approximately 106 minutes after THP-1 cells became Syt G-positive, marking the onset of cell death (**Fig. 20D**). In hMDMs, time-lapse imaging demonstrated that 32% of dead cells released DNA and formed extracellular web-like structures (**Fig. 20A** and **E**, **SVs 9** and **10**). Among ~2600 analyzed uninfected hMDMs, only 10 necrotic cells were detected, of which 5 released DNA. Notably, in 3 of 6 independent repeats, no necrotic cells were observed. Consequently, the percentage of DNA release among total Syt G^+ hMDMs could not be quantified in **Fig. 20E**. During Mtb infection, approximately 22% of hMDMs underwent necrosis (**Fig. 20F**). Zoomed-in images of these trap-like structures and the corresponding time-lapse videos are shown in **Fig. 21A** and **SV. 11** (THP-1) and **12** (hMDM). Suicidal NETosis induced by PMA in human neutrophils (hNeu) was imaged and used as one of the references to define criteria to distinguish DNA-releasing cells from cells without DNA release (**Fig. 21B**, **SV 13**). The criteria are described in the **Materials and Methods** section.

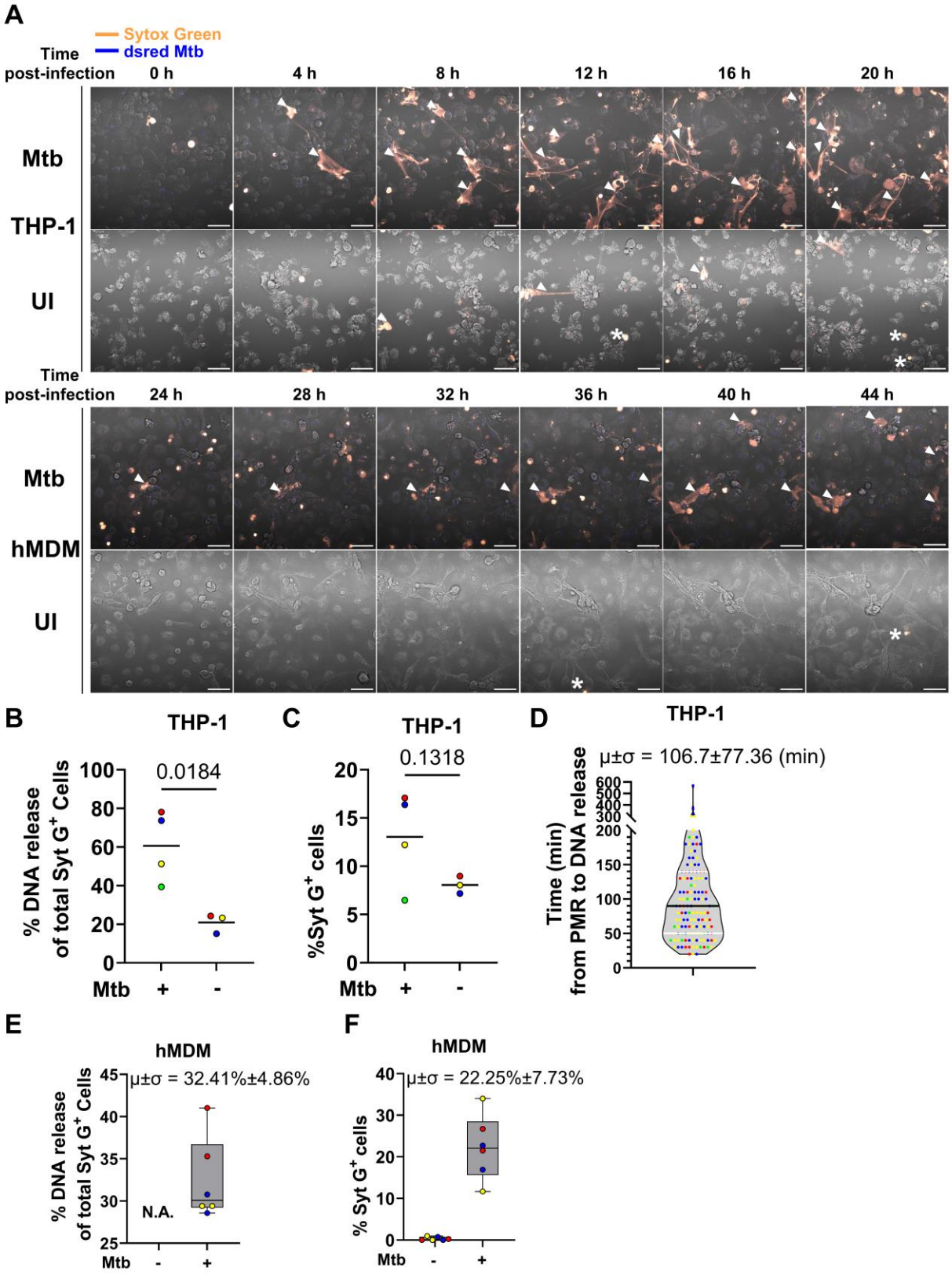
A
Sytox Green
dsred Mtb
Time post-infection
0 h
4 h
8 h
12 h
16 h
20 h
Mtb
THP-1
UI
Time post-infection
24 h
28 h
32 h
36 h
40 h
44 h
Mtb
hMDM
UI
B
THP-1
% DNA release of total Syt G+ Cells
0.0184
Mtb + -
C
THP-1
%Syt G+ cells
0.1318
Mtb + -
D
THP-1
μ±σ = 106.7±77.36 (min)
Time (min) from PMR to DNA release
E
hMDM
% DNA release of total Syt G+ Cells
μ±σ = 32.41%±4.86%
N.A.
Mtb - +
F
hMDM
% Syt G+ cells
μ±σ = 22.25%±7.73%
Mtb - +

Fig. 20: Mtb induces DNA release in THP-1 cells and hMDMs during the infection.
A. THP-1 cell images extracted from the same time-lapse video shown in **Fig. 18A** and time-lapse confocal microscopic images of Mtb-infected hMDMs. THP-1 cells or hMDMs were infected with dsRed H37Rv Mtb (blue) at MOI 2 and then stained with Syt G (orange). The white arrowheads indicate extracellular, web-like DNA structures, while asterisks label cells that do not exhibit DNA release. Scale bars represent 50 μm. **B, C** Quantification of DNA release or plasma membrane rupture (PMR) ratios in uninfected and Mtb-infected THP-1 cells. DNA release events and total cell numbers in frame 1 of each video were quantified using FIJI software (the same for **E** and **F**). Each colored data point represents the average of 4 fields (N = 4 for Mtb; N = 3 for UI) and includes over 200 cells. Statistical analysis was performed using unpaired Welch's t-tests, and *p*-values are shown in the graphs. **D** Quantification of the time duration from PMR to DNA release in Mtb-infected THP-1 cells. The number of frames between the two events was manually counted and converted to time (in minutes). The black dot line indicates the median, and the white dashed lines represent the 25th and 75th percentiles. Each dot represents a single trackable cell. The mean (μ) and standard deviation (σ) are indicated; the same notation is used hereinafter. Each color represents an independent experiment (N = 4). **E, F** Quantification of DNA release or PMR ratios in Mtb-infected or uninfected hMDMs. Each data point represents the average of 4 fields from an independent experiment (N = 6), with more than 200 cells analyzed per condition. Each color corresponds to a distinct human donor (N = 3). μ and σ are shown only for the infected groups. N.A.: Not applicable.

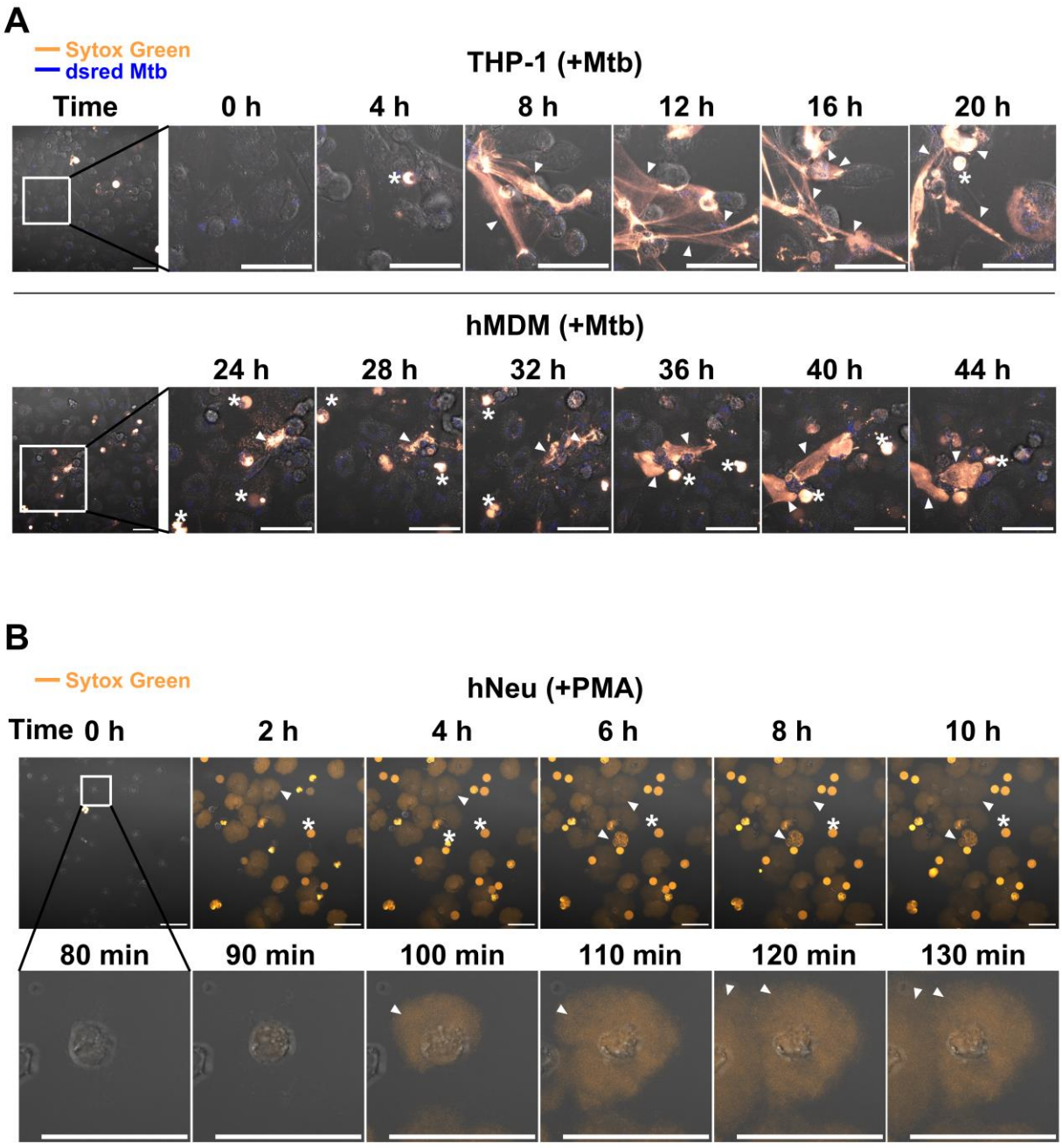

Fig. 21: Zoomed-in images illustrating the structures of released or expelled DNA.
A Zoomed-in images corresponding to **Fig. 20A** showing the structures of released DNA from Mtb-infected THP-1 cells or hMDMs. **B** Time-lapse live-cell imaging of PMA-treated human neutrophils (hNeu) (N = 1). Image acquisition began immediately after the addition of 50 ng/mL

PMA to hNeu. For **A** and **B**, White arrowheads indicate extracellular, web-like DNA structures, while asterisks label cells that do not exhibit DNA release. Scale bars represent 50 μm.

7.3.2 Characterization of the molecular composition and biological relevance of eDNA released by Mtb-infected THP-1 cells

eDNA released from Mtb-infected THP-1 cells and hMDMs exhibits a morphology resembling NETs (**Fig. 20A**). We therefore questioned whether DNA released from infected THP-1 cells follows mechanisms associated with NETosis. To investigate the mechanisms underlying DNA release from THP-1 cells during Mtb infection, we performed a comparative analysis of eDNA composition between THP-1 cells and human neutrophils.

Immunofluorescence microscopy was used to assess the localization of MPO and citrullinated histone H3 (CitH3). Notably, the extracellular DNA released by Mtb-infected THP-1 cells was positively stained with antibodies against MPO and CitH3 (**Fig. 22A–C**, **Fig. 23A**), indicating their association with the DNA structures visualized by DAPI staining. However, compared with Mtb-infected neutrophils, the abundance of MPO and CitH3 on extracellular DNA from THP-1 cells was markedly lower (**Fig. 22D, E**). While neutrophils displayed considerable variability in MPO and CitH3 deposition on extracellular DNA, THP-1 cells consistently exhibited lower levels of these markers. Airyscan confocal microscopy analysis suggested that the eDNA released from THP-1 cells could associate with extracellular Mtb bacilli (**Fig. 22F**, **SV 14**).

We investigated the effects of released DNA on host cells and extracellular Mtb bacilli by using DNase I to remove DNA web-like structures during infection. DNase I was used to treat uninfected THP-1 cells or THP-1 cells infected with w.t. H37Rv Mtb in the absence of gentamycin in the chase medium. Control experiments demonstrate that DNase I neither killed Mtb nor inhibited Mtb growth in 7H9 culture medium (**Fig. 24A**). DNase I in the culture medium effectively digested DNA and removed the trap-like structures formed by Mtb-infected THP-1 cells, as shown in **Fig. 24B** and **C**. DNase I treatment significantly reduced LDH release from

Mtb-infected THP-1 cells by ~10%, while it had no effect on the viability of uninfected THP-1 cells (**Fig. 24E**). CFU analysis indicated that DNase I treatment reduced extracellular bacilli by an average of ~75% compared with untreated controls across four independent replicates (**Fig. 24F**). However, this reduction did not reach statistical significance. Collectively, these findings suggest that extracellular DNA may modestly exacerbate cell death in infected or bystander cells during Mtb infection, while the trap-like structures do not directly kill extracellular Mtb.

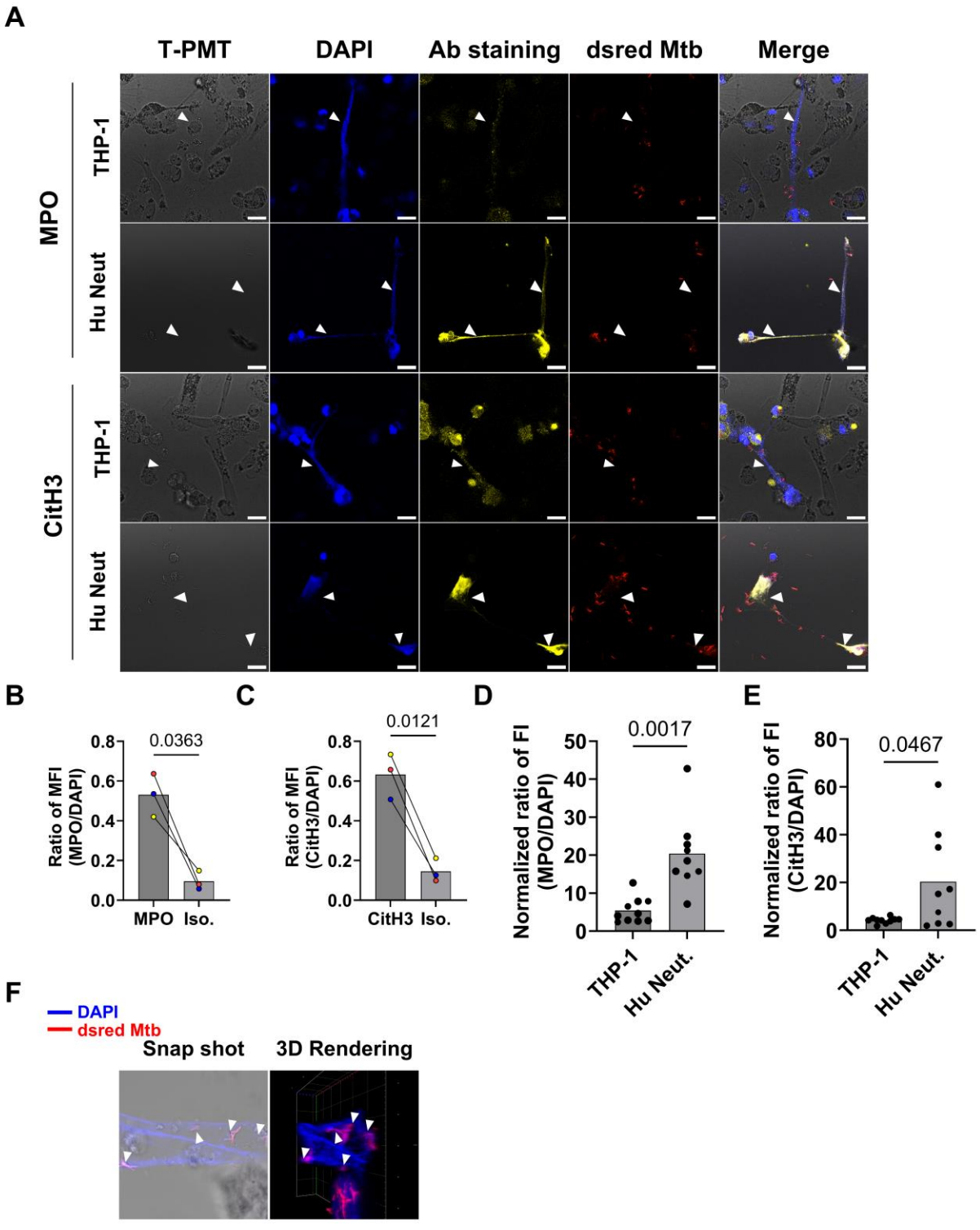

Fig. 22: Markers of NETosis are detected on the extracellular DNA released by Mtb-infected THP-1 cells.

A THP-1 cells or human neutrophils (hNeu) (from 1 donor) were infected with dsred H37Rv Mtb (red) at MOI 2 for 20 h and fixed and stained with DAPI (blue) to visualize DNA. Alexa Fluor 647-conjugated antibodies (yellow) were applied to detect myeloperoxidase (MPO) or citrullinated Histone 3 (CitH3). White arrowheads indicate extracellular web-like DNA structures. Scale bars represent 20 μm. **B, C** Bar graphs showing the mean fluorescence intensity (MFI) ratios for DAPI and antibody staining on extracellular DNA. Intracellular fluorescence signals were manually excluded, and the MFI of DAPI or antibody staining on extracellular web-like DNA was quantified using FIJI. Paired t-tests were performed; *p*-values are reported in each graph. Each data point represents the average of 3-4 fields from an independent experiment, with each color denoting an independent experiment (N = 3). **D** Airyscan confocal image showing extracellular DNA released by infected THP-1 cells interacting with extracellular Mtb (N = 1). The left image is a 0.53 μm optical slice with merged signals from brightfield, DAPI (blue), and dsRed Mtb (red). 3D volume rendering (on the right) was performed using ZEISS Zen 3.6, showing the X-Y view. Each square in the background grid represents a 10 μm × 10 μm area.

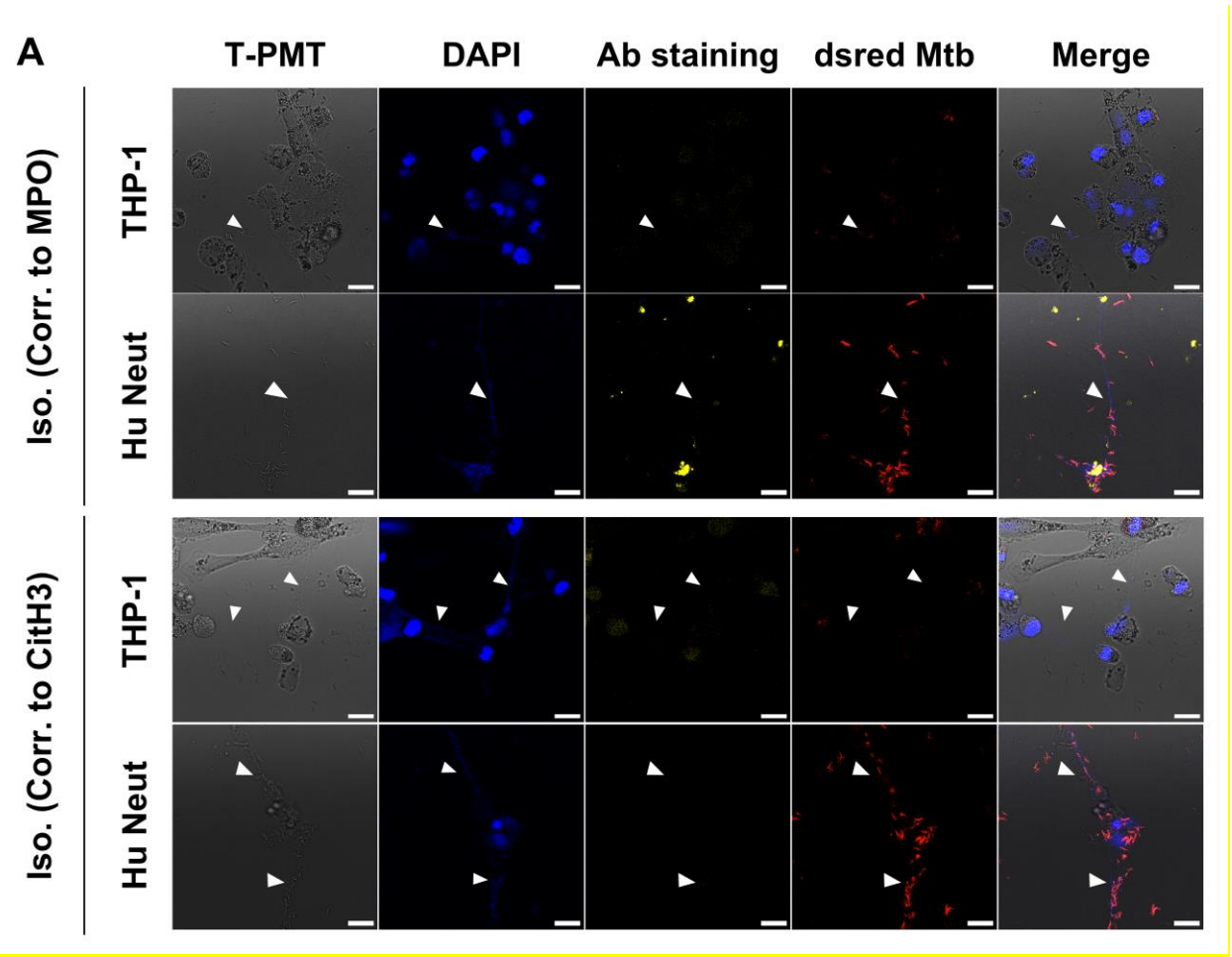

Fig. 23: Isotype control stainings for anti-MPO and anti-CitH3 antibodies.
A Representative confocal immunofluorescence images of dsRed H37Rv Mtb-infected THP-1 cells and hNeu undergoing DNA release. Cells were infected with dsRed H37Rv Mtb (red) at MOI 2 for 20 h, then fixed and stained with DAPI (blue) to visualize DNA. Alexa Fluor 647-conjugated mouse or rabbit IgG isotype control antibodies (yellow) were used to assess background staining. White arrowheads indicate extracellular web-like DNA structures. Scale bars: 50 µm.

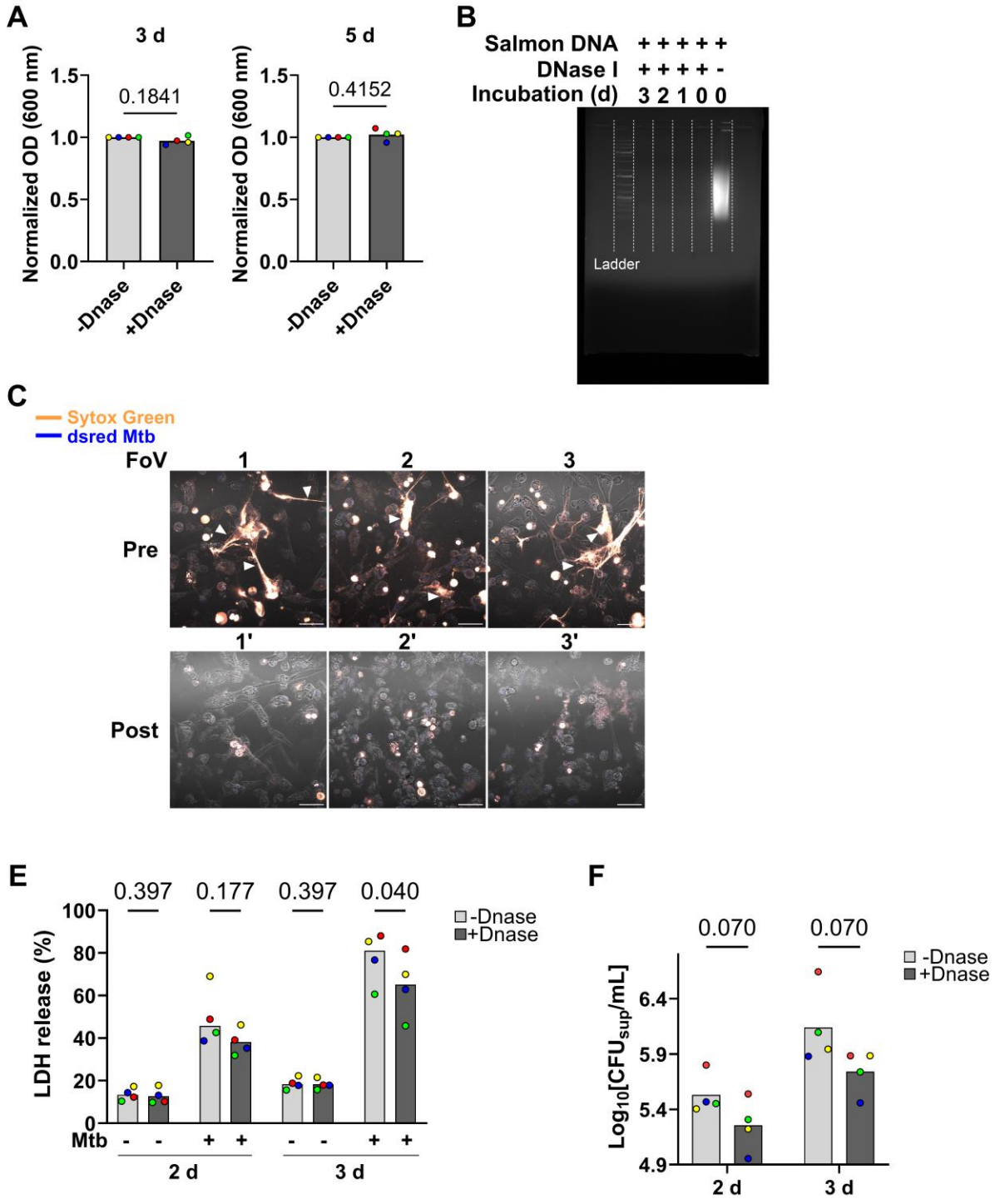

Fig. 24: Assessment of the effect of eDNA on host THP-1 cells and Mtb bacilli.
A Comparisons of ODs between DNase I-treated and untreated Mtb 7H9 cultures. Well-grown Mtb cultures were diluted to $OD_{600} = 0.2$ from different initial ODs. DNase I was added to the cultures at 100 U/mL, and the cultures were shaken at 140 rpm at 37 °C. OD_{600} values were measured at 3

and 5 d post-DNase treatment (N = 4). For each repeat, values from DNase-treated cultures were normalized to their untreated counterparts. **B** Analysis of DNase I activity in THP-1 culture medium at different time points by agarose gel electrophoresis. DNase I was diluted in THP-1 growth medium to 100 U/mL and incubated at 37 °C for 0, 1, 2, or 3 days. After the incubation, 10 µL of the pre-incubated DNase I solutions from all groups were mixed with 10 µg (1 µL) of shredded salmon sperm DNA and incubated at 37 °C for 1 hour. Then the reaction mixtures were mixed with loading buffer and analyzed by agarose gel electrophoresis (N = 1). **C** Confocal fluorescence images of Mtb-infected THP-1 cells pre- and post-DNase I treatment. THP-1 cells were infected with dsRed H37Rv Mtb (blue) at MOI 5. 4 h after bacterial addition (defined as time 0), cells were washed twice with DPBS and replenished with fresh culture medium. At 24 h post-infection, cells were stained with Syt G (orange) and imaged, with three random fields of view (FoVs) acquired. DNase I (100 U/mL) was then added to the same well, and cells were incubated for 1 h at 37 °C under 5% CO_2. Three additional FoVs from the same well were imaged post-DNase treatment using identical microscope settings (N = 1). **D** LDH release assay showing the percentage of cell death in each group, calculated by normalizing absorbance values to the lysis control. THP-1 cells were infected with w.t. H37Rv Mtb at MOI:5 for 4 hours, washed with DPBS twice, and replenished with fresh medium. DNase I was added to half of the UI and infected groups at 100 U/mL, while the remaining groups were left untreated. Supernatants were collected at 2 and 3 d post-infection for LDH release analysis (**D**) and CFU enumeration (**E**) (N = 4 for both panels). **E** CFU analysis reflecting the number of viable extracellular Mtb bacilli. Supernatants from infected groups were harvested and plated on 7H11 agar plates. Samples were diluted 1:10 and 1:100 prior to plating, and only plates containing >20 colonies were used for quantification. Plates were monitored daily to ensure optimal colony size for counting, and CFUs were enumerated at 21 days post-plating.

7.3.3 Assessment of whether pyroptosis induction is required for eDNA release

To identify potential regulators of eDNA release, we investigated whether known cell death executioners are essential for this phenomenon. For instance, vital METosis requires GSDMD activation during pyroptosis induction[288]. Given the significant pyroptosis observed in THP-1 cells upon Mtb infection, we examined whether eDNA release results from GSDMD or inflammasome activation.

To assess the involvement of GSDMD in DNA release, we treated infected THP-1 cells with Disulfiram (DIS). Time-lapse live-cell imaging indicated that disulfiram, the GSDMD inhibitor, did not alter the extent of DNA release during Mtb infection (**Fig. 25A** and **B**, **SVs 15** and **16**). Furthermore, disulfiram did not inhibit the induction of necrosis, as assessed by Syt G staining (**Fig. 25C**) and the LDH release (**Fig. 25D**). The control experiment shows that the disulfiram still effectively inhibited GSDMD activation in THP-1 cells after 20-hour treatment (**Fig. 25E**). These data indicate that GSDMD is not required for either Mtb-induced cell death or DNA release in THP-1 cells.

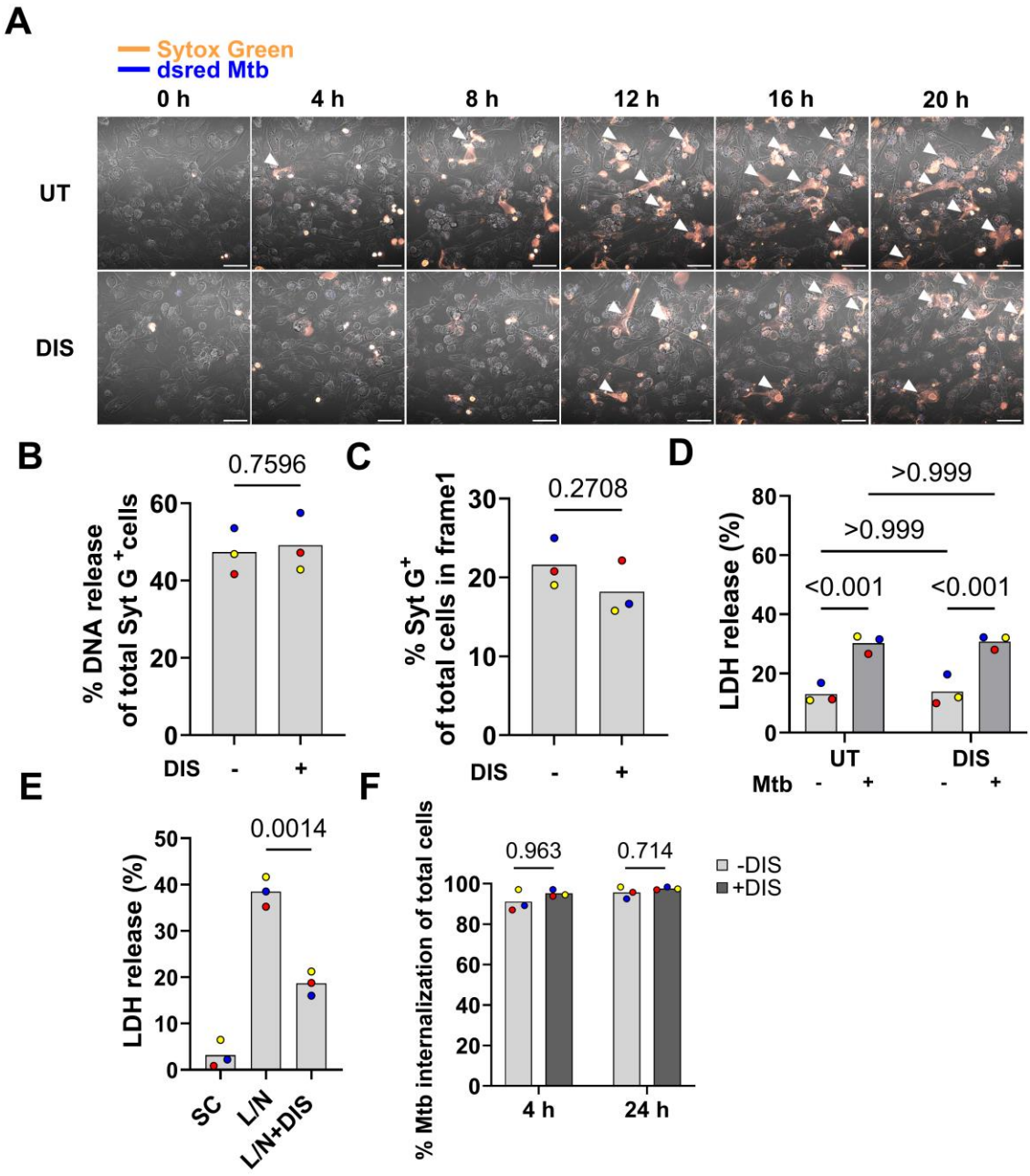

Fig. 25: GSDMD does not promote DNA release.

A Representative confocal time-lapse images showing Mtb-infected THP-1 cells undergoing DNA release in the presence or absence of disulfiram. Cells were infected with dsRed H37Rv Mtb (blue) at MOI:2 for 20 h and stained with Syt G (orange) to visualize DNA. Infected THP-1 cells were treated with disulfiram (20 µM). UT, untreated. DIS, disulfiram. White arrowheads indicate extracellular web-like DNA structures. Scale bars represent 50 µm. **B, C** Quantification of DNA release and the percentage of Syt G+ cells. Welch's t-tests were applied for statistical analysis, with

p-values reported in decimal format. **D, E** Quantification of LDH release expressed as a percentage of the lysis control. THP-1 cells were infected with dsRed H37Rv Mtb at MOI:2 for 20 h in the presence or absence of disulfiram (20 μM). Two-way ANOVA with Šidák correction was performed, and *p*-values are shown (**D**). Bar graph showing the control experiment demonstrating the efficacy of disulfiram (20 μM). THP-1 cells were untreated or treated with disulfiram at 20 μM for 20 h prior to the addition of LPS, followed by stimulation with LPS and NIG as described in Methods. SC, solvent control; L/N, LPS and nigericin. **F**, Bar graph showing the percentage of cells with internalized Mtb among total cells in the corresponding frames. Multiple unpaired t-tests with Welch's correction were performed to compare the disulfiram-treated and untreated cells.

CASP4 and CASP5 have been recently reported to play critical roles in inflammasome activation in THP-1 cells during Mtb infection[227]. To assess their involvement, we employed *CASP4/5*$^{-/-}$ THP-1 cells. Time-lapse live-cell imaging demonstrated an increased frequency of DNA release events in *CASP4/5*$^{-/-}$ cells compared to the wild-type THP-1 cells control (**Fig. 26A** and **B**, **SVs 17** and **18**), despite comparable levels of cell necrosis between the two cell lines (**Fig. 26C** and **D**). ELISA revealed markedly reduced IL-1β secretion in *CASP 4,5*$^{-/-}$ cells during Mtb infection (**Fig. 26F**), and WB confirmed gene deletion (**Fig. 26E**). The abolishment of IL-1β release is consistent with previous findings[231]. Collectively, these results indicate that CASP4/5-mediated inflammasome activation is associated with Mtb infection but is dispensable for the induction of necrosis and DNA release in THP-1 cells.

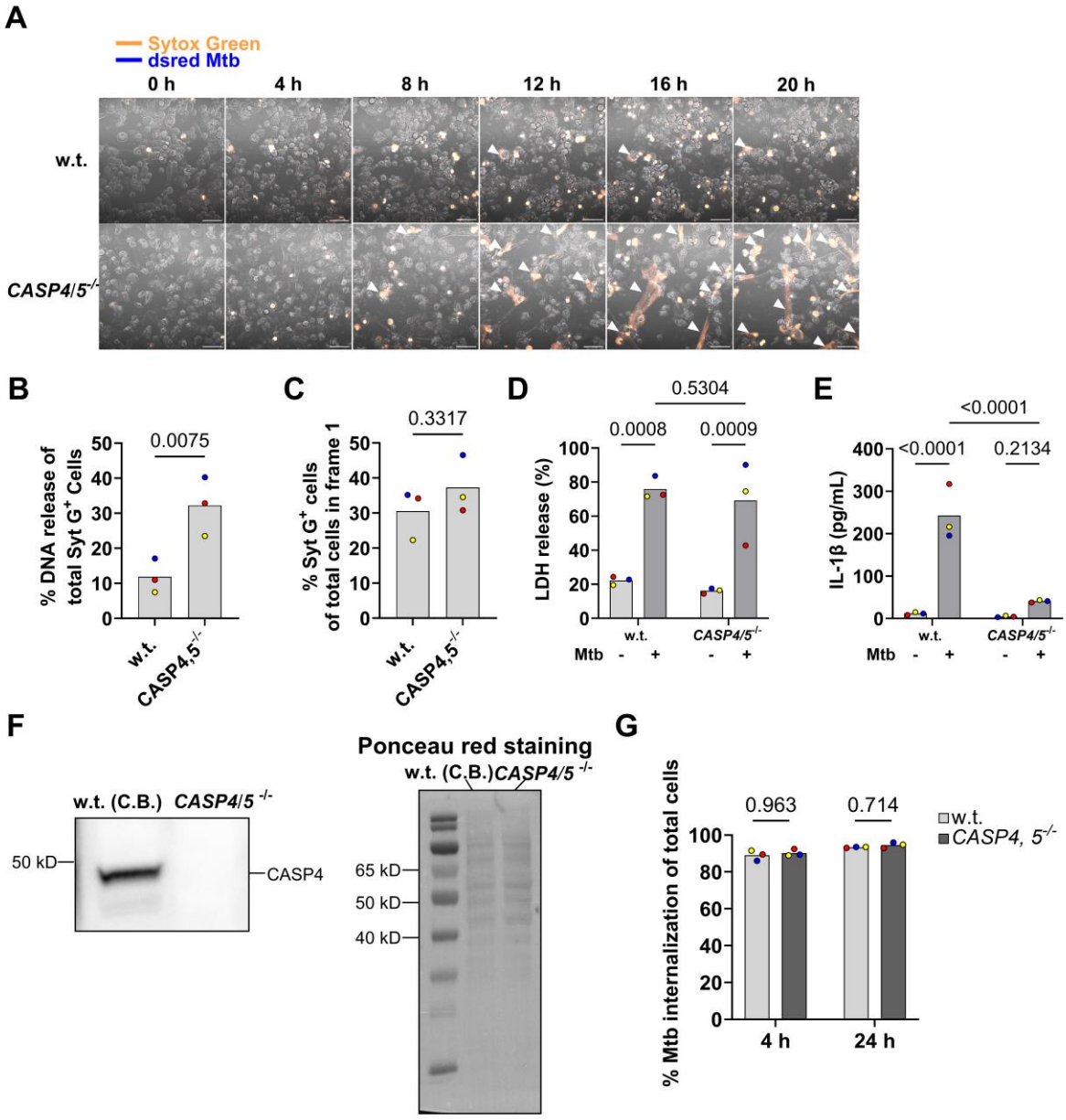

Fig. 26: CASP4 or 5 does not promote DNA release.

A Representative confocal time-lapse images showing infected *CASP4/5*$^{-/-}$ and w.t. THP-1 cells undergoing DNA release. THP-1 cells were a kind gift from Dr. Clare Bryant. The cells were infected with dsRed H37Rv Mtb (blue) at MOI:2 for 20 h and stained with Syt G (orange) to visualize DNA. White arrowheads indicate extracellular web-like DNA structures. Scale bars represent 50 µm. **B, C** Bar graphs showing the quantification of DNA release and PMR percentages. Each colored data point represents an independent experiment (N = 3) (the same applies to **D, E, and G)**. Welch's t-tests were performed, and *p*-values are shown in the graph. **D, E** Bar graphs showing the percentage of LDH release or the concentration of secreted IL-1β. Two-way ANOVA was used for statistical analysis, with *p*-values shown in the graphs. The ELISA was performed by Akshaya Ganesh (ORCID: 0000-0002-5432-118X)

F Immunoblot and Ponceau red staining confirming the genotype of THP-1 cell lines (N = 1). THP-1 cells were differentiated and left untreated. **G** Quantification of the percentage of Mtb internalization relative to the total cells in corresponding frames. Welch's t-tests were performed, and *p*-values are shown in the graph.

Finally, we examined NINJ1, a protein implicated in secondary necrosis, pyroptosis, and ferroptosis[141,176,285,289]. Time-lapse live-cell imaging revealed no significant differences between *NINJ1*$^{-/-}$ and wild-type THP-1 cells in either the proportion of necrotic cells or DNA release at 20 hours post-infection (**Fig. 27A–E**, **SVs 19** and **20**). Cell genotypes were validated by WB (**Fig. 27G)**, and phagocytic capacity was assessed by fluorescence microscopy (**Fig. 27H)**, and no difference was observed between the w.t. and *NINJ1*$^{-/-}$ cells. Notably, *NINJ1*$^{-/-}$ THP-1 cells did not exhibit delayed membrane rupture during Mtb infection as reflected by the Syt G staining (**Fig. 27D**). However, LDH release assay suggested that NINJ1 promotes cell lysis during Mtb infection. Overall, these data imply that, while initial PMR may occur via NINJ1-independent mechanisms in this context, final cell lysis depends on NINJ1.

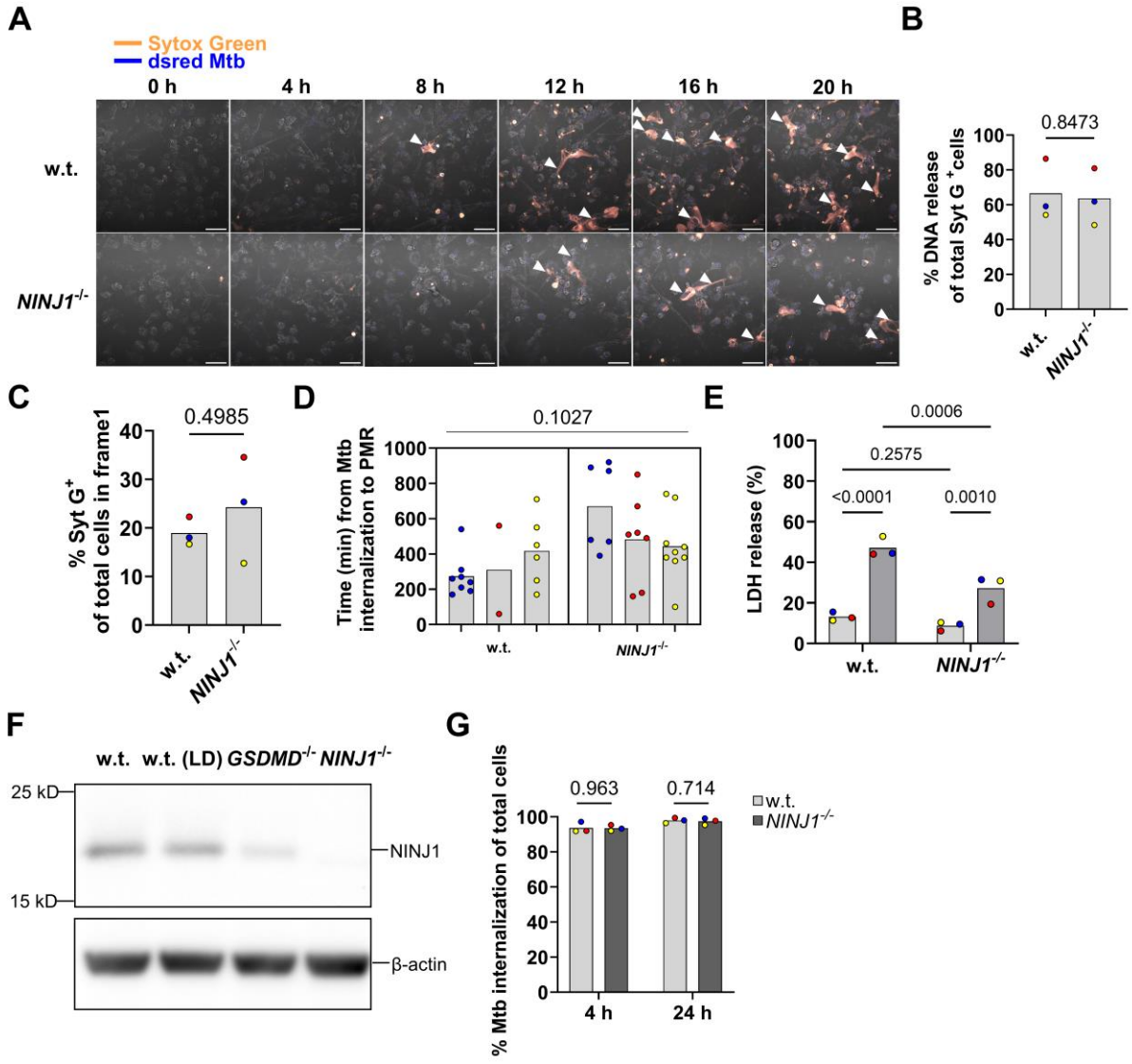

Fig. 27: NINJ1 promotes cell lysis of Mtb-infected THP-1 cells but is not required for DNA release.

A Representative confocal time-lapse images showing Mtb-infected *NINJ1*$^{-/-}$ and wildtype (w.t.) THP-1 cells undergoing DNA release. *NINJ1*$^{-/-}$ and its w.t. counterpart are kind gifts from Dr. Liron David. Cells were infected with dsRed H37Rv Mtb (blue) at MOI:2 for 20 h and stained with Syt G (orange) to visualize DNA (N = 3). White arrowheads indicate extracellular web-like DNA structures. Scale bars represent 50 µm. **B, C** Quantification of the percentage of DNA release (**B**) and Syt G^{+} cells (**C**). Welch's t-tests were applied for statistical analysis, with *p*-values reported in decimal format. **D** Quantification of time durations from Mtb internalization to PMR. A nested t-test was performed, and the *p*-value is shown. **E** LDH release relative to the lysis control. Two-way ANOVA was applied for statistical analysis, with *p*-values reported in the graph. **F** Immunoblot confirming *NINJ1* genotype in differentiated, untreated THP-1 cells (*N* = 1). **G** Quantification of the percentage of Mtb internalization relative to the total cells in corresponding frames (N = 3). Welch's t-tests were performed.

7.4 Discussion

Our live cell imaging approach demonstrates the release of DNA from dead, Mtb-infected THP-1 cells (**Fig. 19**). Similar observations have been reported in Mtb-infected hMDMs, where METosis was claimed[174]. Notably, we are the first to directly visualize the dynamic process of DNA release from dying, Mtb-infected THP-1 cells and hMDMs using time-lapse live-cell imaging (**Fig. 19A, SVs 7** and **9**). This analysis revealed that Mtb induces PMR preceding DNA release, which contrasts with the vital NETosis observed during Mtb infection of neutrophils[250]. This approach also allowed us, for the first time, to quantify the relative contribution of the DNA-release phenotype to total cell death. We find that ~60% of Mtb-infected THP-1 cells and ~30% of hMDMs deaths were associated with DNA release (**Fig. 19B, C, E,** and **F**). In addition, we observed that the movement of surrounding, live macrophages appears to expand the extracellular DNA, forming web-like structures (**Fig. 19A** and **B**, **SVs 7** and **9**), which could not be captured using microscopy approaches on fixed cells[246,287].

The importance of eDNA on host cells and Mtb was further assessed, and our data indicate that eDNA modestly exacerbates THP-1 cell death during Mtb infection, while not directly killing extracellular Mtb bacilli. Whether DNA release in human macrophages represents a distinct cell death modality governed by a specific signaling pathway remains unclear. For example, some studies have suggested that NETosis is closely linked to neutrophil GSDMD activation and pyroptosis[290]. Our findings indicate that all observed DNA release events occurred only after PMR and were independent of the pyroptosis pathway (**Figs. 24–26**). Moreover, given the minimal abundance of MPO and citH3 on the extracellular DNA (**Fig. 21A, D,** and **E**), it is unlikely that the DNA release in THP-1 cells follows the established NETosis signaling pathway.

Chapter 8: Comprehensive Discussion

8.1 Conclusions

This research project, titled *"Characterization of Programmed Cell Death Activated in Mycobacterium tuberculosis-infected THP-1 cells and human monocyte-derived macrophages"*, focuses on systematically analyzing the activation of cell death pathways during Mtb infection. Specifically, this study screened known cell death executioners in host cells and characterized a previously poorly defined phenomenon associated with Mtb-induced necrosis. Immunoblotting (WB) and confocal microscopy were the primary techniques used to investigate cell death pathways, supported by LDH release assays, ELISA, and inhibitor-based analyses.

We first characterized the kinetics of cell death induced by Mtb in THP-1 cells and hMDMs and selected the first three days post-infection as the optimal time window for sample acquisition and analysis (**Fig. 5**). We next showed that IFN-β secretion from infected THP-1 cells was minimal during Mtb infection, although STAT1 phosphorylation was detectable. However, blocking this IFNAR-mediated signaling pathway did not rescue THP-1 cells from cell death (**Figs. 6** and **7**), indicating that IFN-β signaling is not required for cell death induction during *ex vivo* Mtb infection in THP-1 cells.

We then examined apoptosis, a well-established non-necrotic form of cell death. YO-PRO-1 staining combined with confocal microscopy revealed minimal apoptosis induction in both THP-1 cells and hMDMs during Mtb infection. In contrast, bulk population immunoblotting detected CASP-3 activation in THP-1 cells but not in hMDMs **(Figs. 8–11**). Among the programmed necrotic pathways examined—pyroptosis, necroptosis, and ferroptosis—only pyroptosis was found to be moderately induced in Mtb-infected THP-1 cells (**Fig. 12**). Our data demonstrate that

necroptosis and ferroptosis were not induced in either Mtb-infected THP-1 cells or hMDMs (**Figs. 12–17**).

To further investigate terminal cell death events, we employed time-lapse live-cell imaging to assess lysosomal integrity within the final 2 h preceding plasma membrane rupture (PMR). Lysosomal membrane permeabilization (LMP) was not detected during the terminal phase of cell death execution in Mtb-infected THP-1 cells (**Figs. 18** and **19**). These largely negative findings are either consistent with or contrast with published reports, and such discrepancies may arise from differences in host cell types, infection protocols, or kinetic analyses.

Finally, we identified eDNA release from Mtb-infected THP-1 cells and hMDMs and termed this phenomenon DNA release-associated necrosis (DRAN). By focusing on the DNA release event, we characterized its kinetics, molecular composition, and biological relevance (**Figs. 20–24**). We concluded that DRAN observed in THP-1 cells during Mtb infection does not conform to the classical NETosis model, despite morphological similarities between the web-like eDNA structures and NETs.

To determine whether DRAN represents an independent cell death pathway, we examined the contribution of key pyroptosis signaling components to DRAN induction. Inhibition of GSDMD did not alter PMR or DNA release, indicating that while pyroptosis is induced during Mtb infection in THP-1 cells, it is not required for cell death execution (**Fig. 25**). Notably, eDNA release was significantly increased in the absence of CASP4/5, whereas IL-1β secretion was completely abolished (**Fig. 26**). Finally, the pan-executioner of cell lysis, NINJ1, was shown to contribute to Mtb-induced cell lysis but not to DNA release from infected, dying THP-1 cells (**Fig. 27**).

8.2 Novelty

This research is novel in its scope, experimental approaches, and conceptual findings. We performed a comprehensive and systematic analysis of multiple established programmed cell death (PCD) pathways in the context of Mtb infection in human macrophage models, including THP-1 cells and hMDMs. In parallel, we characterized DNA release-associated necrosis (DRAN) and directly compared this phenomenon with previously proposed METosis and NETosis models. Such a broad and integrated evaluation of cell death modalities remains rare in human macrophage models of tuberculosis.

A major methodological innovation of this study is the extensive use of time-lapse live-cell imaging to analyze LMP and DRAN at the single-cell level. Owing to biosafety constraints associated with live Mtb, this type of single-cell, long-term live imaging remains uncommon across the field. The resulting 20-h time-lapse datasets capturing Mtb-induced cell death in THP-1 cells and hMDMs, therefore, constitute a unique resource. This approach enabled precise temporal resolution of lysosomal integrity and quantitative assessment of DNA release events, information that cannot be obtained from fixed samples or static imaging alone.

Conceptually, this work advances the understanding of eDNA release in macrophages. In the NETosis field, the roles of inflammasome activation, GSDMD, and necrosis remain areas of active debate, and METosis research has largely followed conceptual frameworks established in neutrophils. However, mechanistic insight into METosis remains limited, and clear molecular criteria defining this process are lacking. Our study demonstrates a DNA-releasing necrotic phenotype in Mtb-infected THP-1 cells that shares some features with NETosis and METosis but exhibits markedly reduced engagement of canonical NETosis markers, including MPO and CitH3, and therefore does not conform to the established NETosis models. Importantly, DNase I-mediated

removal of extracellular DNA improved host macrophage survival without affecting extracellular Mtb growth, revealing a previously unrecognized biological relevance of DRAN in macrophage-Mtb interactions.

Furthermore, we demonstrate that DRAN occurs independently of pyroptosis in Mtb-infected THP-1 cells. Although pyroptosis is modestly induced, inhibition of its key executioner does not prevent PMR or DNA release. The relationship between DNA release and other programmed necrotic pathways has rarely been examined in macrophage models.

Finally, we provide novel insight into the role of NINJ1 during Mtb infection. Together with a recent, independent report by Dr. Trude Flo[291], our study is among the first to identify NINJ1 as a contributor to macrophage cell lysis during Mtb infection. Importantly, our data show that NINJ1 deficiency neither rescues THP-1 cells from early PMR nor inhibits extracellular DNA release. These findings exclude NINJ1 as the terminal executioner of Mtb-induced cell death and define its role as permissive rather than determinative, a distinction that was previously unknown.

8.3 Limitations

This research has several limitations related to experimental models, methodologies, scope, and mechanistic depth.

First, limitations related to experimental models should be acknowledged. THP-1 cells were used for most pathway analyses and phenotypic characterizations. Although the differentiation protocol employed here has been reported to generate macrophage-like cells that transcriptionally resemble unactivated hMDMs, differentiated THP-1 cells are not equivalent to primary human macrophages. Genes involved in cell death pathways may be transcriptionally or translationally regulated in unexpected ways. A relevant example is that SARM1 is not expressed in THP-1 cells but is expressed in hMDMs, highlighting intrinsic differences between the two

models. Another limitation of the THP-1 model is the relatively high baseline cell death observed in uninfected, untreated differentiated cells (<10% per day). This background cell death is non-negligible, particularly in experiments where total infection-associated cell death reaches only ~30–40%. Importantly, this phenomenon was consistently observed not only in our THP-1 cells but also in THP-1 cell lines obtained from other laboratories, although it has rarely been reported previously. This may reflect variability in differentiation protocols across the field or a lack of systematic investigation and reporting. Elevated baseline cell death could partially confound interpretations related to novel phenotypes such as DRAN. For hMDMs, monocytes were obtained from donors of unknown age and ethnicity, introducing biological heterogeneity that may contribute to increased variability, particularly when the number of biological replicates is limited. In addition, the characteristics of hMDMs differentiated using PMA in our laboratory were not comprehensively characterized, and differences in differentiation protocols may contribute to discrepancies observed between THP-1 cells and hMDMs. Notably, some hMDM donor groups exhibited strong resistance to Mtb infection, precluding robust cell death analyses (data not shown). This suggests that the hMDM infection model could be further optimized. For example, higher multiplicities of infection or cytokine priming may amplify differences between infected and uninfected groups and potentially enhance clinical relevance. Furthermore, although published studies indicate that Mtb can induce ferroptosis at later time points in hMDMs, we did not establish a long-term infection model, which may limit conclusions regarding the involvement or biological significance of ferroptosis.

Second, several methodological limitations related to fluorescence microscopy should be considered. Fluorophore selection could be further optimized. Syt G, commonly used in NETosis studies, has a broad emission spectrum that overlaps with dsRed expressed by Mtb and Lysoview,

constraining fluorophore combinations and image processing and presentation. It remains unclear whether alternative dyes, such as Draq7 or other nucleic acid stains, could provide eDNA signals comparable to Syt G. For Airyscan microscopy, DAPI was used to visualize DNA. However, DAPI is cytotoxic and requires ultraviolet excitation, which limits its suitability for live-cell imaging. Additionally, we did not systematically evaluate whether alternative fluorophore-labeled Mtb strains could provide brighter signals than dsRed-expressing H37Rv without altering bacterial virulence. Improved bacterial fluorescence could enhance quantitative analysis and data presentation. Quantification methods also have limitations. The percentage of Syt G-positive cells was determined by manual scoring, which may introduce subjectivity and variability. In comparative imaging analyses involving neutrophils and THP-1 cells, the number of selected ROIs was limited. Moreover, normalizing antibody fluorescence intensity to total DAPI intensity rather than to the volume of DAPI-positive regions may reduce quantitative precision. Finally, although our laboratory has established single-cell tracking and quantification pipelines, we did not systematically correlate key phenotypes with bacterial burden at the single-cell level, representing an important opportunity for future studies.

Third, the scope of this study was primarily host-focused. While this work aimed to systematically analyze host PCD pathways during Mtb infection, it did not directly investigate bacterial virulence factors known to modulate host cell death, such as PDIM, EsxA, or TNT. Potential direct interactions between Mtb virulence factors and host PCD machinery were therefore not addressed, which may result in the omission of important mechanisms. For example, recent work from Dr. Trude Flo and colleagues suggests a novel mode of cell death induction during Mtb infection[291], raising the possibility that Mtb may directly activate NINJ1 through specific virulence factors and induce cell lysis independently of canonical PCD pathways.

Additionally, a substantial portion of this study focused on evaluating established cell death pathways to contextualize novel findings. While this approach contributes to a broader understanding of macrophage cell death during Mtb infection, some results are not fully aligned with published data and are not themselves novel. Although discrepancies were discussed, they were not experimentally resolved.

Finally, the mechanistic depth of this work remains limited. Although this study systematically examined several established PCD pathways during Mtb infection and identified a DNA-release-associated necrotic phenotype, we did not define molecular hallmarks that could be used to quantitatively or conceptually delineate this phenomenon. The underlying mechanism by which infected macrophages release DNA into the extracellular space remains unresolved. This lack of mechanistic insight limits the biological interpretation and broader impact of the findings and highlights important directions for future investigation.

8.4 Biological significance

This research provides a systematic analysis of multiple host cell death pathways in THP-1 cells during Mtb infection, thereby contributing to a more nuanced understanding of this widely used human macrophage-like model in tuberculosis and cell death research. The absence or limited engagement of certain programmed cell death pathways in both THP-1 cells and hMDMs highlights important differences between human macrophage models and murine or zebrafish macrophage models, in which distinct cell death modalities have been repeatedly reported. These interspecies differences underscore the need for caution when extrapolating mechanistic findings across model systems. In the context of eDNA release, the inclusion of primary human neutrophils as a comparative model further emphasizes that morphologically similar DNA-release phenomena may arise from fundamentally different cellular programs. Understanding these discrepancies

across models may advance our knowledge of conserved versus context-dependent principles of cell biology.

A major strength of this work is the application of a recently developed single-cell tracking framework that enables longitudinal analysis of individual host cells during Mtb infection. In addition, we generated and shared a Cellpose model optimized for THP-1 cell segmentation, facilitating reproducibility and reuse. The image analysis and quantification pipelines were implemented in Python and released as open-source code by Dr. Jacques Augenstreich[276], allowing the analytical principles described here to be adapted broadly to other imaging-based studies of host-pathogen interactions

Importantly, this study demonstrates Mtb-induced host cell death using long-duration (20 h) live-cell imaging, enabling visualization of cell death as a dynamic process rather than a static endpoint. This approach captures morphological changes, intercellular interactions, and the temporal sequence of events leading from bacterial phagocytosis to terminal plasma membrane rupture. Notably, the full DRAN process can be observed, including the partial efferocytosis of dying cells and the apparent expansion of extracellular, trap-like DNA structures driven by macrophage motility. The ability to visualize these events in real time provides a mechanistic context that is not accessible through endpoint assays alone and may improve conceptual understanding of infection-induced cell death.

Furthermore, this work highlights the importance of distinguishing DRAN from previously described METosis or NETosis. Studies of NETosis have demonstrated that morphologically similar outcomes can be driven by distinct molecular mechanisms and can have divergent biological consequences. By demonstrating limited engagement of canonical NETosis markers while observing robust DNA release in infected macrophages, this study raises the possibility that

DRAN represents a mechanistically distinct process. These findings may prompt more rigorous definitions of DNA-release-associated phenomena and encourage deeper mechanistic investigations in future work.

Finally, the observed difference in LDH release between untreated and DNase I-treated conditions suggests that extracellular DNA may actively contribute to secondary cell damage rather than serving solely as a passive byproduct of cell death. This observation supports the hypothesis that DNA released from dying cells may amplify tissue injury through additional signaling pathways *in vivo*. Such mechanisms remain poorly explored in TB research and may have broader implications for understanding inflammation, tissue pathology, and HDT strategies. Further dissection of the mechanisms underlying this phenomenon could identify novel HDT targets to pharmacologically augment host defense against Mtb infection.

8.5 Future directions

Building on the findings of this study, several avenues of investigation could further advance understanding of host cell death during Mtb infection.

First, host cell metabolism represents an important and underexplored dimension of infection-induced cell death. Ferroptosis is intrinsically linked to cellular metabolic states, including lipid metabolism, redox balance, and iron homeostasis. A systematic analysis of metabolic remodeling in Mtb-infected macrophages may help explain why ferroptosis was not observed in our human cell models but has been reported in murine macrophages. In addition, metabolic profiling may uncover the engagement of other metabolism-dependent cell death pathways that were not addressed in this study.

Second, the involvement of subcellular organelles beyond lysosomes warrants further investigation. While this work investigates lysosomal membrane permeabilization, other organelles, particularly mitochondria and the endoplasmic reticulum, also play critical roles in regulating cell death signaling. The use of macrophage models expressing fluorophore-labeled organelles could enable real-time visualization of organelle dynamics during infection and may reveal previously unrecognized mechanisms of cell death induction or regulation.

Third, the direct contribution of Mtb virulence factors to host cell death pathways remains insufficiently defined. Several bacterial determinants are known to promote or inhibit macrophage death. However, their host targets and mechanisms of action are largely unknown. Elucidating the molecular interactions between specific Mtb virulence factors and host cell death machinery, as well as identifying additional bacterial factors associated with cell death regulation, would significantly strengthen the mechanistic framework of host-pathogen interactions.

Fourth, further differentiation of DRAN from METosis and NETosis requires deeper molecular characterization. Although studies of NETosis and METosis constitute an independent research field, applying proteomic approaches to the macrophage models described here may help resolve conceptual and mechanistic distinctions. For example, histone citrullination, particularly CitH3, is considered a hallmark of NETosis. However, histone citrullination in human cells is a complex and heterogeneous process involving multiple histone species and modification sites, making targeted, single-epitope analyses insufficient to comprehensively characterize this modification landscape. While the analysis of citrullination by MS has historically been challenging, recent methodological advances now enable more sensitive detection of histone citrullination events[292], which are thought to facilitate chromatin decondensation and DNA release.

Finally, the downstream and bystander effects of extracellular DNA release require further investigation. NETs bind and activate pattern recognition receptors, including TLRs[293], thereby amplifying inflammatory signaling. By analogy, it will be important to determine whether eDNA released during DRAN engages similar receptor-mediated pathways and contributes to intercellular communication, inflammation, or tissue damage during infection.

Appendices

Appendix A: Antibodies used in this research

Primary antibodies					
Target	**Manufacturer**	**Cat. no.**	**Conc.**	**Application**	**Dilution**
CL-CASP-3	Cell Signaling Technology	9664S	40 µg/mL	WB	1:1000
FL-CASP-3	Cell Signaling Technology	9662S	49 µg/mL	WB	1:1000
CASP-8	Enzo	ALX-804-242-C100	1 mg/mL	WB	1:1000
CASP-9	Cell Signaling Technology	9502S	52 µg/mL	WB	1:1000
GSDMD	NOVUS	NBP2-33422	0.15 mg/mL	WB	1:1000
GSDMD	Cell Signaling Technology	39754S	150 µg/mL	WB	1:1000
GSDME	Cell Signaling Technology	19453S	100 µg/mL	WB	1:1000
pMLKL	Cell Signaling Technology	EPR9514	0.642 mg/mL	WB	1:1000
MLKL	Cell Signaling Technology	14993S	Unknown	WB	1:1000
GPX4	Cell Signaling Technology	52455S	Unknown	WB	1:1000
NINJ1	BD Biosciences	610777	250 µg/mL	WB	1:1000
β-actin	Cell Signaling Technology	3700S	312 µg/mL	WB	1:1000
STAT1	Cell Signaling Technology	14994S	53 µg/mL	WB	1:1000
pSTAT1	Cell Signaling Technology	9167S	59 µg/mL	WB	1:1000
CASP4	Santa Cruz Biotechnology	sc-56056	100 µg/mL	WB	1:200
MPO	Santa Cruz Biotechnology	sc-52707	100 µg/mL	IFM	1:200
CitH3	Abcam	ab5103	1 mg/mL	IFM	1:200
Rabbit IgG Isotype Control	Cell Signaling Technology	3900S	2.5 mg/mL	IFM	1:5000
Mouse IgG1 Isotype Control	Cell Signaling Technology	5415S	2.5 mg/mL	IFM	1:5000
Neutralization antibodies					
Mouse Mab to Human IFN Alpha/Beta RC2	pbl assay science	21385-1	1 mg/mL	Neutralization	1:10000

Mouse IgG2a kappa Isotype	Invitrogen	14-4724-82	0.5 mg/mL	Neutralization	1:5000
Secondary antibodies					
Alexa Fluor 647-conjugated Goat anti-mouse IgG (H+L)	Jackson ImmunoResearch	115-605-062	1 mg/mL	IFM	1:200
Alexa Fluor 647-conjugated Goat anti-rabbit IgG (H+L)	Jackson ImmunoResearch	111-605-045	1 mg/mL	IFM	1:200
Peroxidase-conjugated AffinityPure Donkey anti-sheep IgG (H+L)	Jackson ImmunoResearch	713-035-003	0.8 mg/mL	WB	1:25 000
Peroxidase-conjugated AffinityPure Goat anti-rabbit IgG (H+L)	Jackson ImmunoResearch	115-035-062	0.8 mg/mL	WB	1:25 000
Peroxidase-conjugated AffinityPure Goat anti-mouse IgG (H+L)	Jackson ImmunoResearch	111-035-144	0.8 mg/mL	WB	1:25 000

Appendix B: Other materials used in this research

Cell culture materials ("-" represents uncertainty or not applicable)				
Material	**Manufacturer**	**Cat. no.**	**Final Conc.**	**Dilution Factor**
RPMI	ATCC	302001	-	85-90%
FBS	Gibco	A52567-01	-	10%
Human Serum	GeminiBio	100-110	-	5%
human Serum off the clot	GeminiBio	100-318	-	5%
DPBS	Gibco	14190144	-	-
Gentamicin	Corning	30-005-CR	500 µg/mL	1:100
PMA	Invivogen	tlrl-pma	50 ng/mL	-
hMCSF	R&D Systems	216-MC-010	10 ng/mL	-
Bacterial culture materials				
7H9	BD	271310	-	~88%
7H11	Sigma-Aldrich	M0428-500G	-	-
OADC	BD	212351	-	10%
Tween-80	Fisher Scientific	BP338-500	-	0.05%
Zeocin	Invivogen	ZEL-45-05	100 µg/mL	1:1000
Glycerol	Fisher Scientific	G33-4	-	0.2%
Kits, reagents, and dyes				
YO-PRO-1 (Oxazole Yellow)	Biotium	40089	0.5 µM	1:2000
CytoTox 96 Non-Radioactive Cytotoxicity assay	Promega	G1782	-	-
ToxLight BioAssay Kit	Lonza	LT07-217	-	-
Pierce BCA Protein Assay Kit	ThermoFisher	23225	-	-
SuperSignal West Pico PLUS Chemilumminescent Substrate	ThermoFisher	34577	-	-
PVDF Transfer Membrane 0.45 µM, 26.5 cm x 3.75 m roll	ThermoFisher	88518	-	-
SuperBlock Blocking Buffer - Blotting in PBS	ThermoFisher	37537	-	-
SurePAGE, Bis-Tris, 10x8	GenScript	M00668	-	-
Halt Protease & Phosphatase Single-use Inhibitor Cocktail (100X)	ThermoFisher	78442	-	-
Tween-20	Fisher Scientific	BP337-500	-	0.1% (WB)/0.2% (IFM)

Paraformaldehyde Solution, 4% in PBS	ThermoFisher	J19943-K2	-	-
Goat Serum	Gibco	16210-064	-	10%
Bovine Serum Albumin Solution	SIGMA	A9576	-	3% (blocking)/1% (staining)
Human IFN-beta DuoSet ELISA	R&D Systems	DY814-05	-	-
Human IL-1 beta/IL-1F2 DuoSet ELISA	R&D Systems	DY201	-	-
EasySep Direct Human Neutrophil Isolation Kit	Stemcell	19666	-	-
CD14 MicroBeads human	Miltenyi	130-050-201	-	1/3 of the instructed conc.
SYTOX™ Green Nucleic Acid Stain - 5 mM Solution in DMSO	Invitrogen	S7020	100 nM	1:50 000
Draq 7	Invitrogen	D15105	0.3 mM	1:1000
Liperfluo	Doujindo	L248	20 µM	-
Lysoview	Biotium	70058-1	-	1:2000
DAPI (1 mg/mL)	Invitrogen	62248	1 µg/mL	1:1000
Cell treatments				
Staurosporine	Sigma-Aldrich	S6942	1 mM	1:500
LPS-EB (Standard)	Invitrogen	tlrl-eblps	100 ng/mL	-
Nigericin	Invitrogen	tlrl-nig	20 µM	-
Raptino	Sigma-Aldrich	SML-1745	10 µM	-
MG132	Cell signaling Technology	2194S	1 µM	-
Cumyl hydroperoxide, tech. 80%	ThermoFisher	L06866.22	100 µM	-
LLoMe	BACHEM	16689-14-8	1 µM	-
RSL-3	MedChemExpress	HY-100218A	10 µM	-
Ferrostatin-1	MedChemExpress	HY-100579	10 µM	-
hTNF-α	R&D Systems	10291-TA-020	100 ng/mL	-
SM-164	Cell signaling Technology	56003S	10 µM	-
z-VAD-FMK	Cell signaling Technology	60332S	20 µM	-
Necrostatin-1	Sigma-Aldrich	480065	10 µM	-
Disulfiram	MedChemExpress	HY-B0240	20 µM	-
Dnase I	Invitrogen	90083	2,500 U/mL	1:25

Appendix C: Video labeling

SV	Description
1	THP-1 cells treated with MG132
2	Uninfected and untreated THP-1 cells
3	Uninfected and LLoMe-treated THP-1 cells
4	dsRed Mtb-infected THP-1 cells exhibiting increased LV intensity
5	dsRed Mtb-infected THP-1 cells exhibiting unchanged LV intensity
6	dsRed Mtb-infected THP-1 cells exhibiting decreased LV intensity
7	dsRed Mtb-infected THP-1 cells undergoing DNA release
8	Uninfected THP-1 cells undergoing DNA release
9	dsRed Mtb-infected hMDMs undergoing DNA release
10	Uninfected hMDMs does not undergoing DNA release
11	Zoomed-in region (Corr. SV7)
12	Zoomed-in region (Corr. SV9)
13	hNeu treated with PMA
14	3D rendering of Airyscan microscopic imaged infected THP-1 cells
15	untreated dsRed Mtb-infected THP-1 cells, (Corr. SV16)
16	DIS-treated dsRed Mtb-infected THP-1 cells
17	w.t.THP-1 cells infected with dsRed (Corr. SV18)
18	*CASP4/5*$^{-/-}$ THP-1 cells infected with dsRed Mtb
19	w.t. THP-1 cells infected with dsRed Mtb (Corr. SV20)
20	*NINJ1*$^{-/-}$ THP-1 cells infected with dsRed Mtb

Bibliography

1. *Global Tuberculosis Report 2024*. World Health Organization; 2024. https://www.who.int/teams/global-programme-on-tuberculosis-and-lung-health/tb-reports/global-tuberculosis-report-2024

2. Tuberculosis (TB). October 30, 2024. https://www.cdc.gov/tb/index.html

3. Trajman A, Campbell JR, Kunor T, et al. Tuberculosis. *Lancet*. 2025;405(10481):850-866. doi:10.1016/s0140-6736(24)02479-6

4. Gong W, Wu X. Differential Diagnosis of Latent Tuberculosis Infection and Active Tuberculosis: A Key to a Successful Tuberculosis Control Strategy. *Front Microbiol*. 2021;12:745592. doi:10.3389/fmicb.2021.745592

5. Delogu G, Sali M, Fadda G. THE BIOLOGY OF MYCOBACTERIUM TUBERCULOSIS INFECTION. *Mediterr J Hematol Infect Dis*. 2013;5(1):2013070. doi:10.4084/mjhid.2013.070

6. Flynn JL, Chan J. IMMUNOLOGY OF TUBERCULOSIS. *Annu Rev Immunol*. 2001;19(1):93-129. doi:10.1146/annurev.immunol.19.1.93

7. Rahlwes KC, Dias BRS, Campos PC, Alvarez-Arguedas S, Shiloh MU. Pathogenicity and virulence of Mycobacterium tuberculosis. *Virulence*. 2023;14(1):2150449. doi:10.1080/21505594.2022.2150449

8. Plumlee CR, Barrett HW, Shao DE, et al. Assessing vaccine-mediated protection in an ultra-low dose Mycobacterium tuberculosis murine model. *PLOS Pathog*. 2023;19(11):e1011825. doi:10.1371/journal.ppat.1011825

9. Pfyffer GE, Palicova F. Manual of Clinical Microbiology. Published online 2022:472-502. doi:10.1128/9781555816728.ch28

10. Sharpe S, White A, Gleeson F, et al. Ultra low dose aerosol challenge with Mycobacterium tuberculosis leads to divergent outcomes in rhesus and cynomolgus macaques. *Tuberculosis*. 2016;96:1-12. doi:10.1016/j.tube.2015.10.004

11. Nardell EA. Transmission and Institutional Infection Control of Tuberculosis. *Cold Spring Harb Perspect Med*. 2016;6(2):a018192. doi:10.1101/cshperspect.a018192

12. Lee J, Remold HG, Ieong MH, Kornfeld H. Macrophage Apoptosis in Response to High Intracellular Burden of Mycobacterium tuberculosis Is Mediated by a Novel Caspase-Independent Pathway. *J Immunol*. 2006;176(7):4267-4274. doi:10.4049/jimmunol.176.7.4267

13. Guirado E, Schlesinger LS, Kaplan G. Macrophages in tuberculosis: friend or foe. *Semin Immunopathol*. 2013;35(5):563-583. doi:10.1007/s00281-013-0388-2

14. Waal AM de, Hiemstra PS, Ottenhoff TH, Joosten SA, Does AM van der. Lung epithelial cells interact with immune cells and bacteria to shape the microenvironment in tuberculosis. *Thorax*. 2022;77(4):408-416. doi:10.1136/thoraxjnl-2021-217997

15. Scordo JM, Knoell DL, Torrelles JB. Alveolar Epithelial Cells in Mycobacterium tuberculosis Infection: Active Players or Innocent Bystanders? *J Innate Immun*. 2016;8(1):3-14. doi:10.1159/000439275

16. Chandra P, Grigsby SJ, Philips JA. Immune evasion and provocation by Mycobacterium tuberculosis. *Nat Rev Microbiol*. 2022;20(12):750-766. doi:10.1038/s41579-022-00763-4

17. Ganchua SKC, White AG, Klein EC, Flynn JL. Lymph nodes—The neglected battlefield in tuberculosis. *PLoS Pathog*. 2020;16(8):e1008632. doi:10.1371/journal.ppat.1008632

18. Flynn JL, Chan J. Immune cell interactions in tuberculosis. *Cell*. 2022;185(25):4682-4702. doi:10.1016/j.cell.2022.10.025

19. Sankar P, Mishra BB. Early innate cell interactions with Mycobacterium tuberculosis in protection and pathology of tuberculosis. *Front Immunol*. 2023;14:1260859. doi:10.3389/fimmu.2023.1260859

20. Gu Y, Lawrence T, Mohamed R, Liang Y, Yahaya BH. The emerging roles of interstitial macrophages in pulmonary fibrosis: A perspective from scRNA-seq analyses. *Front Immunol*. 2022;13:923235. doi:10.3389/fimmu.2022.923235

21. Borkute RR, Woelke S, Pei G, Dorhoi A. Neutrophils in Tuberculosis: Cell Biology, Cellular Networking and Multitasking in Host Defense. *Int J Mol Sci*. 2021;22(9):4801. doi:10.3390/ijms22094801

22. Liu Q, Que S, Qiu Y, et al. Host Immune Response to Mycobacterium tuberculosis Infection: Implications for Vaccine Development. *J Inflamm Res*. 2025;18(0):8429-8445. doi:10.2147/jir.s517034

23. Chowdhury CS, Kinsella RL, McNehlan ME, et al. Type I IFN-mediated NET release promotes Mycobacterium tuberculosis replication and is associated with granuloma caseation. *Cell Host & Microbe*. 2024;32(12):2092-2111.e7. doi:10.1016/j.chom.2024.11.008

24. Kim H, Shin SJ. Pathological and protective roles of dendritic cells in Mycobacterium tuberculosis infection: Interaction between host immune responses and pathogen evasion. *Front Cell Infect Microbiol*. 2022;12:891878. doi:10.3389/fcimb.2022.891878

25. Mihret A. The role of dendritic cells in Mycobacterium tuberculosis infection. *Virulence*. 2012;3(7):654-659. doi:10.4161/viru.22586

26. Stewart P, Patel S, Comer A, et al. Role of B Cells in Mycobacterium Tuberculosis Infection. *Vaccines*. 2023;11(5):955. doi:10.3390/vaccines11050955

27. Achkar JM, Chan J, Casadevall A. B cells and antibodies in the defense against Mycobacterium tuberculosis infection. *Immunol Rev*. 2015;264(1):167-181. doi:10.1111/imr.12276

28. Loxton AG. Bcells and their regulatory functions during Tuberculosis: Latency and active disease. *Mol Immunol*. 2019;111:145-151. doi:10.1016/j.molimm.2019.04.012

29. Rao M, Valentini D, Poiret T, et al. B in TB: B Cells as Mediators of Clinically Relevant Immune Responses in Tuberculosis. *Clin Infect Dis*. 2015;61(suppl_3):S225-S234. doi:10.1093/cid/civ614

30. Kozakiewicz L, Phuah J, Flynn J, Chan J. The New Paradigm of Immunity to Tuberculosis. *Adv Exp Med Biol*. 2013;783:225-250. doi:10.1007/978-1-4614-6111-1_12

31. Pagán AJ, Ramakrishnan L. The Formation and Function of Granulomas. *Annu Rev Immunol*. 2012;36(1):1-27. doi:10.1146/annurev-immunol-032712-100022

32. Hughes EJ, Tobin DM. Decoding the tuberculous granuloma. *Immunity*. 2022;55(5):819-821. doi:10.1016/j.immuni.2022.04.009

33. Sholeye AR, Williams AA, Loots DT, Furth AMT van, Kuip M van der, Mason S. Tuberculous Granuloma: Emerging Insights From Proteomics and Metabolomics. *Front Neurol*. 2022;13:804838. doi:10.3389/fneur.2022.804838

34. Lyu J, Narum DE, Baldwin SL, et al. Understanding the development of tuberculous granulomas: insights into host protection and pathogenesis, a review in humans and animals. *Front Immunol*. 2024;15:1427559. doi:10.3389/fimmu.2024.1427559

35. Ramakrishnan L. Revisiting the role of the granuloma in tuberculosis. *Nat Rev Immunol*. 2012;12(5):352-366. doi:10.1038/nri3211

36. Zhang Q ao, Ma S, Li P, Xie J. The dynamics of Mycobacterium tuberculosis phagosome and the fate of infection. *Cell Signal*. 2023;108:110715. doi:10.1016/j.cellsig.2023.110715

37. Ehrt S, Schnappinger D. Mycobacterial survival strategies in the phagosome: defence against host stresses. *Cell Microbiol*. 2009;11(8):1170-1178. doi:10.1111/j.1462-5822.2009.01335.x

38. Behar SM, Briken V. Apoptosis inhibition by intracellular bacteria and its consequence on host immunity. *Current Opinion in Immunology*. 2019;60:103-110. doi:10.1016/j.coi.2019.05.007

39. Shim D, Kim H, Shin SJ. Mycobacterium tuberculosis Infection-Driven Foamy Macrophages and Their Implications in Tuberculosis Control as Targets for Host-Directed Therapy. *Front Immunol*. 2020;11:910. doi:10.3389/fimmu.2020.00910

40. Cambier CJ, Falkow S, Ramakrishnan L. Host Evasion and Exploitation Schemes of Mycobacterium tuberculosis. *Cell*. 2014;159(7):1497-1509. doi:10.1016/j.cell.2014.11.024

41. Marakalala MJ, Raju RM, Sharma K, et al. Inflammatory signaling in human tuberculosis granulomas is spatially organized. *Nat Med*. 2016;22(5):531-538. doi:10.1038/nm.4073

42. Cadena AM, Fortune SM, Flynn JL. Heterogeneity in tuberculosis. *Nat Rev Immunol*. 2017;17(11):691-702. doi:10.1038/nri.2017.69

43. Lenaerts A, Barry CE, Dartois V. Heterogeneity in tuberculosis pathology, microenvironments and therapeutic responses. *Immunol Rev*. 2015;264(1):288-307. doi:10.1111/imr.12252

44. Tewoldemedhin B, Al-Ethawi S, Abouzeid W, et al. Persistent Fever in Tuberculosis: Clinical Experience and Literature Review. *Cureus*. 2024;16(9):e69391. doi:10.7759/cureus.69391

45. Luies L, Preez I du. The Echo of Pulmonary Tuberculosis: Mechanisms of Clinical Symptoms and Other Disease-Induced Systemic Complications. *Clin Microbiol Rev*. 2020;33(4):10.1128/cmr.00036-20. doi:10.1128/cmr.00036-20

46. Ruhl CR, Pasko BL, Khan HS, et al. Mycobacterium tuberculosis Sulfolipid-1 Activates Nociceptive Neurons and Induces Cough. *Cell*. 2020;181(2):293-305.e11. doi:10.1016/j.cell.2020.02.026

47. Behr MA, Edelstein PH, Ramakrishnan L. SLeuthing Tuberculous Cough. *Cell*. 2020;181(2):230-232. doi:10.1016/j.cell.2020.03.057

48. Dinkele R, Khan PY, Warner DF. Mycobacterium tuberculosis transmission: the importance of precision. *Lancet Infect Dis*. 2024;24(7):679-681. doi:10.1016/s1473-3099(24)00154-3

49. Churchyard G, Kim P, Shah NS, et al. What We Know About Tuberculosis Transmission: An Overview. *J Infect Dis*. 2017;216(suppl_6):S629-S635. doi:10.1093/infdis/jix362

50. Angelidou A, Diray-Arce J, Conti MG, et al. BCG as a Case Study for Precision Vaccine Development: Lessons From Vaccine Heterogeneity, Trained Immunity, and Immune Ontogeny. *Front Microbiol*. 2020;11:332. doi:10.3389/fmicb.2020.00332

51. Kumar P. A Perspective on the Success and Failure of BCG. *Front Immunol*. 2021;12:778028. doi:10.3389/fimmu.2021.778028

52. Gonzalo-Asensio J, Marinova D, Martin C, Aguilo N. MTBVAC: Attenuating the Human Pathogen of Tuberculosis (TB) Toward a Promising Vaccine against the TB Epidemic. *Front Immunol*. 2017;8:1803. doi:10.3389/fimmu.2017.01803

53. Ari MM, Beig M, Sholeh M, Khoshmirsafa M. The BCG vaccine, advantages, and disadvantages of introducing new generation vaccines against Mycobacterium tuberculosis. *Clin Exp Vaccine Res*. 2024;13(3):184-201. doi:10.7774/cevr.2024.13.3.184

54. Saukkonen JJ, Duarte R, Munsiff SS, et al. Updates on the Treatment of Drug-Susceptible and Drug-Resistant Tuberculosis: An Official ATS/CDC/ERS/IDSA Clinical Practice Guideline. *Am J Respir Crit Care Med*. 2025;211(1):15-33. doi:10.1164/rccm.202410-2096st

55. Warner DF, Barczak AK, Gutierrez MG, Mizrahi V. Mycobacterium tuberculosis biology, pathogenicity and interaction with the host. *Nat Rev Microbiol*. Published online 2025:1-17. doi:10.1038/s41579-025-01201-x

56. Riojas MA, McGough KJ, Rider-Riojas CJ, Rastogi N, Hazbón MH. Phylogenomic analysis of the species of the Mycobacterium tuberculosis complex demonstrates that Mycobacterium africanum, Mycobacterium bovis, Mycobacterium caprae, Mycobacterium microti and Mycobacterium pinnipedii are later heterotypic synonyms of Mycobacterium tuberculosis. *Int J Syst Evol Microbiol*. 2017;68(1):324-332. doi:10.1099/ijsem.0.002507

57. Reichmann M, Tezera LB, Denney L, et al. A co-evolutionary perspective on humans and Mycobacterium tuberculosis in the era of systems biology. Published online 2025. doi:10.7554/elife.108175.1

58. Cook GM, Berney M, Gebhard S, et al. Physiology of Mycobacteria. *Adv Microb Physiol*. 2009;55:81-319. doi:10.1016/s0065-2911(09)05502-7

59. Daffé M, Marrakchi H. Unraveling the Structure of the Mycobacterial Envelope. *Microbiol Spectr*. 2019;7(4):10.1128/microbiolspec.gpp3-0027-2018. doi:10.1128/microbiolspec.gpp3-0027-2018

60. Kalscheuer R, Palacios A, Anso I, et al. The Mycobacterium tuberculosis capsule: a cell structure with key implications in pathogenesis. *Biochem J*. 2019;476(14):1995-2016. doi:10.1042/bcj20190324

61. Hart EM, Bernhardt TG. The mycomembrane. *Curr Biol*. 2025;35(3):R85-R86. doi:10.1016/j.cub.2024.11.002

62. Jackson M. The Mycobacterial Cell Envelope—Lipids. *Cold Spring Harb Perspect Med*. 2014;4(10):a021105. doi:10.1101/cshperspect.a021105

63. Augenstreich J, Briken V. Host Cell Targets of Released Lipid and Secreted Protein Effectors of Mycobacterium tuberculosis. *Frontiers in Cellular and Infection Microbiology*. 2020;10:595029. doi:10.3389/fcimb.2020.595029

64. Ramon-Luing LA, Palacios Y, Ruiz A, Téllez-Navarrete NA, Chavez-Galan L. Virulence Factors of Mycobacterium tuberculosis as Modulators of Cell Death Mechanisms. *Pathogens*. 2023;12(6):839. doi:10.3390/pathogens12060839

65. Quigley J, Hughitt VK, Velikovsky CA, Mariuzza RA, El-Sayed NM, Briken V. The Cell Wall Lipid PDIM Contributes to Phagosomal Escape and Host Cell Exit of \textitMycobacterium tuberculosis. ["Kaufmann", Stefan"] "H. E., eds. *mBio*. 2017;8(2):e00148-17. doi:10.1128/mbio.00148-17

66. Queval CJ, Brosch R, Simeone R. The Macrophage: A Disputed Fortress in the Battle against Mycobacterium tuberculosis. *Front Microbiol*. 2017;8:2284. doi:10.3389/fmicb.2017.02284

67. Weiss G, Schaible UE. Macrophage defense mechanisms against intracellular bacteria. *Immunol Rev*. 2015;264(1):182-203. doi:10.1111/imr.12266

68. Maphasa RE, Meyer M, Dube A. The Macrophage Response to Mycobacterium tuberculosis and Opportunities for Autophagy Inducing Nanomedicines for Tuberculosis Therapy. *Front Cell Infect Microbiol*. 2021;10:618414. doi:10.3389/fcimb.2020.618414

69. Bo H, Moure UAE, Yang Y, et al. Mycobacterium tuberculosis-macrophage interaction: Molecular updates. *Front Cell Infect Microbiol*. 2023;13:1062963. doi:10.3389/fcimb.2023.1062963

70. Mittal E, Prasad GVRK, Upadhyay S, et al. Mycobacterium tuberculosis virulence lipid PDIM inhibits autophagy in mice. *Nat Microbiol*. 2024;9(11):2970-2984. doi:10.1038/s41564-024-01797-5

71. Ricky J. The Dual Role of Mitochondrial ROS in Mycobacterial Infections. *Journal of Biology and Today's World*. 2024;13(1):007. doi:10.35248/2322-3308-13.1.007

72. Prolo C, Álvarez MN, Radi R. Peroxynitrite, a potent macrophage-derived oxidizing cytotoxin to combat invading pathogens. *BioFactors*. 2014;40(2):215-225. doi:10.1002/biof.1150

73. Jayaraman P, Sada-Ovalle I, Nishimura T, et al. IL-1β Promotes Antimicrobial Immunity in Macrophages by Regulating TNFR Signaling and Caspase-3 Activation. *J Immunol*. 2013;190(8):4196-4204. doi:10.4049/jimmunol.1202688

74. Giacomini E, Iona E, Ferroni L, et al. Infection of Human Macrophages and Dendritic Cells with Mycobacterium tuberculosis Induces a Differential Cytokine Gene Expression That Modulates T Cell Response. *J Immunol*. 2001;166(12):7033-7041. doi:10.4049/jimmunol.166.12.7033

75. Algood HMS, Lin PL, Yankura D, Jones A, Chan J, Flynn JL. TNF Influences Chemokine Expression of Macrophages In Vitro and That of CD11b+ Cells In Vivo during Mycobacterium tuberculosis Infection. *J Immunol*. 2004;172(11):6846-6857. doi:10.4049/jimmunol.172.11.6846

76. Domingo-Gonzalez R, Prince O, Cooper A, Khader SA. Cytokines and Chemokines in Mycobacterium tuberculosis Infection. *Microbiol Spectr*. 2016;4(5):10.1128/microbiolspec.tbtb2-0018-2016. doi:10.1128/microbiolspec.tbtb2-0018-2016

77. Roca FJ, Whitworth LJ, Redmond S, Jones AA, Ramakrishnan L. TNF Induces Pathogenic Programmed Macrophage Necrosis in Tuberculosis through a Mitochondrial-Lysosomal-Endoplasmic Reticulum Circuit. *Cell*. 2019;178(6):1344-1361.e11. doi:10.1016/j.cell.2019.08.004

78. Silvério D, Gonçalves R, Appelberg R, Saraiva M. Advances on the Role and Applications of Interleukin-1 in Tuberculosis. *mBio*. 2021;12(6):e03134-21. doi:10.1128/mbio.03134-21

79. Mazewski C, Perez RE, Fish EN, Platanias LC. Type I Interferon (IFN)-Regulated Activation of Canonical and Non-Canonical Signaling Pathways. *Front Immunol*. 2020;11:606456. doi:10.3389/fimmu.2020.606456

80. Schoggins JW. Interferon-Stimulated Genes: What Do They All Do? *Annu Rev Virol*. 2019;6(1):1-18. doi:10.1146/annurev-virology-092818-015756

81. Donovan ML, Schultz TE, Duke TJ, Blumenthal A. Type I Interferons in the Pathogenesis of Tuberculosis: Molecular Drivers and Immunological Consequences. *Front Immunol*. 2017;8:1633. doi:10.3389/fimmu.2017.01633

82. Kotov DI, Lee OV, Fattinger SA, et al. Early cellular mechanisms of type I interferon-driven susceptibility to tuberculosis. *Cell*. 2023;186(25):5536-5553.e22. doi:10.1016/j.cell.2023.11.002

83. Ji DX, Yamashiro LH, Chen KJ, et al. Type I interferon-driven susceptibility to Mycobacterium tuberculosis is mediated by IL-1Ra. *Nat Microbiol*. 2019;4(12):2128-2135. doi:10.1038/s41564-019-0578-3

84. Moreira-Teixeira L, Sousa J, McNab FW, et al. Type I IFN Inhibits Alternative Macrophage Activation during Mycobacterium tuberculosis Infection and Leads to Enhanced Protection in the Absence of IFN-γ Signaling. *J Immunol*. 2016;197(12):4714-4726. doi:10.4049/jimmunol.1600584

85. Zhang L, Jiang X, Pfau D, Ling Y, Nathan CF. Type I interferon signaling mediates Mycobacterium tuberculosis-induced macrophage death. *The Journal of Experimental Medicine*. 2021;218(2):e20200887. doi:10.1084/jem.20200887

86. Olson GS, Murray TA, Jahn AN, et al. Type I interferon decreases macrophage energy metabolism during mycobacterial infection. *Cell Rep*. 2021;35(9):109195. doi:10.1016/j.celrep.2021.109195

87. Lee AM, Nathan CF. Type I interferon exacerbates Mycobacterium tuberculosis induced human macrophage death. *EMBO Reports*. 2024;25(7):3064-3089. doi:10.1038/s44319-024-00171-0

88. Elmore S. Apoptosis: A Review of Programmed Cell Death. *Toxicol Pathol*. 2007;35(4):495-516. doi:10.1080/01926230701320337

89. Newton K, Strasser A, Kayagaki N, Dixit VM. Cell death. *Cell*. 2024;187(2):235-256. doi:10.1016/j.cell.2023.11.044

90. Vitale I, Pietrocola F, Guilbaud E, et al. Apoptotic cell death in disease—Current understanding of the NCCD 2023. *Cell Death Differ*. 2023;30(5):1097-1154. doi:10.1038/s41418-023-01153-w

91. Lossi L. The concept of intrinsic versus extrinsic apoptosis. *Biochem J*. 2022;479(3):357-384. doi:10.1042/bcj20210854

92. Nair P, Lu M, Petersen S, Ashkenazi A. Chapter Five Apoptosis Initiation Through the Cell-Extrinsic Pathway. *Methods Enzym*. 2014;544:99-128. doi:10.1016/b978-0-12-417158-9.00005-4

93. Dickens LS, Powley IR, Hughes MA, MacFarlane M. The 'complexities' of life and death: Death receptor signalling platforms. *Exp Cell Res*. 2012;318(11):1269-1277. doi:10.1016/j.yexcr.2012.04.005

94. Orning P, Lien E. Multiple roles of caspase-8 in cell death, inflammation, and innate immunity. *J Leucoc Biol*. 2020;109(1):121-141. doi:10.1002/jlb.3mr0420-305r

95. Mandal R, Barrón JC, Kostova I, Becker S, Strebhardt K. Caspase-8: The double-edged sword. *Biochim Biophys Acta (BBA) - Rev Cancer*. 2020;1873(2):188357. doi:10.1016/j.bbcan.2020.188357

96. Tummers B, Green DR. Caspase-8: regulating life and death. *Immunol Rev*. 2017;277(1):76-89. doi:10.1111/imr.12541

97. D'Arcy MS. Cell death: a review of the major forms of apoptosis, necrosis and autophagy. *Cell Biol Int*. 2019;43(6):582-592. doi:10.1002/cbin.11137

98. Sedlackova L, Korolchuk VI. Mitochondrial quality control as a key determinant of cell survival. *Biochim Biophys Acta (BBA) - Mol Cell Res*. 2019;1866(4):575-587. doi:10.1016/j.bbamcr.2018.12.012

99. Li P, Zhou L, Zhao T, et al. Caspase-9: structure, mechanisms and clinical application. *Oncotarget*. 2017;8(14):23996-24008. doi:10.18632/oncotarget.15098

100. Twiddy D, Cain K. Caspase-9 cleavage, do you need it? *Biochem J*. 2007;405(1):e1-2. doi:10.1042/bj20070617

101. Mustafa M, Ahmad R, Tantry IQ, et al. Apoptosis: A Comprehensive Overview of Signaling Pathways, Morphological Changes, and Physiological Significance and Therapeutic Implications. *Cells*. 2024;13(22):1838. doi:10.3390/cells13221838

102. Qian S, Wei Z, Yang W, Huang J, Yang Y, Wang J. The role of BCL-2 family proteins in regulating apoptosis and cancer therapy. *Front Oncol*. 2022;12:985363. doi:10.3389/fonc.2022.985363

103. Singh R, Letai A, Sarosiek K. Regulation of apoptosis in health and disease: the balancing act of BCL-2 family proteins. *Nat Rev Mol Cell Biol*. 2019;20(3):175-193. doi:10.1038/s41580-018-0089-8

104. Silke J, Vucic D. Chapter Two IAP Family of Cell Death and Signaling Regulators. *Methods Enzym*. 2014;545:35-65. doi:10.1016/b978-0-12-801430-1.00002-0

105. Silke J, Meier P. Inhibitor of Apoptosis (IAP) Proteins–Modulators of Cell Death and Inflammation. *Cold Spring Harb Perspect Biol*. 2013;5(2):a008730. doi:10.1101/cshperspect.a008730

106. YANG YL, LI XM. The IAP family: endogenous caspase inhibitors with multiple biological activities. *Cell Res*. 2000;10(3):169-177. doi:10.1038/sj.cr.7290046

107. Cosentino K, Hertlein V, Jenner A, et al. The interplay between BAX and BAK tunes apoptotic pore growth to control mitochondrial-DNA-mediated inflammation. *Mol Cell*. 2022;82(5):933-949.e9. doi:10.1016/j.molcel.2022.01.008

108. Moldoveanu T, Czabotar PE. BAX, BAK, and BOK: A Coming of Age for the BCL-2 Family Effector Proteins. *Cold Spring Harb Perspect Biol*. 2020;12(4):a036319. doi:10.1101/cshperspect.a036319

109. Kantari C, Walczak H. Caspase-8 and Bid: Caught in the act between death receptors and mitochondria. *Biochim Biophys Acta (BBA) - Mol Cell Res*. 2011;1813(4):558-563. doi:10.1016/j.bbamcr.2011.01.026

110. Eskander G, Abdelhamid SG, Wahdan SA, Radwan SM. Insights on the crosstalk among different cell death mechanisms. *Cell Death Discov*. 2025;11(1):56. doi:10.1038/s41420-025-02328-9

111. Galbán S, Duckett CS. XIAP as a ubiquitin ligase in cellular signaling. *Cell Death Differ*. 2010;17(1):54-60. doi:10.1038/cdd.2009.81

112. Obexer P, Ausserlechner MJ. X-Linked Inhibitor of Apoptosis Protein – A Critical Death Resistance Regulator and Therapeutic Target for Personalized Cancer Therapy. *Front Oncol*. 2014;4:197. doi:10.3389/fonc.2014.00197

113. Mehrotra P, Ravichandran KS. Drugging the efferocytosis process: concepts and opportunities. *Nat Rev Drug Discov*. 2022;21(8):601-620. doi:10.1038/s41573-022-00470-y

114. Boada-Romero E, Martinez J, Heckmann BL, Green DR. The clearance of dead cells by efferocytosis. *Nat Rev Mol Cell Biol*. 2020;21(7):398-414. doi:10.1038/s41580-020-0232-1

115. Doran AC, Yurdagul A, Tabas I. Efferocytosis in health and disease. *Nat Rev Immunol*. 2020;20(4):254-267. doi:10.1038/s41577-019-0240-6

116. Morioka S, Maueröder C, Ravichandran KS. Living on the Edge: Efferocytosis at the Interface of Homeostasis and Pathology. *Immunity*. 2019;50(5):1149-1162. doi:10.1016/j.immuni.2019.04.018

117. Liao XX, Dai YZ, Zhao YZ, Nie K. Gasdermin E: A Prospective Target for Therapy of Diseases. *Front Pharmacol*. 2022;13:855828. doi:10.3389/fphar.2022.855828

118. Rogers C, Alnemri ES. Gasdermins in Apoptosis: New players in an Old Game. *Yale J Biol Med*. 2019;92(4):603-617.

119. Galluzzi L, Kroemer G. Secondary Necrosis: Accidental No More. *Trends Cancer*. 2017;3(1):1-2. doi:10.1016/j.trecan.2016.12.001

120. Silva MT. Secondary necrosis: The natural outcome of the complete apoptotic program. *FEBS Lett*. 2010;584(22):4491-4499. doi:10.1016/j.febslet.2010.10.046

121. Sachet M, Liang YY, Oehler R. The immune response to secondary necrotic cells. *Apoptosis*. 2017;22(10):1189-1204. doi:10.1007/s10495-017-1413-z

122. Hao W, Feng C. Research progress on pyroptosis and its effect on the central nervous system. *Neurobiol Dis*. 2023;188:106333. doi:10.1016/j.nbd.2023.106333

123. Chai R, Li Y, Shui L, Ni L, Zhang A. The role of pyroptosis in inflammatory diseases. *Front Cell Dev Biol*. 2023;11:1173235. doi:10.3389/fcell.2023.1173235

124. Tang D, Wang H, Billiar TR, Kroemer G, Kang R. Emerging mechanisms of immunocoagulation in sepsis and septic shock. *Trends Immunol*. 2021;42(6):508-522. doi:10.1016/j.it.2021.04.001

125. Galluzzi L, Vitale I, Aaronson SA, et al. Molecular mechanisms of cell death: recommendations of the Nomenclature Committee on Cell Death 2018. *Cell Death Differ*. 2018;25(3):486-541. doi:10.1038/s41418-017-0012-4

126. Anderson MJ, Hartigh AB den, Fink SL. Pyroptosis, Methods and Protocols. *Methods Mol Biol*. 2023;2641:1-16. doi:10.1007/978-1-0716-3040-2_1

127. Yu P, Zhang X, Liu N, Tang L, Peng C, Chen X. Pyroptosis: mechanisms and diseases. *Signal Transduct Target Ther*. 2021;6(1):128. doi:10.1038/s41392-021-00507-5

128. Dai Y, Zhou J, Shi C. Inflammasome: structure, biological functions, and therapeutic targets. *MedComm*. 2023;4(5):e391. doi:10.1002/mco2.391

129. Zheng D, Liwinski T, Elinav E. Inflammasome activation and regulation: toward a better understanding of complex mechanisms. *Cell Discov*. 2020;6:36. doi:10.1038/s41421-020-0167-x

130. Liao Y, Kong Y, Chen H, Xia J, Zhao J, Zhou Y. Unraveling the priming phase of NLRP3 inflammasome activation: Molecular insights and clinical relevance. *Int Immunopharmacol*. 2025;146:113821. doi:10.1016/j.intimp.2024.113821

131. Blevins HM, Xu Y, Biby S, Zhang S. The NLRP3 Inflammasome Pathway: A Review of Mechanisms and Inhibitors for the Treatment of Inflammatory Diseases. *Front Aging Neurosci*. 2022;14:879021. doi:10.3389/fnagi.2022.879021

132. Paik S, Kim JK, Silwal P, Sasakawa C, Jo EK. An update on the regulatory mechanisms of NLRP3 inflammasome activation. *Cell Mol Immunol*. 2021;18(5):1141-1160. doi:10.1038/s41423-021-00670-3

133. Kelley N, Jeltema D, Duan Y, He Y. The NLRP3 Inflammasome: An Overview of Mechanisms of Activation and Regulation. *Int J Mol Sci*. 2019;20(13):3328. doi:10.3390/ijms20133328

134. Swanson KV, Deng M, Ting JPY. The NLRP3 inflammasome: molecular activation and regulation to therapeutics. *Nat Rev Immunol*. 2019;19(8):477-489. doi:10.1038/s41577-019-0165-0

135. Gangopadhyay A, Devi S, Tenguria S, et al. NLRP3 licenses NLRP11 for inflammasome activation in human macrophages. *Nat Immunol*. 2022;23(6):892-903. doi:10.1038/s41590-022-01220-3

136. Opdenbosch NV, Lamkanfi M. Caspases in Cell Death, Inflammation, and Disease. *Immunity*. 2019;50(6):1352-1364. doi:10.1016/j.immuni.2019.05.020

137. Rojas-Lopez M, Gil-Marqués ML, Kharbanda V, et al. NLRP11 is a pattern recognition receptor for bacterial lipopolysaccharide in the cytosol of human macrophages. *Sci Immunol*. 2023;8(85):eabo4767. doi:10.1126/sciimmunol.abo4767

138. Elkayam E, Gervais FG, Wu H, Crackower MA, Lieberman J. New insights into the noncanonical inflammasome point to caspase-4 as a druggable target. *Nat Rev Immunol*. Published online 2025:1-11. doi:10.1038/s41577-025-01142-9

139. Wright SS, Vasudevan SO, Rathinam VA. Mechanisms and Consequences of Noncanonical Inflammasome-Mediated Pyroptosis. *J Mol Biol*. 2022;434(4):167245. doi:10.1016/j.jmb.2021.167245

140. Downs KP, Nguyen H, Dorfleutner A, Stehlik C. An overview of the non-canonical inflammasome. *Mol Asp Med*. 2020;76:100924. doi:10.1016/j.mam.2020.100924

141. Kayagaki N, Kornfeld OS, Lee BL, et al. NINJ1 mediates plasma membrane rupture during lytic cell death. *Nature*. 2021;591(7848):131-136. doi:10.1038/s41586-021-03218-7

142. Degen M, Santos JC, Pluhackova K, et al. Structural basis of NINJ1-mediated plasma membrane rupture in cell death. *Nature*. 2023;618(7967):1065-1071. doi:10.1038/s41586-023-05991-z

143. David L, Borges JP, Hollingsworth LR, et al. NINJ1 mediates plasma membrane rupture by cutting and releasing membrane disks. *Cell*. 2024;187(9):2224-2235.e16. doi:10.1016/j.cell.2024.03.008

144. Zhu Y, Xiao F, Wang Y, et al. NINJ1 regulates plasma membrane fragility under mechanical strain. *Nature*. 2025;644(8078):1088-1096. doi:10.1038/s41586-025-09222-5

145. Broz P. Pyroptosis: molecular mechanisms and roles in disease. *Cell Res*. 2025;35(5):334-344. doi:10.1038/s41422-025-01107-6

146. Dhuriya YK, Sharma D. Necroptosis: a regulated inflammatory mode of cell death. *J Neuroinflammation*. 2018;15(1):199. doi:10.1186/s12974-018-1235-0

147. Pasparakis M, Vandenabeele P. Necroptosis and its role in inflammation. *Nature*. 2015;517(7534):311-320. doi:10.1038/nature14191

148. Ye K, Chen Z, Xu Y. The double-edged functions of necroptosis. *Cell Death Dis*. 2023;14(2):163. doi:10.1038/s41419-023-05691-6

149. Chen X yu, Dai Y hong, Wan X xing, et al. ZBP1-Mediated Necroptosis: Mechanisms and Therapeutic Implications. *Molecules*. 2022;28(1):52. doi:10.3390/molecules28010052

150. Grootjans S, Berghe TV, Vandenabeele P. Initiation and execution mechanisms of necroptosis: an overview. *Cell Death Differ*. 2017;24(7):1184-1195. doi:10.1038/cdd.2017.65

151. Wu X, Nagy LE, Gautheron J. Mediators of necroptosis: from cell death to metabolic regulation. *EMBO Mol Med*. 2024;16(2):219-237. doi:10.1038/s44321-023-00011-z

152. Gough P, Myles IA. Tumor Necrosis Factor Receptors: Pleiotropic Signaling Complexes and Their Differential Effects. *Front Immunol*. 2020;11:585880. doi:10.3389/fimmu.2020.585880

153. Seo J, Nam YW, Kim S, Oh DB, Song J. Necroptosis molecular mechanisms: Recent findings regarding novel necroptosis regulators. *Exp Mol Med*. 2021;53(6):1007-1017. doi:10.1038/s12276-021-00634-7

154. Wang Q, Fan D, Xia Y, et al. The latest information on the RIPK1 post-translational modifications and functions. *Biomed Pharmacother*. 2021;142:112082. doi:10.1016/j.biopha.2021.112082

155. Lork M, Verhelst K, Beyaert R. CYLD, A20 and OTULIN deubiquitinases in NF-κB signaling and cell death: so similar, yet so different. *Cell Death Differ*. 2017;24(7):1172-1183. doi:10.1038/cdd.2017.46

156. Zhang W, Zhu C, Liao Y, Zhou M, Xu W, Zou Z. Caspase-8 in inflammatory diseases: a potential therapeutic target. *Cell Mol Biol Lett*. 2024;29(1):130. doi:10.1186/s11658-024-00646-x

157. Morgan MJ, Kim YS. Roles of RIPK3 in necroptosis, cell signaling, and disease. *Exp Mol Med*. 2022;54(10):1695-1704. doi:10.1038/s12276-022-00868-z

158. Liccardi G, Annibaldi A. MLKL post-translational modifications: road signs to infection, inflammation and unknown destinations. *Cell Death Differ*. 2023;30(2):269-278. doi:10.1038/s41418-022-01061-5

159. Boyd DF, Jordan SV, Balachandran S. ZBP1-driven cell death in severe influenza. *Trends Microbiol*. 2025;33(5):521-532. doi:10.1016/j.tim.2024.12.008

160. Kuriakose T, Kanneganti TD. ZBP1: Innate Sensor Regulating Cell Death and Inflammation. *Trends Immunol*. 2018;39(2):123-134. doi:10.1016/j.it.2017.11.002

161. Faizan MI, Ahmad T. Altered mitochondrial calcium handling and cell death by necroptosis: An emerging paradigm. *Mitochondrion*. 2021;57:47-62. doi:10.1016/j.mito.2020.12.004

162. An X, Yu W, Liu J, Tang D, Yang L, Chen X. Oxidative cell death in cancer: mechanisms and therapeutic opportunities. *Cell Death Dis*. 2024;15(8):556. doi:10.1038/s41419-024-06939-5

163. Liu S, Perez P, Sun X, et al. MLKL polymerization-induced lysosomal membrane permeabilization promotes necroptosis. *Cell Death Differ*. 2024;31(1):40-52. doi:10.1038/s41418-023-01237-7

164. Dixon SJ, Olzmann JA. The cell biology of ferroptosis. *Nat Rev Mol Cell Biol*. 2024;25(6):424-442. doi:10.1038/s41580-024-00703-5

165. Dai E, Chen X, Linkermann A, et al. A guideline on the molecular ecosystem regulating ferroptosis. *Nat Cell Biol*. 2024;26(9):1447-1457. doi:10.1038/s41556-024-01360-8

166. Jiang X, Stockwell BR, Conrad M. Ferroptosis: mechanisms, biology and role in disease. *Nat Rev Mol Cell Biol*. 2021;22(4):266-282. doi:10.1038/s41580-020-00324-8

167. Li J, Cao F, Yin H liang, et al. Ferroptosis: past, present and future. *Cell Death Dis*. 2020;11(2):88. doi:10.1038/s41419-020-2298-2

168. Sun Y, Chen P, Zhai B, et al. The emerging role of ferroptosis in inflammation. *Biomed Pharmacother*. 2020;127:110108. doi:10.1016/j.biopha.2020.110108

169. Li Y, Du Y, Zhou Y, et al. Iron and copper: critical executioners of ferroptosis, cuproptosis and other forms of cell death. *Cell Commun Signal*. 2023;21(1):327. doi:10.1186/s12964-023-01267-1

170. Liang D, Minikes AM, Jiang X. Ferroptosis at the intersection of lipid metabolism and cellular signaling. *Mol Cell*. 2022;82(12):2215-2227. doi:10.1016/j.molcel.2022.03.022

171. Zhang W, Liu Y, Liao Y, Zhu C, Zou Z. GPX4, ferroptosis, and diseases. *Biomed Pharmacother*. 2024;174:116512. doi:10.1016/j.biopha.2024.116512

172. Lee J, Roh JL. SLC7A11 as a Gateway of Metabolic Perturbation and Ferroptosis Vulnerability in Cancer. *Antioxidants*. 2022;11(12):2444. doi:10.3390/antiox11122444

173. Lu SC. Glutathione synthesis. *Biochim Biophys Acta (BBA) - Gen Subj*. 2013;1830(5):3143-3153. doi:10.1016/j.bbagen.2012.09.008

174. Saimoto Y, Kusakabe D, Morimoto K, et al. Lysosomal lipid peroxidation contributes to ferroptosis induction via lysosomal membrane permeabilization. *Nat Commun*. 2025;16(1):3554. doi:10.1038/s41467-025-58909-w

175. Feng J, Wang ZX, Bin JL, et al. Pharmacological approaches for targeting lysosomes to induce ferroptotic cell death in cancer. *Cancer Lett*. 2024;587:216728. doi:10.1016/j.canlet.2024.216728

176. Ramos S, Hartenian E, Santos JC, Walch P, Broz P. NINJ1 induces plasma membrane rupture and release of damage-associated molecular pattern molecules during ferroptosis. *EMBO J*. 2024;43(7):1164-1186. doi:10.1038/s44318-024-00055-y

177. Dixon SJ, Lemberg KM, Lamprecht MR, et al. Ferroptosis: An Iron-Dependent Form of Nonapoptotic Cell Death. *Cell*. 2012;149(5):1060-1072. doi:10.1016/j.cell.2012.03.042

178. Tang D, Chen X, Kang R, Kroemer G. Ferroptosis: molecular mechanisms and health implications. *Cell Res*. 2021;31(2):107-125. doi:10.1038/s41422-020-00441-1

179. Xiao L, Huang H, Fan S, et al. Ferroptosis: A mixed blessing for infectious diseases. *Front Pharmacol*. 2022;13:992734. doi:10.3389/fphar.2022.992734

180. Chen X, Kang R, Kroemer G, Tang D. Ferroptosis in infection, inflammation, and immunity. *J Exp Med*. 2021;218(6):e20210518. doi:10.1084/jem.20210518

181. Behar SM, Martin CJ, Booty MG, et al. Apoptosis is an innate defense function of macrophages against Mycobacterium tuberculosis. *Mucosal Immunol*. 2011;4(3):279-287. doi:10.1038/mi.2011.3

182. Augenstreich J, Briken V. Host Cell Targets of Released Lipid and Secreted Protein Effectors of Mycobacterium tuberculosis. *Front Cell Infect Microbiol*. 2020;10:595029. doi:10.3389/fcimb.2020.595029

183. Srinivasan L, Ahlbrand S, Briken V. Interaction of Mycobacterium tuberculosis with Host Cell Death Pathways. *Cold Spring Harb Perspect Med*. 2014;4(8):a022459. doi:10.1101/cshperspect.a022459

184. Keane J, Balcewicz-Sablinska MK, Remold HG, et al. Infection by Mycobacterium tuberculosis promotes human alveolar macrophage apoptosis. *Infect Immun*. 1997;65(1):298-304. doi:10.1128/iai.65.1.298-304.1997

185. Keane J, Remold HG, Kornfeld H. Virulent Mycobacterium tuberculosis Strains Evade Apoptosis of Infected Alveolar Macrophages. *J Immunol*. 2000;164(4):2016-2020. doi:10.4049/jimmunol.164.4.2016

186. Velmurugan K, Chen B, Miller JL, et al. Mycobacterium tuberculosis nuoG Is a Virulence Gene That Inhibits Apoptosis of Infected Host Cells. Bishai"] ["William, ed. *PLoS Pathog*. 2007;3(7):e110. doi:10.1371/journal.ppat.0030110

187. Gan H, Lee J, Ren F, Chen M, Kornfeld H, Remold HG. Mycobacterium tuberculosis blocks crosslinking of annexin-1 and apoptotic envelope formation on infected macrophages to maintain virulence. *Nat Immunol*. 2008;9(10):1189-1197. doi:10.1038/ni.1654

188. Davis JM, Ramakrishnan L. The Role of the Granuloma in Expansion and Dissemination of Early Tuberculous Infection. *Cell*. 2009;136(1):37-49. doi:10.1016/j.cell.2008.11.014

189. Kundu M, Pathak SK, Kumawat K, et al. A TNF- and c-Cbl-dependent FLIPS-degradation pathway and its function in Mycobacterium tuberculosis–induced macrophage apoptosis. *Nat Immunol*. 2009;10(8):918-926. doi:10.1038/ni.1754

190. Grover S, Sharma T, Singh Y, et al. The PGRS Domain of Mycobacterium tuberculosis PE_PGRS Protein Rv0297 Is Involved in Endoplasmic Reticulum Stress-Mediated Apoptosis through Toll-Like Receptor 4. *mBio*. 2018;9(3):10.1128/mbio.01017-18. doi:10.1128/mbio.01017-18

191. Matsumura K, Takaki S, Kirikae T. Mycobacterial protein PE_PGRS30 induces macrophage apoptosis through prohibitin 2 mitochondrial function interference. *Front Microbiol*. 2023;14:1080369. doi:10.3389/fmicb.2023.1080369

192. Augenstreich J, Arbues A, Simeone R, et al. ESX-1 and phthiocerol dimycocerosates of Mycobacterium tuberculosis act in concert to cause phagosomal rupture and host cell apoptosis. *Cell Microbiol*. 2017;19(7):e12726. doi:10.1111/cmi.12726

193. Sohn H, Kim JS, Shin SJ, et al. Targeting of Mycobacterium tuberculosis Heparin-Binding Hemagglutinin to Mitochondria in Macrophages. *PLoS Pathog*. 2011;7(12):e1002435. doi:10.1371/journal.ppat.1002435

194. Chen M, Gan H, Remold HG. A Mechanism of Virulence: Virulent Mycobacterium tuberculosis Strain H37Rv, but Not Attenuated H37Ra, Causes Significant Mitochondrial Inner Membrane Disruption in Macrophages Leading to Necrosis. *J Immunol*. 2006;176(6):3707-3716. doi:10.4049/jimmunol.176.6.3707

195. Aguiló N, Uranga S, Marinova D, Martín C, Pardo J. Bim is a crucial regulator of apoptosis induced byMycobacterium tuberculosis. *Cell Death Dis*. 2014;5(7):e1343-e1343. doi:10.1038/cddis.2014.313

196. Vu A, Glassman I, Campbell G, et al. Host Cell Death and Modulation of Immune Response against Mycobacterium tuberculosis Infection. *Int J Mol Sci*. 2024;25(11):6255. doi:10.3390/ijms25116255

197. Peng YT, Chen P, Ouyang RY, Song L. Multifaceted role of prohibitin in cell survival and apoptosis. *Apoptosis*. 2015;20(9):1135-1149. doi:10.1007/s10495-015-1143-z

198. Martin CJ, Booty MG, Rosebrock TR, et al. Efferocytosis Is an Innate Antibacterial Mechanism. *Cell Host Microbe*. 2012;12(3):289-300. doi:10.1016/j.chom.2012.06.010

199. Miller JL, Velmurugan K, Cowan MJ, Briken V. The Type I NADH Dehydrogenase of Mycobacterium tuberculosis Counters Phagosomal NOX2 Activity to Inhibit TNF-α-Mediated Host Cell Apoptosis. Deretic"] ["Vojo, ed. *PLoS Pathog*. 2010;6(4):e1000864. doi:10.1371/journal.ppat.1000864

200. Danelishvili L, Yamazaki Y, Selker J, Bermudez LE. Secreted Mycobacterium tuberculosis Rv3654c and Rv3655c Proteins Participate in the Suppression of Macrophage Apoptosis. *PLoS ONE*. 2010;5(5):e10474. doi:10.1371/journal.pone.0010474

201. Poirier V, Bach H, Av-Gay Y. Mycobacterium tuberculosis Promotes Anti-apoptotic Activity of the Macrophage by PtpA Protein-dependent Dephosphorylation of Host GSK3α*. *J Biol Chem*. 2014;289(42):29376-29385. doi:10.1074/jbc.m114.582502

202. Joseph S, Yuen A, Singh V, Hmama Z. Mycobacterium tuberculosis Cpn60.2 (GroEL2) blocks macrophage apoptosis via interaction with mitochondrial mortalin. *Biol Open*. 2017;6(4):481-488. doi:10.1242/bio.023119

203. Zhang W, Lu Q, Dong Y, Yue Y, Xiong S. Rv3033, as an Emerging Anti-apoptosis Factor, Facilitates Mycobacteria Survival via Inhibiting Macrophage Intrinsic Apoptosis. *Front Immunol*. 2018;9:2136. doi:10.3389/fimmu.2018.02136

204. Sun M, Song L, Li Y, Zhou T, Jope RS. Identification of an antiapoptotic protein complex at death receptors. *Cell Death Differ*. 2008;15(12):1887-1900. doi:10.1038/cdd.2008.124

205. Hinchey J, Lee S, Jeon BY, et al. Enhanced priming of adaptive immunity by a proapoptotic mutant of Mycobacterium tuberculosis. *J Clin Investig*. 2007;117(8):2279-2288. doi:10.1172/jci31947

206. Bertheloot D, Latz E, Franklin BS. Necroptosis, pyroptosis and apoptosis: an intricate game of cell death. *Cell Mol Immunol*. 2021;18(5):1106-1121. doi:10.1038/s41423-020-00630-3

207. Chen M, Divangahi M, Gan H, et al. Lipid mediators in innate immunity against tuberculosis: opposing roles of PGE2 and LXA4 in the induction of macrophage death. *J Exp Med*. 2008;205(12):2791-2801. doi:10.1084/jem.20080767

208. Zhang Y, Zhao D, Wang T, et al. Pyroptosis, a double-edged sword during pathogen infection: a review. *Cell Death Discov*. 2025;11(1):289. doi:10.1038/s41420-025-02579-6

209. Brokatzky D, Mostowy S. Pyroptosis in host defence against bacterial infection. *Dis Model Mech*. 2022;15(7):dmm049414. doi:10.1242/dmm.049414

210. Koo IC, Wang C, Raghavan S, Morisaki JH, Cox JS, Brown EJ. ESX-1-dependent cytolysis in lysosome secretion and inflammasome activation during mycobacterial infection. *Cell Microbiol*. 2008;10(9):1866-1878. doi:10.1111/j.1462-5822.2008.01177.x

211. Carlsson F, Kim J, Dumitru C, et al. Host-Detrimental Role of Esx-1-Mediated Inflammasome Activation in Mycobacterial Infection. *PLoS Pathog*. 2010;6(5):e1000895. doi:10.1371/journal.ppat.1000895

212. Kurenuma T, Kawamura I, Hara H, et al. The RD1 Locus in the Mycobacterium tuberculosis Genome Contributes to Activation of Caspase-1 via Induction of Potassium Ion Efflux in Infected Macrophages. *Infect Immun*. 2009;77(9):3992-4001. doi:10.1128/iai.00015-09

213. Yamada H, Mizumo S, Horai R, Iwakura Y, Sugawara I. Protective Role of Interleukin-1 in Mycobacterial Infection in IL-1 α/β Double-Knockout Mice. *Lab Investig*. 2000;80(5):759-767. doi:10.1038/labinvest.3780079

214. Mayer-Barber KD, Barber DL, Shenderov K, et al. Cutting Edge: Caspase-1 Independent IL-1β Production Is Critical for Host Resistance to Mycobacterium tuberculosis and Does Not Require TLR Signaling In Vivo. *J Immunol*. 2010;184(7):3326-3330. doi:10.4049/jimmunol.0904189

215. Dorhoi A, Nouailles G, Jörg S, et al. Activation of the NLRP3 inflammasome by Mycobacterium tuberculosis is uncoupled from susceptibility to active tuberculosis. *Eur J Immunol*. 2012;42(2):374-384. doi:10.1002/eji.201141548

216. Amaral EP, Riteau N, Moayeri M, et al. Lysosomal Cathepsin Release Is Required for NLRP3-Inflammasome Activation by Mycobacterium tuberculosis in Infected Macrophages. *Front Immunol*. 2018;9:1427. doi:10.3389/fimmu.2018.01427

217. Saiga H, Kitada S, Shimada Y, et al. Critical role of AIM2 in Mycobacterium tuberculosis infection. *Int Immunol*. 2012;24(10):637-644. doi:10.1093/intimm/dxs062

218. Rastogi S, Ellinwood S, Augenstreich J, Mayer-Barber KD, Briken V. Mycobacterium tuberculosis inhibits the NLRP3 inflammasome activation via its phosphokinase PknF. *PLoS Pathog*. 2021;17(7):e1009712. doi:10.1371/journal.ppat.1009712

219. Chai Q, Yu S, Zhong Y, et al. A bacterial phospholipid phosphatase inhibits host pyroptosis by hijacking ubiquitin. *Science*. 2022;378(6616):eabq0132. doi:10.1126/science.abq0132

220. Yu Y, Yu S, Lu Z, et al. Pathogenic phosphorylation of linear ubiquitin machinery causes inflammasome sensor degradation. *Cell Rep*. 2025;44(9):116286. doi:10.1016/j.celrep.2025.116286

221. Shah S, Bohsali A, Ahlbrand SE, et al. Cutting Edge: Mycobacterium tuberculosis but Not Nonvirulent Mycobacteria Inhibits IFN-β and AIM2 Inflammasome–Dependent IL-1β Production via Its ESX-1 Secretion System. *J Immunol*. 2013;191(7):3514-3518. doi:10.4049/jimmunol.1301331

222. Afonina IS, Müller C, Martin SJ, Beyaert R. Proteolytic Processing of Interleukin-1 Family Cytokines: Variations on a Common Theme. *Immunity*. 2015;42(6):991-1004. doi:10.1016/j.immuni.2015.06.003

223. Mishra BB, Moura-Alves P, Sonawane A, et al. Mycobacterium tuberculosis protein ESAT-6 is a potent activator of the NLRP3/ASC inflammasome. *Cell Microbiol*. 2010;12(8):1046-1063. doi:10.1111/j.1462-5822.2010.01450.x

224. Wong K, Jr WRJ. Critical role for NLRP3 in necrotic death triggered by Mycobacterium tuberculosis. *Cell Microbiol*. 2011;13(9):1371-1384. doi:10.1111/j.1462-5822.2011.01625.x

225. Abdallah AM, Bestebroer J, Savage NDL, et al. Mycobacterial Secretion Systems ESX-1 and ESX-5 Play Distinct Roles in Host Cell Death and Inflammasome Activation. *J Immunol*. 2011;187(9):4744-4753. doi:10.4049/jimmunol.1101457

226. Beckwith KS, Beckwith MS, Ullmann S, et al. Plasma membrane damage causes NLRP3 activation and pyroptosis during Mycobacterium tuberculosis infection. *Nat Commun*. 2020;11(1):2270. doi:10.1038/s41467-020-16143-6

227. Szczerba M, Ganesh A, Gil-Marqués ML, Briken V, Goldberg MB. NLRP11 is required for canonical NLRP3 and non-canonical inflammasome activation during human macrophage infection with mycobacteria. *bioRxiv*. Published online 2025:2024.12.11.627830. doi:10.1101/2024.12.11.627830

228. Arnett E, Wolff J, Wager CML, et al. Cutting Edge: Cytosolic Receptor AIM2 Is Induced by Peroxisome Proliferator-activated Receptor γ following Mycobacterium tuberculosis Infection of Human Macrophages but Does Not Contribute to IL-1β Release. *J Immunol*. 2024;212(5):765-770. doi:10.4049/jimmunol.2300418

229. Roca FJ, Ramakrishnan L. TNF Dually Mediates Resistance and Susceptibility to Mycobacteria via Mitochondrial Reactive Oxygen Species. *Cell*. 2013;153(3):521-534. doi:10.1016/j.cell.2013.03.022

230. Tobin DM, Roca FJ, Oh SF, et al. Host Genotype-Specific Therapies Can Optimize the Inflammatory Response to Mycobacterial Infections. *Cell*. 2012;148(3):434-446. doi:10.1016/j.cell.2011.12.023

231. Roca FJ, Whitworth LJ, Redmond S, Jones AA, Ramakrishnan L. TNF Induces Pathogenic Programmed Macrophage Necrosis in Tuberculosis through a Mitochondrial-Lysosomal-Endoplasmic Reticulum Circuit. *Cell*. 2019;178(6):1344-1361.e11. doi:10.1016/j.cell.2019.08.004

232. Tanzer MC, Matti I, Hildebrand JM, et al. Evolutionary divergence of the necroptosis effector MLKL. *Cell Death Differ*. 2016;23(7):1185-1197. doi:10.1038/cdd.2015.169

233. Zhao X, Khan N, Gan H, et al. Bcl-xL mediates RIPK3-dependent necrosis in M. tuberculosis-infected macrophages. *Mucosal Immunol*. 2017;10(6):1553-1568. doi:10.1038/mi.2017.12

234. Pajuelo D, Gonzalez-Juarbe N, Tak U, Sun J, Orihuela CJ, Niederweis M. NAD+ Depletion Triggers Macrophage Necroptosis, a Cell Death Pathway Exploited by Mycobacterium tuberculosis. *Cell Rep*. 2018;24(2):429-440. doi:10.1016/j.celrep.2018.06.042

235. Weindel CG, Martinez EL, Zhao X, et al. Mitochondrial ROS promotes susceptibility to infection via gasdermin D-mediated necroptosis. *Cell*. 2022;185(17):3214-3231.e23. doi:10.1016/j.cell.2022.06.038

236. Stutz MD, Ojaimi S, Allison C, et al. Necroptotic signaling is primed in Mycobacterium tuberculosis-infected macrophages, but its pathophysiological consequence in disease is restricted. *Cell Death Differ*. 2018;25(5):951-965. doi:10.1038/s41418-017-0031-1

237. Amaral EP, Costa DL, Namasivayam S, et al. A major role for ferroptosis in Mycobacterium tuberculosis–induced cell death and tissue necrosis. *J Exp Med*. 2019;216(3):556-570. doi:10.1084/jem.20181776

238. Amaral EP, Foreman TW, Namasivayam S, et al. GPX4 regulates cellular necrosis and host resistance in Mycobacterium tuberculosis infection. *J Exp Med*. 2022;219(11):e20220504. doi:10.1084/jem.20220504

239. Wang H, Liu D, Ge X, Wang Y, Zhou X. Mycobacterium bovis Mb3523c protein regulates host ferroptosis via chaperone-mediated autophagy. *Autophagy*. 2025;21(6):1335-1352. doi:10.1080/15548627.2025.2468139

240. Amaral EP, Namasivayam S, Queiroz ATL, et al. BACH1 promotes tissue necrosis and Mycobacterium tuberculosis susceptibility. *Nat Microbiol*. 2024;9(1):120-135. doi:10.1038/s41564-023-01523-7

241. Qiang L, Zhang Y, Lei Z, et al. A mycobacterial effector promotes ferroptosis-dependent pathogenicity and dissemination. *Nat Commun*. 2023;14(1):1430. doi:10.1038/s41467-023-37148-x

242. Wang F, Gómez-Sintes R, Boya P. Lysosomal membrane permeabilization and cell death. *Traffic*. 2018;19(12):918-931. doi:10.1111/tra.12613

243. Repnik U, Česen MH, Turk B. Lysosomal membrane permeabilization in cell death: Concepts and challenges. *Mitochondrion*. 2014;19:49-57. doi:10.1016/j.mito.2014.06.006

244. Lee J, Repasy T, Papavinasasundaram K, Sassetti C, Kornfeld H. Mycobacterium tuberculosis Induces an Atypical Cell Death Mode to Escape from Infected Macrophages. *PLoS ONE*. 2011;6(3):e18367. doi:10.1371/journal.pone.0018367

245. Yang Z, Zhang L, Ottavi S, et al. ACOD1-mediated lysosomal membrane permeabilization contributes to Mycobacterium tuberculosis–induced macrophage death. *Proc Natl Acad Sci*. 2025;122(12):e2425309122. doi:10.1073/pnas.2425309122

246. Doster RS, Rogers LM, Gaddy JA, Aronoff DM. Macrophage Extracellular Traps: A Scoping Review. *J Innate Immun*. 2018;10(1):3-13. doi:10.1159/000480373

247. Jensen M, Thorsen NW, Hallberg LAE, Hägglund P, Hawkins CL. New insight into the composition of extracellular traps released by macrophages exposed to different types of inducers. *Free Radic Biol Med*. 2023;202:97-109. doi:10.1016/j.freeradbiomed.2023.03.025

248. Wong KW, Jacobs WR. Mycobacterium tuberculosis Exploits Human Interferon γ to Stimulate Macrophage Extracellular Trap Formation and Necrosis. *J Infect Dis*. 2013;208(1):109-119. doi:10.1093/infdis/jit097

249. Kalsum S, Braian C, Koeken VACM, et al. The Cording Phenotype of Mycobacterium tuberculosis Induces the Formation of Extracellular Traps in Human Macrophages. *Front Cell Infect Microbiol*. 2017;7:278. doi:10.3389/fcimb.2017.00278

250. Chowdhury CS, Kinsella RL, McNehlan ME, et al. Type I IFN-mediated NET release promotes Mycobacterium tuberculosis replication and is associated with granuloma caseation. *Cell Host Microbe*. 2024;32(12):2092-2111.e7. doi:10.1016/j.chom.2024.11.008

251. Hunter RL. Tuberculosis as a three-act play: A new paradigm for the pathogenesis of pulmonary tuberculosis. *Tuberculosis*. 2016;97:8-17. doi:10.1016/j.tube.2015.11.010

252. Miranda MS, Breiman A, Allain S, Deknuydt F, Altare F. The Tuberculous Granuloma: An Unsuccessful Host Defence Mechanism Providing a Safety Shelter for the Bacteria? *J Immunol Res*. 2012;2012(1):139127. doi:10.1155/2012/139127

253. Jr. AMD, Sugimoto M. Liquefaction of Caseous Foci in Tuberculosis1, 2. *Am Rev Respir Dis*. 2015;113(3):257-259. doi:10.1164/arrd.1976.113.3.257

254. Ehlers S, Schaible UE. The Granuloma in Tuberculosis: Dynamics of a Host–Pathogen Collusion. *Front Immunol*. 2013;3:411. doi:10.3389/fimmu.2012.00411

255. Ríos-Barrera VA, Campos-Peña V, Aguilar-León D, et al. Macrophage and T lymphocyte apoptosis during experimental pulmonary tuberculosis: their relationship to mycobacterial virulence. *Eur J Immunol*. 2006;36(2):345-353. doi:10.1002/eji.200535202

256. Watson VE, Hill LL, Owen-Schaub LB, et al. Apoptosis in Mycobacterium tuberculosis infection in mice exhibiting varied immunopathology. *J Pathol*. 2000;190(2):211-220. doi:10.1002/(sici)1096-9896(200002)190:2<211::aid-path530>3.0.co;2-3

257. Stutz MD, Allison CC, Ojaimi S, et al. Macrophage and neutrophil death programs differentially confer resistance to tuberculosis. *Immunity*. 2021;54(8):1758-1771.e7. doi:10.1016/j.immuni.2021.06.009

258. Kilinç G, Saris A, Ottenhoff THM, Haks MC. Host-directed therapy to combat mycobacterial infections*. *Immunol Rev*. 2021;301(1):62-83. doi:10.1111/imr.12951

259. Li J, Wang Y, He L, et al. Host-directed therapeutic targets in macrophages and their ligands against mycobacteria tuberculosis. *Infect Immun*. Published online 2025:e0006325. doi:10.1128/iai.00063-25

260. Stadler JAM, Maartens G, Meintjes G, Wasserman S. Clofazimine for the treatment of tuberculosis. *Front Pharmacol*. 2023;14:1100488. doi:10.3389/fphar.2023.1100488

261. Fukutomi Y, Maeda Y, Makino M. Apoptosis-Inducing Activity of Clofazimine in Macrophages. *Antimicrob Agents Chemother*. 2011;55(9):4000-4005. doi:10.1128/aac.00434-11

262. Kaufmann SHE, Lange C, Rao M, et al. Progress in tuberculosis vaccine development and host-directed therapies—a state of the art review. *Lancet Respir Med*. 2014;2(4):301-320. doi:10.1016/s2213-2600(14)70033-5

263. Singh M, Sarhan MO, Damiba NNL, et al. Proapoptotic Bcl-2 inhibitor as potential host directed therapy for pulmonary tuberculosis. *Nat Commun*. 2025;16(1):3003. doi:10.1038/s41467-025-58190-x

264. Mayer-Barber KD, Andrade BB, Oland SD, et al. Host-directed therapy of tuberculosis based on interleukin-1 and type I interferon crosstalk. *Nature*. 2014;511(7507):99-103. doi:10.1038/nature13489

265. Zhang L, Jiang X, Pfau D, Ling Y, Nathan CF. Type I interferon signaling mediates Mycobacterium tuberculosis-induced macrophage death. *J Exp Med*. 2021;218(2):e20200887. doi:10.1084/jem.20200887

266. Song R, Gao Y, Dozmorov I, et al. IRF1 governs the differential interferon-stimulated gene responses in human monocytes and macrophages by regulating chromatin accessibility. *Cell Rep*. 2021;34(12):108891. doi:10.1016/j.celrep.2021.108891

267. Lee AM, Nathan CF. Type I interferon exacerbates Mycobacterium tuberculosis induced human macrophage death. *EMBO Rep*. 2024;25(7):3064-3089. doi:10.1038/s44319-024-00171-0

268. Shuster MJ. *Inhibition of Type One Interferon Signaling Through Crosstalk With Toll-Like Receptor Signaling*. University of Maryland, College Park; 2024.

269. Augenstreich J, Phan AT, Allen CNS, et al. Dynamic interplay of autophagy and membrane repair during Mycobacterium tuberculosis Infection. Salgame"] ["Padmini, ed. *PLOS Pathogens*. 2025;21(1):e1012830. doi:10.1371/journal.ppat.1012830

270. Ding G. Videos and image analysis. Published online 2025. doi:10.17632/rkbw676zf2

271. Nisa A, Kipper FC, Panigrahy D, Tiwari S, Kupz A, Subbian S. Different modalities of host cell death and their impact on Mycobacterium tuberculosis infection. *Am J Physiol-Cell Physiol*. 2022;323(5):C1444-C1474. doi:10.1152/ajpcell.00246.2022

272. Riendeau CJ, Kornfeld H. THP-1 Cell Apoptosis in Response to Mycobacterial Infection. *Infection and Immunity*. 2003;71(1):254-259. doi:10.1128/iai.71.1.254-259.2003

273. Theobald SJ, Gräb J, Fritsch M, et al. Gasdermin D mediates host cell death but not interleukin-1β secretion in Mycobacterium tuberculosis-infected macrophages. *Cell Death Discov*. 2021;7(1):327. doi:10.1038/s41420-021-00716-5

274. Beckwith KS, Beckwith MS, Ullmann S, et al. Plasma membrane damage causes NLRP3 activation and pyroptosis during Mycobacterium tuberculosis infection. *Nature Communications*. 2020;11(1):2270. doi:10.1038/s41467-020-16143-6

275. Sugisawa R, Shanahan KA, Davis GM, Davey GP, Bowie AG. SARM1 regulates pro-inflammatory cytokine expression in human monocytes by NADase-dependent and -independent mechanisms. *iScience*. 2024;27(6):109940. doi:10.1016/j.isci.2024.109940

276. Augenstreich J, Poddar A, Belew AT, El-Sayed NM, Briken V. da_Tracker: Automated workflow for high throughput single cell and single phagosome tracking in infected cells. *Biology Open*. 2024;13(9):bio060555. doi:10.1242/bio.060555

277. Gaschler MM, Stockwell BR. Lipid peroxidation in cell death. *Biochemical and Biophysical Research Communications*. 2017;482(3):419-425. doi:10.1016/j.bbrc.2016.10.086

278. Qiang L, Zhang Y, Lei Z, et al. A mycobacterial effector promotes ferroptosis-dependent pathogenicity and dissemination. *Nat Commun*. 2023;14(1):1430. doi:10.1038/s41467-023-37148-x

279. Hristova K, Wimley WC. Determining the statistical significance of the difference between arbitrary curves: A spreadsheet method. Han"] ["Gang, ed. *PLOS ONE*. 2023;18(10):e0289619. doi:10.1371/journal.pone.0289619

280. Park W, Wei S, Kim BS, et al. Diversity and complexity of cell death: a historical review. *Exp Mol Med*. 2023;55(8):1573-1594. doi:10.1038/s12276-023-01078-x

281. Srinivasan L, Gurses SA, Hurley BE, Miller JL, Karakousis PC, Briken V. Identification of a Transcription Factor That Regulates Host Cell Exit and Virulence of Mycobacterium tuberculosis. Sassetti"] ["Christopher M., ed. *PLOS Pathogens*. 2016;12(5):e1005652. doi:10.1371/journal.ppat.1005652

282. Aits S, Jäättelä M. Lysosomal cell death at a glance. *Journal of Cell Science*. 2013;126(9):1905-1912. doi:10.1242/jcs.091181

283. Wong KW, Jacobs WR. Mycobacterium tuberculosis Exploits Human Interferon γ to Stimulate Macrophage Extracellular Trap Formation and Necrosis. *The Journal of Infectious Diseases*. 2013;208(1):109-119. doi:10.1093/infdis/jit097

284. Kalsum S, Braian C, Koeken VACM, et al. The Cording Phenotype of Mycobacterium tuberculosis Induces the Formation of Extracellular Traps in Human Macrophages. *Frontiers in Cellular and Infection Microbiology*. 2017;7:278. doi:10.3389/fcimb.2017.00278

285. David L, Borges JP, Hollingsworth LR, et al. NINJ1 mediates plasma membrane rupture by cutting and releasing membrane disks. *Cell*. 2024;187(9):2224-2235.e16. doi:10.1016/j.cell.2024.03.008

286. Man SM, Tourlomousis P, Hopkins L, Monie TP, Fitzgerald KA, Bryant CE. Salmonella Infection Induces Recruitment of Caspase-8 to the Inflammasome To Modulate IL-1β Production. *J Immunol*. 2013;191(10):5239-5246. doi:10.4049/jimmunol.1301581

287. Weng W, Hu Z, Pan Y. Macrophage Extracellular Traps: Current Opinions and the State of Research regarding Various Diseases. Xu"] ["Huaxi, ed. *Journal of Immunology Research*. 2022;2022:1-10. doi:10.1155/2022/7050807

288. Lee Y, Brenner M, Aziz M, Wang P. Molecular and subcellular mechanisms of vital macrophage extracellular trap formation. *Front Immunol*. 2025;16:1608428. doi:10.3389/fimmu.2025.1608428

289. Wang Y, Shao F. NINJ1, rupturing swollen membranes for cataclysmic cell lysis. *Mol Cell*. 2021;81(7):1370-1371. doi:10.1016/j.molcel.2021.03.005

290. Sollberger G, Choidas A, Burn GL, et al. Gasdermin D plays a vital role in the generation of neutrophil extracellular traps. *Sci Immunol*. 2018;3(26). doi:10.1126/sciimmunol.aar6689

291. Sætra RS, Hansen M, Kappelhoff S, et al. NINJ1 is activated by Mycobacterium tuberculosis ESX-1 secreted effector EsxA and mediates necrosis of infected human macrophages. *bioRxiv*. Published online January 1, 2025:2025.11.04.685750. doi:10.1101/2025.11.04.685750

292. Rebak AS, Hendriks IA, Elsborg JD, et al. A quantitative and site-specific atlas of the citrullinome reveals widespread existence of citrullination and insights into PADI4 substrates. *Nat Struct Mol Biol*. 2024;31(6):977-995. doi:10.1038/s41594-024-01214-9

293. Wang H, Kim SJ, Lei Y, et al. Neutrophil extracellular traps in homeostasis and disease. *Signal Transduct Target Ther*. 2024;9(1):235. doi:10.1038/s41392-024-01933-x